Steam-Oxygen Fluidized Bed Gasification of Sewage Sludge

Von der Fakultät 4 Energie-, Verfahrens- und Biotechnik
der Universität Stuttgart zur Erlangung der Würde eines Doktors der
Ingenieurwissenschaften (Dr.-Ing.) genehmigte Abhandlung

vorgelegt von

Max Schmid

aus Stuttgart

Hauptberichter:	Univ.-Prof. Dr. techn. Günter Scheffknecht
Mitberichter:	Univ.-Prof. Dr. techn. Hermann Hofbauer

Tag der Einreichung: 01.03.2023

Tag der mündlichen Prüfung: 30.10.2023

Institut für Feuerungs- und Kraftwerkstechnik (IFK)
der Universität Stuttgart
2023

Acknowledgement

The work presented within this thesis was conducted between 2015 and 2022 while I was employed at the Institute of Combustion and Power Plant Technology (IFK) of the University of Stuttgart. The experimental work was part of the public funded project Res2CNG under the grant number BWB15004 (2015 - 2018). I gratefully acknowledge the financial support from the Ministry of the Environment, Climate Protection and the Energy Sector (BMWK) of "the Länd" Baden-Württemberg. I furthermore acknowledge the constructive cooperation with the project partners DVGW-EBI and EIFER from Karlsruhe and IER from the University of Stuttgart.

I express my deep gratitude to Univ.-Prof. Dr. techn. Günter Scheffknecht for the supervision of this dissertation project. My gratitude is extended to Univ.-Prof. Dr. techn. Hermann Hofbauer who supported my thesis as co-examiner. I furthermore thank apl. Prof. Dr.-Ing. Uwe Schnell for his constant support.

I thank the former heads of my IFK department "Decentralized Energy Conversion" (DEU), Heiko Dieter and Reinhold Spörl, for their guidance. Furthermore, I am deeply grateful to my colleagues from department DEU, Marcel Beirow, Theodor Beisheim, Yen-Hau Chen, Paul Gabris, Harold Garcia, Andreas Gredinger, Heidi Grosch, Selina Hafner, Georg Hartfuß, Gerrit Hofbauer, Heiko Holz, Matthias Hornberger, Thiansiri Kertthong, Nico Mader, Felix Mangold, Joseba Moreno, Lukas Reiner, Steven Scharr, Christian Schmidberger, Daniel Schweitzer, Tim Seitz and Gebhard Waizmann. Their practical help in the lab and the fruitful scientific discussions were central for the development of this thesis. I furthermore thank Thomas Froschmeier, Simon Grathwohl, Beate Koch, Kay Mechling, Ralf Nollert, Antje Radszuweit, Wolfgang Roß and Dieter Straub for mechanical, chemical and administrative support. Special thanks goes to Alessa Angermann, Hongchao Chu, Felix Kirch, Thiansiri Kertthong and Christian Schmidberger whose student theses contributed to this work.

In addition, I deeply thank my parents Michaela and Gerd for their love, care and support.

I express my warmest gratitude to my wife Julia for unlimited love and support: thank you for making my life cheerful every day.

Contents

List of symbols

Latin symbols

symbol	unit	meaning
C	g m^{-3}	mass concentration
d	m	diameter
h	MJ kg^{-1}	specific enthalpy
H	MJ	absolute enthalpy
m	kg	mass
$\widetilde{M}$	kg mol^{-1}	mole mass
$\dot{m}$	kg h^{-1}	mass flow
n	mol	amount of substance
$n_{Ca,S}$	mol mol^{-1}	calcium to sulfur ratio
n_{CaCO3}	kg kg^{-1}	limestone additive ratio as feed ratio of limestone to fuel au.
n_{O2}	mol mol^{-1}	oxygen ratio
n_{SC}	mol mol^{-1}	steam to carbon ratio incl. biomass moisture
n_{WHSV}	h^{-1}	weight hourly space velocity as mass quotient of fuel (waf.) and bed inventory
$\dot{n}$	mol h^{-1}	mole flow
$S_{j,E}$	kg kg^{-1}	elemental yield: yield of fuel element E in product species j
u	m s^{-1}	velocity
u_0	m s^{-1}	superficial velocity
V	m^3	volume
x	kg kg^{-1}	mass fraction
y	m^3 m^{-3}	volume fraction
Y_{gas}	m^3 kg^{-1}	gas yield: yield of syngas (wf.,N_2f) per fuel (waf)
$Y_{j,fuel}$	kg kg^{-1}	species yield: yield of species *j* per fuel

Greek symbols

symbol	unit	meaning
α	mol mol^{-1}	mole ratio, energy ratio
γ	kg kg^{-1}	fuel mass fraction
Δ		difference
η	J J^{-1}	efficiency
ϑ	°C	gasifier temperature
ν	m^2 s^{-1}	kinematic viscosity
ϱ	g m^{-3}	gas density

Subscripts

subscript	meaning
au	as used
CGE	cold gas efficiency
E	chemical element
el	electric
eq	equilibrium
exp	experiment
f	formation
gas	syngas
gasi	gasifier
HHV	higher heating value
isen	isentropic
j	species
k	species
LHV	lower heating value
mech	mechanic
mf	minimum fluidization
moist	moisture
N2f	N_2-free
P	particle
R	reaction
ref	experimental reference point
s	solid

subscript	meaning
S	stream
sim	simulation
SNG	synthetic natural gas
SS	sewage sludge
stoic	stoichiometric
tot	total
waf	water ash free
wf	water free

Superscripts

superscript	meaning
STP	standard temperature and pressure (273.15 K, 1.013 bar)
0	standard state (298.15 K, 1 bar)

Abbreviations

abbreviation	meaning
AbfKlär2017	2017 novellierte Klärschlammverordnung (German sewage sludge law, renewed in 2017)
ASU	air separating unit
BET	Brunauer-Emmett-Teller technique for measurement of specific surface area
BTX	benzene, toluene, xylene
CHP	combined heat and power plant
DFB	dual fluidized bed
DME	dimethyl ether
DüMV	Düngemittelverordnung (German fertilizer law)
DVGW	Deutscher Verein des Gas- und Wasserfaches e. V. (recognized standardization body for the gas and water industry in Germany)
DT	deformation temperature
ECN	Energy Research Centre of the Netherlands
fc	fixed carbon
FID	flame ionization detector
FT	flow temperature
GC	Gas chromatography
HT	hemisphere temperature

abbreviation	meaning
HTW	higher temperature Winkler gasification
ICE	internal combustion engine
ICP	inductively coupled plasma
MS	mass spectroscopy
NDIR	non-dispersive infrared
PAH	polyaromatic hydrocarbons
PEM	polymer electrolyte membrane electrolyzer
PSI	Paul-Scherrer-Institut
RDF	refuse derived fuel
RME	Rapsmethylester (biodiesel made from rape seeds)
SCD	sulfur chemiluminescence detector
SEM	scanning electron microscope
SEM EDX	energy-dispersive X-ray spectroscopy
SNG	synthetic natural gas
SOEC	Solid oxide electrolysis cell
SST	shrinkage starting temperature
TRL	technology readiness level
UV/Vis	ultraviolet-visible
VDI	Verein Deutscher Ingenieure (association of German engineers)
vm	volatile matter
WGS	water-gas shift
WHSV	weight hourly space velocity
WWTP	wastewater treatment plant
XRD	x-ray diffraction

Abstract

Sewage sludge is a residue that is generated unavoidably by the population. On a first sight, sewage sludge may be a hazardous waste that requires safe disposal. By looking closer, it is recognized as secondary resource. The mineral fraction contains valuable elements such as phosphorous, which can be retrieved as secondary raw material. This thesis focuses on the organic fraction, which is a renewable fuel and carbon source and can be used to substitute fossil carbon in fuels and chemicals. The first step in converting sewage sludge to renewable goods is syngas production via gasification.

The experimental work of this thesis demonstrated the feasibility of synthesis gas production from sewage sludge by steam-oxygen fluidized bed gasification. It was shown that the process works reliably in the investigated 20 kW scale and that the syngas contains high H_2 and CO concentrations and is thus suitable for synthesis of fuels and chemicals. The impurities NH_3, H_2S, COS and tar species, including heterocyclic species such as pyridine, were measured in considerable concentrations in the syngas. Small amounts of limestone bed additive enabled cracking of heavy tars and partial capture of H_2S and COS. It was further found that the cold gas efficiency increases with rising gasification temperature due to improved tar and char conversion at higher temperatures. The typical operation temperature 850 °C requires an oxygen ratio of 0.33, obtaining a cold gas efficiency of 63 %. Moreover, the H_2/CO-ratio could be controlled efficiently by altering the steam to carbon ratio, as steam promotes the water gas shift reaction in the gasifier to achieve the desired stoichiometry for synthesis, however, resulting in higher energy demand for steam provision. The experimental results can be utilized for process design, e.g., for a TRL 7-demonstrator.

Furthermore, a gasifier model was developed and an integrated process chain was simulated to assess the conversion of sewage sludge to synthetic natural gas (SNG) with and without inclusion of power-to-gas through electrolysis. The total efficiency of the conversion including own consumption for the case without electrolysis was 51 % with a carbon utilization of 33 %. These values could be enhanced by inclusion of power-to-gas. It was predicted that the produced SNG has a CH_4-concentration of between 0.81 $m^3\ m^{-3}$ and 0.84 $m^3\ m^{-3}$ and nitrogen concentrations of up to 0.16 $m^3\ m^{-3}$ originating from fuel-bound nitrogen. The simulations on process integration showed that up to 20% of the sewage sludge feed can be dried by heat integration. This implies that also external heat sources have to be used for drying.

Overall, the steam-oxygen gasification proved to be an efficient and technically feasible process for sewage sludge treatment and can be considered as an alternative to fluidized bed incineration for future mono-treatment plants.

Kurzfassung

Klärschlamm ist ein unvermeidbarer Reststoff, der durch die Abwasserreinigung produziert wird. Auf den ersten Blick ist Klärschlamm ein schadstoffhaltiger Abfall, der sicher entsorgt werden muss. Bei genauerem Hinsehen handelt es sich um einen Sekundärrohstoff. Der mineralische Anteil enthält wertvolle Elemente wie Phosphor, die zurückgewonnen werden können. Diese Arbeit setzt den Fokus jedoch auf den organischen Anteil, welcher als Ausgangsstoff verwendet werden kann, um fossilen Kohlenstoff in Kraftstoffen und Chemikalien zu ersetzen.

Im experimentellen Teil dieser Arbeit wird die Machbarkeit der Synthesegaserzeugung aus Klärschlamm durch Wasserdampfsauerstoff-Wirbelschichtvergasung nachgewiesen. Es konnte gezeigt werden, dass der Prozess im untersuchten 20-kW-Maßstab zuverlässig funktioniert und dass das Synthesegas hohe H_2- und CO-Konzentrationen enthält und somit für die Synthese von Kraftstoffen und Chemikalien geeignet ist. Die Verunreinigungen NH_3, H_2S, COS und Teerspezies, einschließlich heterozyklischer Spezies wie Pyridin, wurden in beträchtlichen Konzentrationen im Synthesegas gemessen. Kleine Mengen an Kalkstein als Bettadditiv ermöglichten das Cracken von schweren Teeren und die anteilige Abscheidung von H_2S und COS. Der Kaltgaswirkungsgrad erhöhte sich stetig mit steigender Vergasungstemperatur aufgrund einer verbesserten Umwandlung von Teer und Koks. Eine typische Betriebstemperatur von 850 °C erfordert eine Sauerstoffzahl von 0,33 und es wird ein Kaltgaswirkungsgrad von 63 S% erreicht. Darüber hinaus kann das H_2/CO-Verhältnis durch Anpassung der zugeführten Dampfmenge gesteuert werden, um die gewünschte Stöchiometrie für die Synthese zu erreichen, was jedoch zu einem höheren Energiebedarf für die Dampfbereitstellung führt. Die experimentellen Ergebnisse können für die Prozessauslegung genutzt werden, z. B. für einen TRL 7 Demonstrator.

Darüber hinaus wurde ein Vergasermodell entwickelt und eine integrierte Prozesskette simuliert, um die Umwandlung von Klärschlamm zu synthetischem Erdgas (SNG) mit und ohne Einbeziehung von Power-to-Gas zu bewerten. Der Gesamtwirkungsgrad der Umwandlung inkl. Eigenverbrauch beträgt 51 % bei einer Kohlenstoffausnutzung von 33 %. Diese Werte können durch die Einbeziehung von Power-to-Gas gesteigert werden. Für das produzierte SNG wurden CH_4-Konzentrationen von 0,81 $m^3\ m^{-3}$ bis 0,84 $m^3\ m^{-3}$ und N_2-Konzentrationen von bis zu 0,15 $m^3\ m^{-3}$ berechnet, bedingt durch die Umwandlung von brennstoffgebundenen Stickstoff zu im SNG verbleibendem N_2. Zudem ergaben die Simulationen, dass bis zu 20 % des eingesetzten Klärschlamms durch Wärmeintegration getrocknet werden können. Dies impliziert, dass auch externe Wärmequellen zum Trocknen verwendet werden müssen.

Insgesamt hat sich die Wasserdampfsauerstoffvergasung als effiziente und technisch machbare Alternative zur Wirbelschichtverbrennung für zukünftige Monoverwertungsanlagen erwiesen.

1 Introduction

1.1 Motivation for sewage sludge gasification

Climate change mitigation requires extensive measures to reduce greenhouse gas emissions. One of that is substituting fossil carbon in fuels and goods by renewable carbon sources, which include biomass, such as wood and energy crops but also biogenic residues with the advantage of low or even negative feedstock costs.

One of those biogenic residues is sewage sludge, which is generated unavoidably by the population since it is a by-product of wastewater treatment. The generated quantities of sewage sludge are for example $10 \cdot 10^9$ kg a^{-1} in Europe [1], $12 \cdot 10^9$ kg a^{-1} in the USA [2] and $6 \cdot 10^9$ kg a^{-1} in China [3], all on dry basis. Since wastewater treatment is still to be deployed in large parts of the world, further increase of the worldwide-generated amount is expected that needs to be disposed adequately.

Sewage sludge is more than a biogenic fuel and carbon source. It contains high amounts of minerals including phosphorous, which can be recovered to close the nutrient cycle, but also hazardous heavy metals which need to be disposed safely [4]. The currently mostly practiced disposal methods of land-use or landfill fail to recover the sewage sludge's renewable energy, make no or only inefficient use of its phosphorous content and contaminate soil with hazardous substances. Other common disposal methods are co-incineration in coal-fired power plants or cement plants, which allow energy recovery but do not allow phosphorous recovery, since the sewage sludge ash is mixed with coal ash or clinker. In Germany and Switzerland, for instance, the need of phosphorous recovery has already been put into regulation [5], which will effectively ban co-combustion. Consequently, the technology of choice for greenfield plants is currently a thermal mono-treatment such as fluidized bed incineration, which allows the collection of sewage sludge ash for subsequent phosphorous recovery. There is currently too less capacity for appropriate sewage sludge treatment that causes very high disposal fees. Therefore, the construction of numerous mono-treatment plants is expected in the coming decade.

State of the art sewage sludge fluidized bed incineration uses comparably wet sludge with a water content of over 0.4 kg kg^{-1} making the process energetically rather inefficient, thus only little heat and power can be produced. A more innovative and efficient concept is sewage sludge gasification followed by a synthesis process that is able to convert sewage sludge into established carbon-based products, such as transport fuels, chemicals or plastics, utilizing the sludge's renewable carbon.

Also, the recovery of phosphorous can be achieved well from gasification-derived sewage sludge ash [6–8] since it is already partially reduced.

1.2 Motivation for this thesis

Air gasification is state of the art for conversion of sewage sludge to a combustible gas. However, the syngas obtainable from air gasification has N_2 concentrations of up to 0.6 $m^3 m^{-3}$ [9] and is thus not suitable for synthesis purposes. Therefore, this thesis studies a more suitable gasification technology that builds on the state of the art enabling fast adoption by industry but enables the production of N_2-free syngas. Steam-oxygen fluidized bed gasification is particularly suitable for this application, since it produces a nitrogen-lean and thus high calorific syngas that is rich in hydrogen and carbon monoxide and can be used for synthesis of fuels (e.g. synthetic natural gas, dimethyl ether, kerosene) and chemicals (methanol, plastic monomers).

The steam-oxygen gasification uses a mixture of steam and oxygen as gasification agent. Oxygen is used for partial fuel oxidation providing the necessary heat for the endothermic gasification process. Steam serves on the one hand as reactant to enhance gasification reactions and on the other hand as additional fluidization agent to ensure good mixing of the fluidized bed to prevent hot spots. Due to its autothermal operation, steam-oxygen gasification only requires a single fluidized bed reactor which simplifies the process layout in contrast to allothermal indirect dual fluidized bed (DFB) steam gasification. The needed oxygen can be generated by an on-site power-to-gas facility that produces oxygen as by-product from water electrolysis or by state-of-the-art air separation units (ASU) with acceptable energy consumption [10, 11]. Fluidized bed gasification uses dried sewage sludge as feedstock. A combination of mechanical dewatering (e.g. centrifuge) to a dry matter fraction of around 0.25 kg kg^{-1}, followed by solar or thermal drying, using low-temperature heat, can be used to obtain a dry matter fraction of > 0.9 kg kg^{-1} as required for steam oxygen gasification. Similar to state-of-the-art air gasification, the gasifier is operated at temperatures of around 850 °C which enables the thermochemical decomposition of fuel into permanent gases, tar species, char and ash. The produced char and tar species are then gasified or reformed by reaction with oxygen and steam [12]. The main products in the syngas are H_2, CO, CO_2, CH_4 and H_2O, of which H_2 and CO can be used as feedstock for various synthesis processes.

The product gas contains beside the desired syngas species, tar species and other impurities. Especially when using fuels with high S and N content, a high H_2S and NH_3 concentration is observed in the syngas which is not tolerated by downstream synthesis catalysts [13]. Therefore, gas cleaning is required before synthesis. Reducing the costs of gas cleaning is important for the economic feasibility of the process [14]. Tar species from sewage sludge gasification can differ from the well-known polyaromatic hydrocarbons (PAH) of wood gasification [11, 15]. The high amounts of N

and S in the sewage sludge enables the formation of tar species containing these elements, so called heterocyclic aromatics and polyaromatics. Such species are often water-soluble and more toxic than the corresponding aromatics without heteroatoms and thus need to be considered when designing the gas cleaning.

To design and assess the entire process chain consisting of gasification, gas cleaning and synthesis, detailed information on the product gas yield and composition, including impurities, is needed. Therefore, a central goal of this thesis is to conduct an experimental study of the steam-oxygen gasification to assess the syngas composition including impurity concentrations and the efficiency of fuel conversion as well as the effect of gasifier operation conditions thereon. These insights are important for an evaluation of the technical feasibility of the process and as foundation for process modeling and design.

The reduction of tars and impurities by primary measures such as active bed materials is considered economically and technically favorable compared to secondary measures [16, 17]. A CaO-containing bed material, e.g. achieved by addition of limestone ($CaCO_3$) or dolomite is catalytically active for cracking and steam reforming of tars and acts as sorbent to capture H_2S and COS [18]. Therefore, another specific goal of this thesis is to collect experimental data on the application of limestone as tar cracking and sulfur capture agent for sewage sludge steam-oxygen gasification.

To assess the efficiency of a process chain converting sewage sludge to a synthetic fuel, the process integration between the main process steps drying, gasification, gas cleaning and synthesis needs to be taken into account. To conduct a first assessment, the conversion of sewage sludge to substitute natural gas (SNG) is investigated in this thesis. For this, a process model of the complete chain from sewage sludge to SNG including heat integration and integration of water electrolysis (power to gas) was built and the process chain studied by simulative sensitivity studies. The key results contain suggestions for optimized process operation conditions, predictions of the overall process efficiency and SNG composition.

1.3 Objectives and outline of this thesis

This thesis is an experimental and simulative investigation of steam-oxygen gasification of sewage sludge. The specific objectives of the experimental work are:

- to demonstrate production of synthesis gas from sewage sludge by steam-oxygen gasification in a 20 kW fluidized bed using sewage sludge ash as bed material and determine the quality and quantity of all products
- to conduct an experimental sensitivity study on the effect of gasifier operation conditions on the gasification performance including syngas composition, gas yield and impurity concentrations
- to quantify and assess the effect of limestone as bed additive for in-situ gas cleaning.

The specific objectives of the model development and simulative work are:

- to develop a gasifier model based on thermodynamic correlations and experimental data with the ability of
    - describing the gasification mass balance and its sensitivity to the operation parameters according to the experimental findings of this work
    - calculating the energy balance to determine the needed oxygen ratio for autothermal gasification
- to model an exemplary production chain for the conversion of sewage sludge to substitute natural gas (SNG)
- to conduct process simulations to calculate optimized operation parameters for the gasification and the whole process chain for maximized total efficiency including assessment of synergies with power to gas through water electrolysis.

Chapter 2 of this thesis describes the background of thermochemical gasification in general, of steam-oxygen gasification and peculiarities of sewage sludge as feedstock and gives an overview on the state of the art. The experimental methods are described in chapter 3 followed by the experimental results and their discussion in chapter 4. Chapter 5 describes the development of the gasifier model, model validation against experimental data as well as results and discussion of the gasifier simulations. Chapter 6 describes the modeling of an SNG production chain from sewage sludge followed by simulation results and discussion focusing on efficiency assessment of the process chain also including integration with water electrolysis. This thesis' conclusions are presented in chapter 7.

1.4 Author's publications related to this thesis

During the course of this dissertation project, the author of this thesis published five peer-reviewed papers as first author which are used as basis of this thesis. The research covered in these publications as well as the writing of the original drafts were conducted by the author of this thesis. The co-authors of the papers had a supporting role but did not contribute original research. Some passages and figures from these papers were incorporated in this thesis without changes while others were updated and modified. All previously published data and results have been assessed carefully to ensure consistent data evaluation throughout this thesis. For that reason, the results presented in this thesis may slightly deviate from the ones previously published. The publications that were incorporated in this thesis are:

1. M. Schmid, M. Beirow, D. Schweitzer, G. Waizmann, R. Spörl, G. Scheffknecht: Product gas composition for steam-oxygen fluidized bed gasification of dried sewage sludge, straw pellets and wood pellets and the influence of limestone as bed material, Biomass and Bioenergy 117 (2018) 71–77. [10]

2. M. Schmid, S. Hafner, G. Scheffknecht: Experimental Parameter Study on Synthesis gas Production by Steam-Oxygen Fluidized Bed Gasification of Sewage Sludge, Applied Sciences (2021) 11, 579 [19]

3. M. Schmid, S. Hafner, S. Biollaz, J. Schneebeli, G. Waizmann, G. Scheffknecht: Steam-oxygen gasification of sewage sludge: Reduction of tar, H_2S and COS with limestone as bed additive, Biomass and Bioenergy 150 (2021) 106100 [20]

4. M. Schmid, C. Schmidberger, G. Scheffknecht: Modelling and Simulation of Fluidized Bed Steam-Oxygen Gasification of Sewage Sludge using Thermochemical Equilibrium and Experimental Data, Fuel 341 (2023) 127595 [21]

5. M. Schmid, C. Schmidberger, S. Hafner, G. Scheffknecht: Process simulation of SNG production from sewage sludge via steam-oxygen gasification, Fuel 360 (2024) 130491 [22]

2 Background

2.1 Fluidized bed gasification of biogenic residues

This chapter gives a short overview on thermochemical gasification of biogenic residues to provide the background for this work.

2.1.1 Thermochemical gasification

Thermochemical gasification is the conversion of a solid or liquid fuel into a burnable product gas, also known as synthesis gas or syngas. Thermochemical gasification of solid fuels typically takes place at reactor temperatures between 700 °C and 1400 °C and in most cases comprises of the steps drying, pyrolysis, and gasification. During the drying step, the fuel particle releases moisture due to the heat exposure. When the dried fuel is further heated, it undergoes pyrolysis, a cracking of molecular bounds converting the fuel into smaller molecules of which the majority is already volatile. The gasifier contains oxidizing gases, the so-called gasification agent, such as air. In contrast to combustion processes, the gasification takes place at under-stoichiometric oxygen supply or without any molecular oxygen supply. The product gas consists mainly of H_2, CO, CO_2, CH_4, further hydrocarbons and the unreacted components of the gasification agent. The pyrolysis and gasification reactions are briefly described in the following [12].

Pyrolysis

Pyrolysis refers to the decomposition of fuel solemnly due to the influence of temperature and is a complex process with numerous reaction pathways, intermediates and products. However, it can formally be divided into primary pyrolysis and secondary pyrolysis. The primary pyrolysis refers to the thermal cracking of the fuel molecules into permanent gases, primary tar species and char. The primary tar species undergo secondary pyrolysis, a further thermal cracking to permanent gases and secondary tars. These processes can be described by reactions R 1 and R 2 [23]:

Primary pyrolysis:

$$\text{fuel} \rightarrow \text{char} + CO + H_2 + CO_2 + CH_4 + \ldots + \text{primary tar species} \qquad \text{R 1}$$

Secondary pyrolysis:

$$\text{primary tar} \rightarrow CO + H_2 + CO_2 + CH_4 + \ldots + \text{secondary tar species} \qquad \text{R 2}$$

Gasification reactions

Gasification refers to the reactions between pyrolysis products and the gasification agent. A selection of the most relevant gasification reactions and their reaction enthalpies Δh^0_R is given in the following [12]:

Char oxidation:	$C + O_2 \leftrightarrow CO_2$	$\Delta h^0_R = -394$ kJ mol^{-1}	R 3
Carbon monoxide oxidation:	$CO + 0.5\ O_2 \leftrightarrow CO_2$	$\Delta h^0_R = -283$ kJ mol^{-1}	R 4
Hydrogen oxidation:	$H_2 + 0.5\ O_2 \leftrightarrow H_2O$	$\Delta h^0_R = -286$ kJ mol^{-1}	R 5
Water-gas reaction:	$C + H_2O \leftrightarrow CO + H_2$	$\Delta h^0_R = 131$ kJ mol^{-1}	R 6
Bouduard reaction:	$C + CO_2 \leftrightarrow 2\ CO$	$\Delta h^0_R = 172$ kJ mol^{-1}	R 7
Methane reforming:	$CH_4 + H_2O \leftrightarrow CO + 3\ H_2$	$\Delta h^0_R = 225$ kJ mol^{-1}	R 8
Hydrocarbon reforming:	$C_xH_y + x\ H_2O \leftrightarrow x\ CO + (x+\frac{y}{2})\ H_2$	$\Delta h^0_R > 0$	R 9
Tar reforming:	$tar + H_2O \leftrightarrow x\ CO + y\ H_2$	$\Delta h^0_R > 0$	R 10
Water-gas-shift:	$CO + H_2O \leftrightarrow CO_2 + H_2$	$\Delta h^0_R = -41$ kJ mol^{-1}	R 11

R 3 to R 5 describe the combustion reactions, which only take place if the gasification agent contains oxygen. In an autothermal gasification process, like steam-oxygen gasification, these exothermic reactions provide the necessary heat to maintain the gasification temperature. These reactions are typically faster than the other listed reactions. R 6 to R 10 describe the strongly endothermic gasification reactions that convert char and hydrocarbons into CO and H_2. These reactions are comparably slow. The kinetics of char gasification is highly dependent on the char structure [12, 24]. The slightly exothermic water-gas shift reaction R 11 is a temperature dependent equilibrium reaction that influences the H_2/CO-ratio of the syngas.

2.1.2 Autothermal and allothermal gasification

Gasification processes can be classified by means of heat input into the gasifier to achieve the desired reactor temperature and to drive the endothermic gasification reactions. In an autothermal gasification process, the fuel is partially combusted by oxygen or air fed into the gasifier (e.g. steam-oxygen gasification). Autothermal gasification requires less equipment since the gasification process can take place in one reactor. The disadvantage is the requirement of air or oxygen as gasification agent resulting in either dilution of the product gas with N_2 or efforts for oxygen production.

In an allothermal gasification process, the heat is transported from an outside source into the gasifier e.g. by heat exchangers or by heat convection through heated sand or other solids. No air or

oxygen feed is required ensuring undiluted product gas with high heating value and saving additional efforts for producing pure oxygen. However, more equipment is needed for allothermal gasification such as a second reactor in which the heat is produced, e.g. by combustion, as well as means of heat transport into the gasifier, such as heat exchangers, heat pipes or heat transport by a stream of hot solid (i.e. dual fluidized bed gasification).

2.1.3 Tar definition, formation and reduction

Tar is an unavoidable by-product of the pyrolysis step of solid fuels. Contamination of the syngas with tar is a major drawback in gasification and has been one of the main obstacles for broad commercialization of gasification technology. At room temperature, tars become visible as highly viscous liquid. Heavy tars can condense at temperatures below 400 °C and can clog pipes or impair equipment downstream of the gasifier.

Tar definition

Different tar definitions can be found in literature [39–41]. This thesis uses the definition used in the tar sampling standard CEN/TS 15439:2006, also known as "tar protocol" [25]:

"Tar is a term for all organic compounds present in the gasification product gas

excluding hydrocarbons from C1 through C6."

Many references exclude the species benzene from the tar definition. However, in this thesis benzene is regarded as a part of the GC-detectable tar, since benzene concentration is for most gasification processes very important for the gas cleaning system design.

As described in the "tar protocol" [25], tar samples can be analyzed with gravimetric and GC methods. Therefore, tars are further classified in gravimetric tars (ECN1) and GC tars, whereas GC tars are further classified into the classes ECN2 - ECN5 [26], as shown in Table 2.1.

Table 2.1: The ECN tar classification system [26] as applied in this thesis

Tar class	Description
ECN1	Gravimetric tar
ECN2	Heterocyclic species (compounds with heteroatoms e.g. O, N, Cl, S) with considerable water solubility (e.g. pyridine, phenol, cresol, thiophene, benzothiophene).
ECN3	One-ring aromatic species (e.g. toluene, xylene, styrene). These species exhibit low water solubility. Due to comparably low dew point, these species have only minor contribution to condensation and clogging issues.
ECN4	Light polyaromatic species with two or three rings (e.g. naphthalene, fluorene, phenanthrene). These species can condense at intermediate temperatures when present in high concentrations.
ECN5	Heavy polyaromatic species with four or more rings (e.g. pyrene, fluoranthene). These species can condense easily at still relatively high temperatures and cause clogging or facility malfunctioning.

Tar formation

Tar is mainly formed through decomposition of the fuel during pyrolysis in the particle temperature range of 200 °C to 500 °C [12]. The fuel components, for lignocellulosic fuels cellulose, hemicellulose and lignin, for sewage sludge additionally proteins and urea, undergo decomposition to primary tars. Primary tars also include significant amounts of oxygenated, for sewage sludge sulfonated and nitrogenated, species. At temperatures above 500 °C, primary tars undergo secondary pyrolysis and are cracked into permanent gases but also into heavier molecules, the so-called secondary tars. Secondary tars are mostly methyl-derivates of aromatics or olefins. Secondary tars can further react to aromatics and polyaromatics, sometimes classified as tertiary tars. Higher temperatures promote this conversion so that species without substituents (benzene, naphthalene, etc.) are favored [12, 23].

Tar reduction and removal

The tar yield can be reduced by primary measures: The total tar quantity decreases significantly with increasing temperature. The tar concentration is further dependent on the gasification agent, for example, higher oxygen and steam feed reduce the tar concentration. Tar can further be reduced by catalytically active bed material such as olivine, or CaO produced from calcined dolomite or limestone [13, 27–29]. Secondary tar removal can consist of downstream tar scrubbing with water

or organic solvents or downstream catalytic reforming e.g. over nickel or noble metal or natural catalysts [30–34].

2.1.4 Desulfurization of the syngas with CaO

Gasification of sulfur-containing fuel produces gaseous sulfur species such as H_2S and COS. Calcium oxide (CaO) can act as sulfur sorbent. It is present in sewage sludge ash but can also be added in form of limestone ($CaCO_3$) additive that can be calcined in the gasifier (R 12). The H_2S and COS capture follows the equilibrium reactions R 13 and R 14 [17, 35–37]:

$$CaCO_3 \leftrightarrow CaO + CO_2 \qquad \Delta h^0_R = -178 \text{ kJ mol}^{-1} \qquad \text{R 12}$$

$$H_2S + CaO \leftrightarrow CaS + H_2O \qquad \Delta h^0_R = -109 \text{ kJ mol}^{-1} \qquad \text{R 13}$$

$$COS + CaO \leftrightarrow CaS + CO_2 \qquad \Delta h^0_R = -103 \text{ kJ mol}^{-1} \qquad \text{R 14}$$

Since a reducing atmosphere is present in the gasifier, $CaSO_4$ cannot be formed but instead CaS. Therefore, no complete sulfur capture is possible. H_2S or COS capture is limited by the thermodynamic equilibrium as can be calculated from thermodynamic databases using calculator software such as FactSage® or AspenPlus®. Results of equilibrium calculations on desulfurization under relevant conditions can be found in literature [35] and in section 4 and 5 of this thesis. Since R 13 and R 14 are exothermic, high H_2S and COS capture is favored at low temperatures. Moreover, the possible degree of sulfur capture is influenced by the gas atmosphere: e.g. higher steam concentration decreases H_2S-capture while higher CO_2 concentration decrease COS-capture.

2.2 Steam-oxygen gasification

2.2.1 Principle and material streams

Figure 2.1 shows schematic of the steam-oxygen gasification with its main mass flows. Typically, a bubbling fluidized bed gasifier blown with a mixture of steam and oxygen is used. The fuel, with the mass flow $\dot{m}_{fuel,au}$, is fed into or onto the fluidized bed in the condition as used (au.) containing a certain amount of moisture. The fuel reacts with oxygen and steam and is thus gasified. Typical temperatures of the gasifier are ϑ = 600 - 900 °C while the necessary heat to achieve these temperatures is provided by partial fuel oxidation. Particle separators, typically a cyclone and a filter, are placed downstream of the gasifier to remove fly ashes. Ash drained directly from the bed is called bed ash. The particle-free product gas contains different gas species including impurities. In this work, the impurity free syngas, consisting of the species H_2, CO, CO_2, CH_4, C_xH_y and H_2O, is designated $\dot{m}_{gas}$. Although in practice, there are many further components and impurities present,

this work limits the view on the impurities tar species, H_2S, COS and NH_3. For the calculation of gas yields or species concentrations, this work often refers to water free syngas. The main parameters and values describing the operation and performance of steam-oxygen gasification are described in the following subsections.

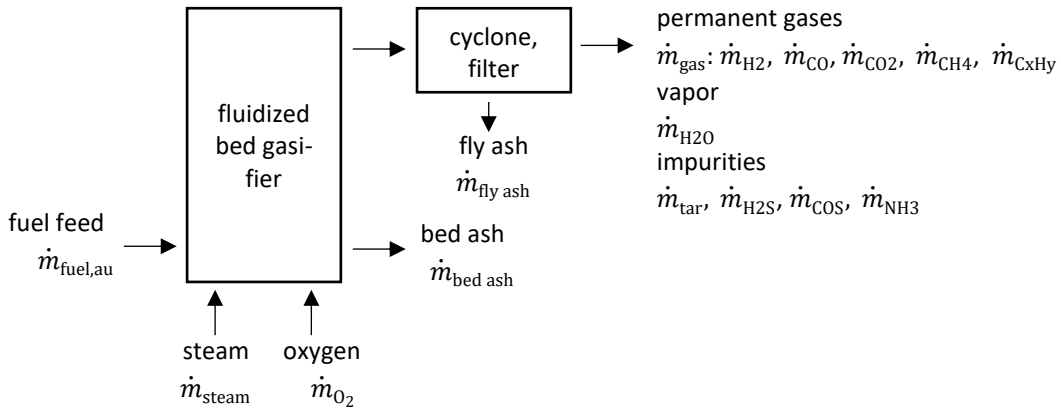

Figure 2.1: Material streams of steam-oxygen gasification

2.2.2 Operation parameters

The main operation parameters for the steam-oxygen gasification process are gasification temperature, steam to carbon ratio, oxygen ratio, weight hourly space velocity and the bed material type.

Gasification temperature ϑ

The gasification temperature ϑ refers to the temperature of the bed. In this work, the bubbling fluidized bed is considered as a well-mixed system and therefore a uniform bed temperature is assumed. In practice, especially in larger fluidized beds, temperature gradients can occur e.g. caused by feeding of the fuel or the gasification agent. For the choice of ϑ, the following trade-off needs to be considered: Higher temperatures lead to faster gasification reactions and thus improved char and tar conversion but, on the other hand, can result into bed agglomeration when the sintering point of the fuel ash is exceeded (see section 2.3.3). In addition, higher gasification temperatures require more oxygen and thus can reduce the overall conversion efficiency. In this work, gasification temperatures from 650 °C to 900 °C were investigated to generate insight in the influence of temperature on the process. Because of the advantages of higher gasification rates and lower tar yields, it is expected that an industrial sewage sludge gasifier will be operated at a temperature above 800 °C but below 900 °C to prevent sintering and agglomeration of the bed.

Steam to carbon ratio n_{SC}

The steam to carbon ratio n_{SC} describes the ratio of the total mole flow of water, including the fuel's moisture, to the mole flow of biomass carbon introduced into the gasifier:

$$n_{SC} = \frac{\dot{N}_{H2O,steam} + \dot{N}_{H2O,moist}}{\dot{N}_{C,fuel}}. \quad (2\text{-}1)$$

Generally, higher n_{SC} result in a reduced overall energetic efficiency, as additional steam is needed. On the other hand, low n_{SC} can reduce char conversion and cause higher tar yields [38]. The water-gas shift reaction (R 11) is severely influenced by the steam to carbon ratio, since H_2O pushes the equilibrium to the right side. Therefore, the H_2-yield as well as the H_2/CO-ratio that is important for downstream synthesis processes, can be increased with increasing n_{SC}.

Oxygen ratio n_{O2}

The oxygen ratio n_{O2} (analogue to air ratio λ in combustion processes) – often also referred to as equivalence ratio ER – expresses the ratio of the amount of oxygen actually used in the process to the amount of oxygen required for stoichiometric oxidation of the fuel:

$$n_{O2} = \frac{\dot{N}_{O2}}{\dot{N}_{O2,stoic}} = \frac{\dot{M}_{O2}}{\dot{M}_{O2,stoic}}. \quad (2\text{-}2)$$

In a technical process, n_{O2} cannot be chosen independently of the gasifier's temperature, but is a function thereof. However, due to the electrical heating of the experimental facility used in this work, n_{O2} is not coupled with the gasifier temperature and hence can be set by the operator.

Weight hourly space velocity n_{WHSV}

The weight hourly space velocity n_{WHSV} is the ratio of the dry ash free fuel feeding rate to bed inventory mass:

$$n_{WHSV} = \frac{\dot{M}_{fuel,waf}}{M_{bed}}. \quad (2\text{-}3)$$

Therefore, n_{WHSV} is a design value that brings the fuel load and the size of the fluidized bed reactor in terms of bed inventory in correlation. The n_{WHSV} is correlated reciprocally to the fuel residence or space time in the bed. That means, for higher n_{WHSV} the fuel has a shorter residence time in the bed.

Limestone additive ratio n_{CaCO3}

The limestone additive ratio n_{CaCO3} expresses the mass ratio of limestone additive to water free fuel feed:

$$n_{CaCO3} = \frac{\dot{M}_{CaCO3}}{\dot{M}_{fuel,wf}}. \quad (2\text{-}4)$$

It directly influences the fraction of CaO in the bed material that is available for catalytic tar cracking and sulfur capture.

Calcium to sulfur ratio $n_{Ca,S}$

The calcium to sulfur ratio is used to assess in-situ desulfurization potential of the system and is calculated as the quotient of the mole flows of calcium and sulfur.

$$n_{Ca,S} = \frac{\dot{N}_{Ca}}{\dot{N}_{S,fuel}}. \quad (2\text{-}5)$$

While the sulfur usually comes only with the fuel, calcium can be introduced by the fuel or by an additive (e.g. limestone). Sulfur capture by calcium can take place through different reactions, however H_2S capture (R 13) and COS capture (R 14) are the most important in gasification. Sulfur capture can only occur until these reactions are in equilibrium or, in other words, until the equilibrium concentration of H_2S and COS are reached in the syngas.

Superficial velocity u_0

The superficial velocity u_0 in the fluidized bed is the quotient of the gas volume flow in the reactor and the cross-sectional area of the gasifier A_{gasi}. For simplification, u_0 is calculated by the inlet volume flows of steam and nitrogen (purge) at reactor conditions (ϑ, p):

$$u_0 = \frac{\dot{V}_{H2O,steam} + \dot{V}_{O2} + \dot{V}_{N2,purge}}{A_{gasi}}. \quad (2\text{-}6)$$

This calculation method does not account for gases produced by the thermochemical conversion of the fuel. Therefore, the so calculated u_0 can be considered a minimum value.

Minimum fluidizing velocity u_{mf}

The minimum fluidizing velocity u_{mf} was derived from the particle Reynolds number at minimum fluidizing conditions $Re_{P,mf}$ which was calculated according to Kunii and Levenspiel [39] using the values for K_1 and K_2 of Wen and Yu [40]

$$Re_{P,mf} = \frac{u_{mf}\, d_P}{\nu_{gas}} = \sqrt{33.7^2 + 0.0408\, Ar_P} - 33.7 \quad (2\text{-}7)$$

and the particle Archimedes number

$$Ar_P = \frac{d_P^3\ (\rho_s - \rho_{gas}) g}{\nu_{gas}^2\, \rho_{gas}}. \quad (2\text{-}8)$$

2.2.3 Heat of formation

The change of enthalpy during the formation of a compound from chemical elements is called heat of formation. It is commonly given in standard state (1 bar, 25 °C). The standard heat of formation

of elements in their standard configuration (e.g. C, H_2, O_2) is zero. The standard heat of formation of chemical compounds with known chemical formula is available in literature. However, for complex mixtures like most solid fuels, it needs to be calculated from a reaction with known stoichiometry and known reaction enthalpy. Thus, a solid fuel's heat of formation can be calculated from its elemental analysis and its higher heating value according to equation (2-8) following the reaction with oxygen:

$$\Delta h^0_{\mathrm{f,fuel,waf}} = \Delta h^0_{\mathrm{f,CO_2}}\,\gamma_{\mathrm{C}}\,\frac{\widetilde{M}_{\mathrm{CO_2}}}{\widetilde{M}_{\mathrm{C}}} + \Delta h^0_{\mathrm{f,H_2O(l)}}\,\gamma_{\mathrm{H}}\,\frac{\widetilde{M}_{\mathrm{H_2O}}}{\widetilde{M}_{\mathrm{H_2}}} + \Delta h^0_{\mathrm{f,SO_2}}\,\gamma_{\mathrm{S}}\,\frac{\widetilde{M}_{\mathrm{SO_2}}}{\widetilde{M}_{\mathrm{S}}} + h_{\mathrm{HHV,fuel,waf}} \qquad (2\text{-}9)$$

With $\Delta h^0_{\mathrm{f,CO2}}$ = -8.94 MJ kg^{-1}, $\Delta h^0_{\mathrm{f,H2O(l)}}$ = -15.88 MJ kg^{-1} and $\Delta h^0_{\mathrm{f,SO2}}$ = 4.64 MJ kg^{-1}. The heat of formation for different sewage sludges and wood pellets as comparison are calculated in 2.3.1.

2.2.4 Concentration of educt and product species

The concentration of a chemical element or a species *j* in a solid stream *S* is expressed in mass fractions

$$x_j = \frac{m_j}{m_S}. \qquad (2\text{-}10)$$

The same principle is used to express fuel composition, however the symbol γ is used and the reference basis is stated, e.g. as used (au), water free (wf) or water and ash free (waf):

$$\gamma_j = \frac{m_j}{m_{\mathrm{fuel,waf}}}. \qquad (2\text{-}11)$$

The gas concentration of species *j* is expressed as volume fraction

$$y_j = \frac{V_j}{V_{\mathrm{gas}}}. \qquad (2\text{-}12)$$

Ideal gas is assumed in this thesis; therefore, volume fractions equal mole factions. Volume fractions are mostly used for the so-called permanent gases: H_2, CO, CO_2, CH_4, C_xH_y, N_2, but also for H_2O (steam) or impurity concentrations such as H_2S, COS, NH_3 and HCl. The gas volume fractions are often used on water free basis since most common syngas analyzers can only measure water-free gas. Moreover, since in practice the N_2-concentration is often not measured, concentrations on a water free and N_2-free (N_2f) basis are common:

$$y_{j,\mathrm{wf,N2f}} = \frac{V_{\mathrm{j}}}{V_{\mathrm{gas,wf,N2f}}}. \qquad (2\text{-}13)$$

Especially for tar species, mass concentrations based on gas volume are used:

$$C_j = \frac{m_j}{V_{\mathrm{gas}}^{\mathrm{STP}}}. \qquad (2\text{-}14)$$

For the above-explained practical reasons the concentrations are often based on water-free and N_2-free gas volume:

$$C_{j,\mathrm{wf,N2f}} = \frac{m_j}{V^{\mathrm{STP}}_{\mathrm{gas,wf,N2f}}}. \tag{2-15}$$

Volume fractions and mass concentrations can be correlated by the gas density at STP conditions.

2.2.5 Yield of product species

The mass yield of individual product streams or species *j* is expressed as species mass per fuel mass:

$$Y_{j,\mathrm{fuel}} = \frac{m_j}{m_{\mathrm{fuel}}}. \tag{2-16}$$

In most cases, the dry and ash free fuel is used as basis. Typical yields are the yield of CH_4, $Y_{\mathrm{CH4,SSwaf}}$, or the yield of total tar, $Y_{\mathrm{tar,SSwaf}}$, per water and ash free sewage sludge.

The total gas yield is one of the key values that is used to describe the gasification process. It is expressed as total gas volume in STP-conditions generated by the gasification of a certain fuel mass

$$Y_{\mathrm{gas}} = \frac{V^{STP}_{gas,wf,N2f}}{m_{\mathrm{fuel,waf}}}. \tag{2-17}$$

It is common to use the yield of water-free and N_2-free gas on the basis of water ash free fuel.

Elemental yields are expressed as yield of a respective element in a product stream based on feed amount of that element in the fuel

$$S_{j,E} = \frac{x_{j,E}\, Y_{\mathrm{j,fuel}}}{\gamma_E}. \tag{2-18}$$

With $x_{j,E}$ as mass fraction of the element E in the species *j*, γ_E as mass fraction of the element *E* in the fuel. For example, $S_{\mathrm{CH4,C}}$ is the yield of fuel-bound carbon (C) in the syngas species CH_4, whereas $S_{\mathrm{H2S,S}}$ is the yield of fuel-bound sulfur in the syngas species H_2S.

2.2.6 Efficiency and performance values

The cold gas efficiency η_{CGE} is used to assess the energetic performance of a gasification process without the need of further analysis of upstream and downstream processes or heat integration. It is calculated as a quotient of the chemical energy in the produced syngas and the used fuel. By considering only chemical energy and no sensible energy, the energy needed for pre-heating of feed streams (e.g. gasification agent) but also the usable heat in product gas is neglected. In the following, the cold gas efficiency is calculated on higher heating value (HHV) basis considering only the main combustible components:

$$\eta_{\mathrm{CGE}} = \frac{\dot{m}_{\mathrm{Gas}}\, \Delta h_{HHV,gas}}{\dot{m}_{\mathrm{fuel,waf}}\, \Delta h_{HHV,fuel,waf}} = \frac{\Sigma \dot{m}_j\, \Delta h_{\mathrm{HHV},j}}{\dot{m}_{\mathrm{fuel,waf}}\, \Delta h_{HHV,fuel,waf}} \quad \text{for } j = H_2,\ CO,\ CH_4,\ C_xH_y. \tag{2-19}$$

The chemical energy in tar species is regarded as not usable and is therefore not considered in η_{CGE}.

To assess the whole process chain for SNG production, a cold gas efficiency, defined as quotient of the chemical energy in the produced SNG and the chemical energy in the utilized fuel, is used:

$$\eta_{CGE,\mathrm{SNG}} = \frac{\dot{m}_{\mathrm{SNG}}\, h_{HHV,SNG}}{\dot{m}_{\mathrm{fuel,waf}}\, h_{HHV,fuel,waf}}. \tag{2-20}$$

To assess the total efficiency of the whole process chain, a more complex definition can be used taking into account process requirements of electrical energy and heat as well as the utilization of potential product heat and power streams:

$$\eta_{\mathrm{tot}} = \frac{\dot{M}_{\mathrm{SNG}}\, \Delta h_{HHV,SNG} + \sum P_{el,out} + \sum Q_{out}}{\dot{M}_{\mathrm{fuel,waf}}\, \Delta h_{HHV,fuel,waf} + \sum P_{el,in} + \sum Q_{in}}. \tag{2-21}$$

Equation (2-21) and (2-20) can be simplified in case that there are no input or output heat streams nor output of electrical power:

$$\eta_{\mathrm{tot,SNG}} = \frac{\dot{m}_{\mathrm{SNG}}\, \Delta h_{\mathrm{HHV,SNG}}}{\dot{m}_{\mathrm{fuel,waf}}\, \Delta h_{\mathrm{HHV,fuel,waf}} + \sum P_{\mathrm{el,in}}}. \tag{2-22}$$

This is the case when the heat demand of the process is satisfied by the process itself e.g. from exothermic reactions, which is very common in gasification processes wherein heat is generated through partial combustion of the fuel. Heat integration can be used to provide needed heat to downstream processes if necessary.

The ratio of the mole concentrations of H_2 and CO is important to assess the suitability of the syngas stoichiometry for synthesis of respective end products. For SNG synthesis $\alpha_{H2,CO}$=3 is preferred, whereas $\alpha_{H2,CO}$ =2 is optimal for a Fischer-Tropsch or methanol synthesis:

$$\alpha_{H2,CO} = \frac{y_{H2}}{y_{CO}} \quad \text{in mol mol}^{-1} \tag{2-23}$$

2.3 Properties of sewage sludge

Sewage sludge is a residue from wastewater treatment that is generated during mechanical, biological and chemical treatment steps. The sludge contains organic and inorganic solids from the wastewater as well as nutrient precipitation agents and their phosphorous salts. The sludge is a pollutant sink in the wastewater treatment process. After its first separation from the wastewater, sewage sludge is typically stabilized, digested for biogas production and mechanically dewatered, i.e. by filter-pressing or centrifugation. The sludge is then sent for treatment or direct disposal.

2.3.1 Organic composition

The organic part of sewage sludge mostly originates from wastewater sediments and bacterial matter from the biological stage of the WWTP but contains also various impurities originating from households, industry and street runoff such as detergents, care products, pharmaceuticals, wood

preservatives, paint and other chemicals. In addition, polymers used as precipitator in the wastewater treatment process can be found. Wet sewage sludge can contain hazardous biologically active compounds such as bacteria, viruses or vermin. It should therefore not be handled without proper safety measures. The biogenic hazard can be reduced if the sludge was heated during the drying step.

The elemental composition ranges of sewage sludge can be found in literature [41–43]. Table 2.2 shows analyses of different sewage sludges from previous projects of the author which are in line with values reported in the above-mentioned references. All analyses in Table 2.2 were performed at IFK's lab. The organic fraction of sewage sludge contains mainly carbon, hydrogen and oxygen, similar to wood or other biomasses. However, high amounts of nitrogen and sulfur are present. Sewage sludge has small concentrations of chlorine. The volatile amount is higher and the fixed carbon lower in comparison to wood. In literature as well as in Table 2.2, it is observed that the concentration of C, H, O as well as Cl on water ash free basis is very similar for different sludges. On the other hand, ash, sulfur and to a lower extent nitrogen contents are varying between different sludges. It can be seen that the composition of the Großbottwar sludge was quite constant in the sampled time from 2013 to 2016.

Table 2.3 shows sewage sludge compositions and heating values from different references on sewage sludge gasification. The sludges originated from various parts of the world. It is noticeable that the ash content varies significantly between different sludge specimens, while the elemental composition and the heating value on water ash free basis has similar values.

The higher heating values presented in Table 2.2 and Table 2.3 are between 18 and 25 MJ kg^{-1} on dry and ash free basis. However, most analyses show values between 21 MJ kg^{-1} and 23 MJ kg^{-1}, which is comparable to wood pellets.

Heat of formation $\Delta h^0_{f,ss,waf}$ was calculated from the elemental analysis and the higher heating value following equation (2-9). Table 2.2 and Table 2.3 show that the heat of formation of the different sludges varies significantly from -4 MJ kg^{-1} to under -10 MJ kg^{-1} which is remarkable since the heat of formation has a huge impact on the energy balance calculation. However, most of the sludges and the wood pellets show a heat of formation between -6 MJ kg^{-1} and -5 MJ kg^{-1}.

Table 2.2: Sewage sludge analyses conducted at IFK's lab, origin of samples: [1]Grade A1 wood pellets Scharr GmbH, [2]sewage sludge drying plant Bioenergie Bottwartal GmbH (sludge mainly from WWTP Marbach), [3]WWTP Büsnau Institute of Sanitary Engineering, Water Quality and Solid Waste Management (ISWA), University of Stuttgart, [4]WWTP Balingen, [5]WWTP Koblenz

			sewage sludge					
	unit	**wood pellets**[1]	**Großbottwar 2013**[2]	**Großbottwar 2014**[2]	**Großbottwar 2016**[2]	**Büsnau 2021**[3]	**Balingen 2021**[4]	**Koblenz 2017**[5]
$\gamma_{ash,wf}$	kg kg^{-1}	0.004	0.489	0.483	0.476	0.402	0.499	0.388
$\gamma_{fc,waf}$	kg kg^{-1}	0.184	0.094	0.081	0.082	0.157	0.088	0.077
$\gamma_{vm,waf}$	kg kg^{-1}	0.816	0.906	0.907	0.912	0.853	0.912	0.923
$\gamma_{C,waf}$	kg kg^{-1}	0.510	0.493	0.524	0.510	0.517	0.507	0.495
$\gamma_{H,waf}$	kg kg^{-1}	0.063	0.092	0.066	0.069	0.068	0.068	0.072
$\gamma_{O,waf}$	kg kg^{-1}	0.425	0.329	0.302	0.321	0.321	0.341	0.340
$\gamma_{N,waf}$	kg kg^{-1}	0.002	0.068	0.077	0.075	0.075	0.064	0.072
$\gamma_{S,waf}$	kg kg^{-1}	0.000	0.016	0.029	0.024	0.018	0.018	0.018
$\gamma_{Cl,waf}$	kg kg^{-1}	0.000	0.002	0.002	0.002	0.002	0.002	0.003
$\Delta h_{HHV,waf}$	MJ kg^{-1}	19.825	21.068	22.021	21.032	21.790	21.132	22.042
$\Delta h_f^0{}_{,waf}$	MJ kg^{-1}	-5.930	-8.391	-4.834	-5.797	-5.048	-5.358	-4.633

Table 2.3: Sewage sludge analyses from different references on sewage sludge gasification

	unit	**Choi et al. 2015 [44]**	**Pinto et al. 2007 [45]**	**André et al. 2016 [15]**	**Calvo et al. 2013 [46]**	**Migliaccio et al. 2021 [47]**		**Niu et al. 2018 [48]**	**Judex et al. 2012 [9]**	**Judex et al. 2012 [9]**
origin		Seoul	Portugal	Madrid	Oakland California	south Italy	south Italy	Zhen-jiang, China	Balingen	Mann-heim
$\gamma_{ash,wf}$	kg kg^{-1}	0.276	0.378	0.417	0.379	0.340	0.270	0.511	0.570	0.395
$\gamma_{fc,waf}$	kg kg^{-1}	0.102	0.114	-	0.114	0.086	0.073	0.119	-	-
$\gamma_{vm,waf}$	kg kg^{-1}	0.898	0.886	-	0.887	0.914	0.927	0.881	-	-
$\gamma_{C,waf}$	kg kg^{-1}	0.556	0.558	0.506	0.583	0.492	0.518	0.497	0.393	0.496
$\gamma_{H,waf}$	kg kg^{-1}	0.073	0.074	0.082	0.072	0.085	0.079	0.086	0.077	0.073
$\gamma_{O,waf}$	kg kg^{-1}	0.293	0.274	0.314	0.237	0.350	0.266	0.309	0.460	0.344
$\gamma_{N,waf}$	kg kg^{-1}	0.079	0.074	0.070	0.090	0.061	0.067	0.087	0.053	0.069
$\gamma_{S,waf}$	kg kg^{-1}	0.018	0.019	0.027	0.018	0.018	0.014	0.018	0.016	0.018
$\gamma_{Cl,waf}$	kg kg^{-1}	-	0.001	-	0.002	0.001	0.056	0.002	-	-
$\Delta h_{HHV,waf}$	MJ kg^{-1}	23.605	23.900	22.470	24.799	17.845	22.527	18.594	19.767	19.835
$\Delta h_f^0{}_{,waf}$	MJ kg^{-1}	-5.241	-5.148	-6.143	-4.836	-10.590	-5.873	-10.231	-4.238	-6.987

2.3.2 Mineral composition

Wastewater sources can be street runoff, residential homes, office buildings, industry facilities, hospitals and others. Therefore, various minerals can be present in wastewater and subsequently in sewage sludge. Typical elements coming from street runoff are silica and calcium originating mainly from dust as well as traces of copper and zinc originating mainly from corrosion of building materials. Further heavy metals like cadmium, lead and mercury usually originate from pipes or industrial processes. Iron and aluminum compounds are added as precipitation agent for phosphorous in the waste water treatment plants and can be found in significant amounts in sewage sludges [43].

Table 2.4 shows analyses of the mineral fraction of different sewage sludges from previous projects of the author. The data is consistent with data from literature [41–43]. According to the data, silica has the highest share in all samples. Phosphorous oxide concentration varies between 0.136 kg kg^{-1} in Balingen sludge and 0.255 kg kg^{-1} in Büsnau sludge. Iron and Aluminum content can also severely vary according to the used phosphorous precipitation agent by the WWTP. The three samples of Großbottwar sludge show considerable differences in aluminum, calcium and iron concentration. With a view to the combustion properties, the potassium content of sewage sludge is also noteworthy, since potassium is known to cause major corrosion in boilers. The potassium oxide contents are between 0.011 kg kg^{-1} and 0.020 kg kg^{-1} for the shown samples. Considering the high ash content of sewage sludge, this means a significant intake of potassium into a boiler and therefore high corrosion potential.

Table 2.4: Composition mineral fraction (ash) of sewage sludge, origin of samples see Table 2.2

	unit	Großbottwar 2013	Großbottwar 2014	Großbottwar 2016	Büsnau 2021	Balingen 2021
γ_{SiO2}		0.348	0.292	0.291	0.162	0.295
γ_{Fe2O3}		0.103	0.183	0.103	0.072	0.169
γ_{P2O5}		0.138	0.148	0.162	0.255	0.136
γ_{CaO}		0.151	0.142	0.223	0.127	0.158
γ_{Al2O3}		0.154	0.110	0.129	0.283	0.165
γ_{SO3}		0.039	0.069	0.045	0.041	0.048
γ_{MgO}	kg kg^{-1}	0.031	0.029	0.028	0.019	0.031
γ_{K2O}		0.020	0.016	0.017	0.011	0.016
γ_{TiO2}		0.007	0.006	0.005	0.005	0.008
γ_{Na2O}		0.005	0.005	0.004	0.005	0.001
γ_{MnO2}		0.003	0.003	0.003	0.001	0.004
γ_{BaO}		0.001	0.001	0.001	0.001	0.001
γ_{SrO}		0.001	0.001	0.001	0.001	0.001

Table 2.5 shows trace elements and impurities of the exemplary sludge samples. It can be seen that the trace element concentrations are varying widely between the different sludges, which is consistent with literature [41–43]. The trace element contents of all samples are slightly below or above the German legal limit for sewage sludge land-use according to the "fertilizer regulation" [49].

Table 2.5: Trace elements in dry sewage sludge, origin of samples see Table 2.2

	unit	Großbottwar 2014	Großbottwar 2016	Büsnau 2021	Balingen 2021	German limit fertilizer [49]
γ_{As}	mg kg^{-1}	1.2	13.8	9.3	4.2	40.0
γ_{Cd}		6.7	1.9	1.0	0.7	4.0
γ_{Cu}		540	496	715	978	900
γ_{Hg}		0.2	0.3	1.2	0.0	1.0
γ_{Ni}		26	26	49	87	80
γ_{Pb}		37	60	23	89	150
γ_{Tl}		n.a.	2.7	0.4	n.a.	1.0
γ_{Zn}		1150	1020	922	2370	4000

2.3.3 Ash sintering, deformation and melting

Melting or sintering of fuel ash can cause bed agglomeration that can ultimately lead to defluidization. Assessment of the ash behavior is thus especially important when a high ash concentration is present in the fluidized bed or if the ash itself is used as bed material as common for sewage sludge gasification. Ash melting behavior analysis of different sewage sludges has been conducted by the IFK laboratory according to DIN EN ISO 21404:2020-06 [50] with wood chips as reference under oxidizing atmosphere (Figure 2.2). Following the standard, the ash melting is assessed by four characteristic temperatures: shrinkage starting temperature (SST), deformation temperature (DT), hemisphere temperature (HT) and the flow temperature (FT). It can be seen that three of the analyzed sludges have an SST of below 1000 °C, whereas the FT lies between 1240 °C and 1340 °C for the analyzed sludges. In contrast, the wood chips have higher SST and HT (DT could not be seen and FT was above the maximum oven temperature of 1500 °C). From these analyses and literature data [51–53], it can be summarized that sewage sludge ash exhibits comparably low sintering and ash melting temperatures. One important mechanism of sintering of sewage sludge ash is described in literature as reaction of hematite with quartz and aluminum silicates [52]. Huang et. al. reported that for sewage sludge ash HT and FT could be lowered by up to 77 K and 80 K, respectively, when switching from oxidizing (air) to reducing atmosphere (CO, H_2) [51].

It can thus be concluded that especially when sewage sludge ash is used as bed material under reducing conditions, special attention needs to be paid to bed agglomeration. Bed temperatures should be kept well below the SST and local hot spots should be avoided. The ash melting behavior shown in Figure 2.2 was analyzed under oxidizing atmosphere, future work should conduct the analyses under reducing atmosphereons to recreate the conditions during gasification.

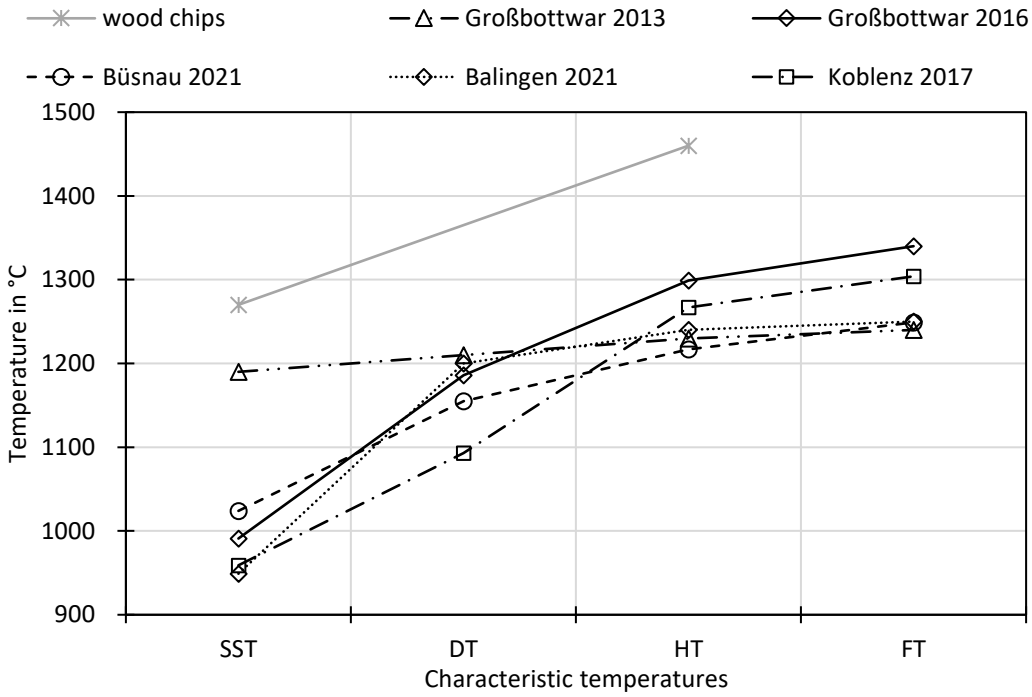

Figure 2.2: Ash melting behavior under oxidizing conditions of different sewage sludge samples and wood chips as reference, origin of samples see Table 2.2, analysis conducted at IFK's laboratory. SST: shrinkage starting temperature, DT: deformation temperature, HT: hemisphere temperature, FT: flow temperature.

2.3.4 Sewage sludge treatment and regulations in Germany

In Germany, $1.8 \cdot 10^6$ t dry sewage sludge is produced per year [54]. Regulations prohibit the landfilling of untreated waste in Germany since 2005, therefore, sewage sludge is not landfilled anymore. A land-use e.g. for utilization as fertilizer is, however, possible in certain cases. The majority (79 % in 2021) of the sludge is currently incinerated in mono-incineration or co-incineration in cement plants or coal-fired power plants [54]. Currently, 22 mono-incineration plants are in operation in Germany treating up to $0.53 \cdot 10^6$ t a^{-1} of dry sewage sludge. Around $0.81 \cdot 10^6$ t a^{-1} dry sludge is co-combusted mainly in cement plants, lignite power plants and waste incinerations. Most of the residual sludge is disposed through land-use. However, the regulation on fertilizer use (DüMV) [49] imposes strict pollutant limits for land-use which cannot be met by all sewage sludges.

The updated sewage sludge regulation (AbfKlär2017) [5] came into effect in 2017. The regulation makes phosphorous recovery mandatory and effectively banns land-use of sewage sludge originating from wastewater treatment plants with a size over 50,000 citizen equivalents from 2029 on. Compulsory phosphorus recovery applies for all sewage sludges with a phosphorus content of more than 20 g phosphorus per kg dry sludge as well as for sewage sludge incineration ashes. Over 50 % of the phosphorous needs to be recovered by the measures. The law also accepts the method of sludge mono-incineration and dedicated deposition of the ash to allow access to the ash for

subsequent phosphorus recovery. However, co-incineration of sludge exceeding 20 g kg^{-1} phosphorous will not be possible any more, since typical co-incineration makes phosphorous recovery impossible due to the dilution of sewage ash with other ashes or materials.

To comply to the updated sewage sludge regulation, waste water treatment plants over 50000 citizen equivalents have from 2029 realistically two options [55]:

1. Reduce the concentration of phosphorous in sewage sludge e.g. value lower than 20 g phosphorus per kg dry sludge. This sludge can then be incinerated e.g. in a cement plant.
2. Apply mono-incineration or mono-gasification of the sewage sludge and subject the ash to P-recovery or deposit the ash in a way that it can be accessed later (e.g. separate dumpsites for sewage sludge ash).

The first option requires major changes in the wastewater treatment process and is therefore not favored by most of the operators. This explains the current trend to mono-treatment plants. The state-of-the-art technology is sewage sludge fluidized bed incineration. However, also gasification plants have been built in Germany. The sewage sludge regulation also encourages the high-value utilization of the sludge, which is a strong motivation to develop the conversion of sewage sludge to high value products.

2.4 State of the art

Fluidized bed gasification of different fossil and biogenic fuels has been studied by several research groups and was applied in commercial plants. Different reactor and process concepts include autothermal gasification in bubbling fluidized beds or circulating fluidized beds as well as dual circulating fluidized beds (indirect gasification) and screw reactors. The most common gasification agent for commercial application is air.

2.4.1 Commercial autothermal fluidized bed sewage sludge gasification

The company KOPF SynGas GmbH & Co. KG offers commercial fluidized bed gasifiers for sewage sludge. Three plants of this type have been built at the sites of wastewater treatment plans. Two of those are currently in operation. Table 2.6 shows the plant location, treatment capacity and operation parameters. The plants operate with air as gasification agent and sewage sludge ash as bed material. The cold gas efficiency can reach up to $\eta_{CGE} = 0.70$ [9]. The syngas is combusted to supply heat for sewage sludge drying or for other purposes or is converted into electrical power and heat via an internal combustion engine CHP.

Table 2.6: Commercial plants of the company KOPF SynGas for air-blown autothermal bubbling fluidized bed sewage sludge gasification using sewage sludge ash as bed material

plant	treatment capacity	operation parameters	comment	operation
Balingen [9, 56]	2000 t a^{-1} dry SS 720 kW th.	ϑ = 850 °C n_{O2} = 0.28 - 0.35 η_{CGE} = 0.66	demonstration plant, syngas combusted to produce heat for sewage sludge drying	since 2002
Mannheim [9, 57]	5000 t a^{-1} dry SS 2.2 MW th.	ϑ = 850 °C - 900 °C n_{O2} = 0.28 - 0.35 η_{CGE} = 0.70	heat production, plant, has been shut down due to a political decision	2011 to 2018
Koblenz [58]	4000 t a^{-1} dry SS 1.8 MW th.	ϑ = 850 °C - 900 °C $n_{O2} \approx 0.3$ η_{CGE} = 0.70	electricity production in gas engine, heat production	since 2021

2.4.2 Research on autothermal fluidized bed sewage sludge gasification

Several references for research on autothermal fluidized bed gasification of sewage sludge were found and summarized in Table 2.7. The main experimental results such as gas composition, gas yield and cold gas efficiency are summarized in Table 2.8. Most studies used air or steam-air as gasification agent. Only one reference was found on steam-oxygen-blown sewage sludge gasification [44] using a 110 mm diameter bubbling fluidized bed at a gasification temperature of 816 °C and n_{O2} of 0.25 mol mol^{-1}. The reported molar gas concentrations calculated to N_2-free basis are shown in

Table 2.8. However, tar concentrations were not measured following CEN/TS 15439:2006 and the research lacks H_2S measurements. The researchers used olivine as bed material and conducted the experiments for up to 30 minutes for each point due to ash accumulation in the fluidized bed. Furthermore, activated carbon and CaO were used in a second fluidized bed stage with promising tar reduction in that publication as well as in another publication by the same research group [59]. The same facility was also used for air-gasification of sewage sludge [60].

In other studies [11, 15, 27], sewage sludge was used in air gasification or steam air gasification, where the main focus was set on the influence of the fuel throughput and different bed materials: dolomite, olivine, alumina. Dolomite was found the most active bed material for tar reduction. Tar concentrations were measured following CEN/TS 15439:2006 and the composition of sewage sludge tar according to ECN tar classes was studied. Since air-steam gasification leads to a significant dilution of the product gas, it is not applicable for synthesis gas production. Anyway, these

studies give a very good understanding of autothermal bubbling fluidized bed gasification of sewage sludge. Several further references are available on sewage sludge air and steam-air gasification. Furthermore, a review paper has recently been published on that subject [61].

It can be summarized that there are many references on fluidized air gasification of sewage sludge, but only one research group did relevant experiments on steam-oxygen gasification. The experiments found in literature used the bed materials sand, olivine, limestone, and dolomite but none used sewage sludge ash as in the commercial gasifiers.

Table 2.7: Autothermal bubbling fluidized bed sewage sludge gasification experimental research (blown by steam-oxygen, steam-air, air)

	experiment description, operation parameters	**operation conditions**	**reactor diameter, fuel feed rate**	**gasification agent, bed material**
Choi et al. 2015 [44]	• steam oxygen gasification • tar measurement by condensation and by GC with gas bag sampling • subsequent reactor with natural catalyst (activated carbon, CaO) was used to achieve tar reduction • gasifier operation <30 min per experimental run	$\vartheta \approx 815°C$ $n_{O2} \approx 0.25$	110 mm, 1.8 kg h^{-1}	steam-oxygen, olivine
Pinto et al. 2007 [45]	• mono- and co-gasification with coal • gas concentration calculated to N_2-free basis although air-steam was used as gasification agent • measurement of H_2S, NH_3 and HCl after gas cooling and condensation • no results for tar concentration	$\vartheta \approx 850$ °C $n_{O2} = 0$ - 0.3	80 mm, 0.3 kg h^{-1}	steam-air, silica sand
Pinto et al. 2008 [62]	• mono- and co-gasification with biomass • gas concentration calculated to N_2-free basis although air-steam was used as gasification agent • NH_3 and HCl concentration measured after gas cooling and condensation for co-gasification • no results for tar concentration	$\vartheta \approx 850$ °C $n_{O2} = 0$ - 0.6	80 mm, 0.3 kg h^{-1}	steam-air, silica sand
André et al. 2012 [63]	• H_2S reduction with dolomite and limestone studied • mono- and co-gasification studied • no permanent gas concentration presented	$\vartheta \approx 850$ °C $n_{O2} \approx 0.2$	80 mm, 0.3 kg h^{-1}	steam-air, olivine
Mun et al. 2012 [60]	• tar measurement by GC with gas bag sampling • subsequent reactor with natural catalyst (activated carbon, zeolite, olivine, dolomite) was used to achieve tar reduction • gasifier operation <30 min per experimental run	$\vartheta \approx 800$ °C $n_{O2} \approx 0.2$	110 mm, 1.8 kg h^{-1}	air

	experiment description, operation parameters	operation conditions	reactor diameter, fuel feed rate	gasification agent, bed material
Pinto et al. 2008 [62]	• mono- and co-gasification with biomass • gas concentration calculated to N_2-free although air was used • measurement of tar, NH_3 and HCl concentration after gas cooling and condensation for co-gasification		80 mm, 0.3 kg h^{-1}	steam-air
Andrés et al. 2011 [27]	• steam-air gasification at ϑ=800°C • air gasification at ϑ=750°C, 800°C, 850°C • additives dolomite, olivine in different feed rates • tar measurement according to CEN/TS 15439:2006	ϑ = 800 °C n_{O2} = 0.3	32 mm, 0.7 kg h^{-1}	steam-air, air, olivine, dolomite
Andrés et al. 2014 [15]	• steam-air gasification at ϑ=800°C • air gasification at ϑ=750°C, 800°C, 850°C • test of dolomite additive • variation of throughput • tar concentration according to CEN/TS 15439:2006	ϑ = 800 °C n_{O2} = 0.2	32 mm, 0.7 kg h^{-1}	steam-air, air, dolomite, sand
Andrés et al. 2016 [11]	• steam-air gasification at ϑ=800°C • air gasification at ϑ=750°C, 800°C, 850°C • tar concentration according to CEN/TS 15439:2006, analysis of tar composition according to ECN classes	ϑ = 750 °C - 850 °C	32 mm, 0.7 kg h^{-1}	steam-air, air, sand, olivine, alumina
Manyà et al. 2005 [64]	• measurement of permanent gases, H_2S • extractive tar sampling • relative low carbon conversion	n_{O2} = 0.25 - 0.36 ϑ = 750 °C - 850 °C	38 mm, 0.3 kg h^{-1}	air, activated alumina
Calvo et al. 2013 [46]	• tar analysis by condensation and methanol scrubbing • alkali vapor measurements	ϑ = 850 °C	73 mm	air, alumina-silicate
Migliaccio et al. 2021 [47]	• experiments with two different sewage sludges, only one experimental run each • SEM EDX analysis of sewage sludge • tar measurement by condensation	ϑ = 850 °C n_{O2} = 0.1 - 0.2	41 mm, 0.1 kg h^{-1}	air-N_2, sand
Niu et al. 2018 [48]	• mono- and co-gasification with straw • bed material variation • GC tar analysis	ϑ = 800°C n_{O2} = 0.3	50 mm	air-oxygen, bauxite, dolomite, olivine

Table 2.8 Operation conditions, gasification performance and syngas composition for steam-oxygen, steam-air and air fluidized bed gasification of sewage sludge from literature

	unit	Choi et al. 2015 [44]	Andrés et al. 2014 [15]	Manya et al. 2005 [64]	Judex et al. 2012 [9]	
					Balingen	Mannheim
gasification agent		steam-oxygen	steam-air	air	air	air
bed material		olivine	sand/olivine	sand	sewage sludge ash	
ϑ	°C	816	800	850	850	870
n_{O2}	-	0.25	0.30	0.25	0.33	0.28
n_{SC}	mol mol^{-1}	0.82	1.23	-	-	-
$S_{gas,C}$	-	0.74	0.45	0.65	-	-
η_{CGE}	-	0.52	0.45	0.42	0.66	0.70
$Y_{tar,SSwaf}$	g kg^{-1}	69.1	5.2	99.0	-	-
$Y_{gas,SSwaf}$	m^3 kg^{-1}	-	2.9	2.1	-	-
$y_{N2,wf}$	m^3 m^{-3}	0.067	0.606	0.649	0.600	0.557
$y_{H2,wf}$	m^3 m^{-3}	0.280	0.111	0.061	0.131	0.131
$y_{CO,wf}$	m^3 m^{-3}	0.193	0.067	0.086	0.081	0.081
$y_{CO2,wf}$	m^3 m^{-3}	0.324	0.137	0.160	0.167	0.130
$y_{CH4,wf}$	m^3 m^{-3}	0.085	0.085	0.027	0.021	0.042
$y_{CxHy,wf}$	m^3 m^{-3}	0.043	0.019	0.028	-	-
$C_{tar,wf}$	g kg^{-1}	4.86	3.40	-	-	-
$y_{NH3,wf}$	10^{-6} m^3 m^{-3}	315	-	-	-	-
$y_{H2S,wf}$		-	-	2.300	-	-
$Y_{gas,wf,N2f,SSwaf}$	m^3 kg^{-1}	-	1.143	0.737	-	-

2.4.3 Research on other sewage sludge gasification processes

There is considerable research on a variety of gasification concepts for sewage sludge. A short and exemplary overview is given in the following. Research on sewage sludge fluidized bed steam gasification – without using oxygen as gasification agent – is available in literature [65–67]. At IFK, preliminary work [68] has been done on dual fluidized bed steam gasification with comparable sewage sludge and using the same gasifier as in this work. However, these experimental studies used additional bed materials such as sand or olivine. In practice the bed material would be replaced by sewage sludge ash due to its high ash content. The complex hydrodynamic operation of a dual fluidized operation may be impaired severely by the inhomogeneous sewage sludge questioning the suitability of DFB processes for sewage sludge gasification. In the experiments of the above-shown references, the process was in all cases not operated long enough to replace original bed material significantly by sewage sludge ash.

Sewage sludge steam oxygen gasification with rotary kilns [69] or screw reactors [70, 71] or supercritical reactors [72] has also been investigated in literature. A commercial fixed bed sewage sludge gasifier is under construction in Australia [73]. Also, there are research endeavors investigating sewage sludge gasification in high temperature fluidized beds or entrained flow reactors with direct phosphorous separation [74, 75]. A demonstration plant for conversion of sewage sludge to methanol was operated at the campus "Schwarze Pumpe" using dried, briquetted sewage sludge in a fixed bed gasifier [76].

These processes cannot be compared directly to the steam-oxygen gasification investigated in this work, since the process conditions, reactor designs and purposes are different.

2.4.4 Research on steam-oxygen gasification of wood and other fuels

The so-called High Temperature Winkler (HTW) fluidized bed gasification of coal with steam and oxygen as gasification agent was developed by BASF around one hundred years ago to produce syngas for chemical production [77]. Meanwhile, syngas production was replaced by other processes such as natural gas reforming. However, there are several further recent references dealing with research and semi-commercial application of steam-oxygen gasification, of which some are mentioned in the following.

A 1000 kW internally circulating bubbling fluidized bed pilot plant was used by [78] to perform steam gasification of almond shells with $n_{O2} = 0.23$. A water free syngas composition of $y_{H2} = 0.30\ m^3\ m^{-3}$, $y_{CO} = 0.30\ m^3\ m^{-3}$, $y_{CO2} = 0.25\ m^3\ m^{-3}$, $y_{CH4} = 0.10\ m^3\ m^{-3}$ and $y_{CxHy} = 0.02\ m^3\ m^{-3}$ was reported as well as impurities of $y_{H2S} = 50 \cdot 10^{-6}\ m^3\ m^{-3}$, $y_{HCl} = 50 \cdot 10^{-6}\ m^3\ m^{-3}$ and $y_{NH3} = 70 \cdot 10^{-6}\ m^3\ m^{-3}$ Also, gravimetric and GC-MS tar concentrations of up to $10\ g\ m^{-3}$ and $18\ g\ m^{-3}$, respectively, were reported referring to water free, STP and N_2-free conditions. Gil et. al. [79] conducted steam-oxygen gasification of wood chips in a silica sand bed in a facility that is comparable in size and setup to the one used in this work. Sebastiani et al. [80] and Chen et al. [81] conducted steam-oxygen gasification of refuse derived fuel in a pilot plant with 0.25 m diameter. The product gas contained considerable higher CH_4 and C_xH_y concentrations than gasification of biomass.

Further references [82, 83] conducted steam-oxygen gasification of wood at ambient pressure and pressures up to 5 bar in a fluidized bed reactor. Increasing pressure enables higher CH_4 yields, which can be beneficial when SNG is the desired synthesis product. However, elevated pressure leads to higher facility investment costs and is not the focus of this work, but can be an option for industrial application. In addition, dolomite was used as bed material in that study and a promising catalytic effect of the bed material on tar cracking was observed. Circulating fluidized bed reactors have also been used in literature: Peat was gasified in a demonstration plant at a pressure of 10 bar [84], wood chips were gasified at 2.5 bar [85] and distillers grain [86] at atmospheric pressure.

It can be summarized that data on steam-oxygen gasification of different fuels is available from research facilities and few demo plants that can be used for comparison with the results of this work. However, fewer data is available than for air gasification or steam gasification.

2.4.5 Synthesis processes

The conversion of synthesis gas to fuels or chemicals is state of the art. Synthesis processes range from alkane production via Fischer-Tropsch-Process over methanation to the synthesis of methanol [87]. The latter can be used as fuel or as basis chemical for various products including plastics. Also, direct synthesis of other plastic monomers is possible from syngas. The most economically and technically feasible synthesis product needs to be chosen for each case.

This work selected a methanation process chain for the production of SNG using the commercially available TREMP™ process by the company Haldor Topsoe. The reasons for this decision are explained in chapter 6. An overview on methanation technology is given in [88]. However, the methanation can be seen as an exemplary case, which can serve as reference to also assess other synthesis routes.

2.4.6 Hydrogen and oxygen provision by electrolysis

The available biomass and biogenic residues are limited. However, the conversion from feedstock to fuels or chemicals via gasification and synthesis has significant conversion losses. These losses manifest mainly in the emission of carbon dioxide. By adding hydrogen, this carbon loss can be reduced or avoided by converting remaining CO_2 to products. Renewable hydrogen can be generated by water electrolysis powered by renewable electricity. There are mainly three electrolysis technologies with different efficiencies [89]: Alkaline electrolyzer with approximately 70 % efficiency, polymer electrolyte membrane (PEM) electrolyzers with 80 % and solid oxide electrolyzers (SOEC) with over 90 % efficiency, all on LHV basis. While alkaline and PEM electrolyzers operate at temperatures of around 100 °C, SOEC electrolyzers can operate up to 850 °C. On the other side, SOECs are less load-flexible since thermal stress to the cells needs to be limited. SOEC is well suited for integration with a high-temperature process that operates without significant load changes, like a gasification process. Further information on SOECs is provided by the leading manufacturer Sunfire GmbH [90, 91]. Besides hydrogen, electrolysis produces oxygen that can be used as gasification agent.

There are references that studied the implementation of SOEC into a biomass to SNG conversion chain [92, 93] as discussed below.

2.4.7 Gasifier modelling and simulation

This section gives a short and exemplary summary on practical approaches for modeling of fluidized bed gasification that can be used for process simulation.

A one-dimensional 2-phase hydrodynamic and kinetic model has previously been developed by Beirow and the author of this thesis [94–96] to simulate sorption enhanced gasification. This model was adapted for steam-oxygen gasification of wood in the master thesis of Kertthong [97] supervised by the author of this work. The simulation used the geometry of the 20 kW bubbling fluidized bed gasifier used in the experiments of this thesis. The model showed a sufficient accuracy compared to experimental data for the main product gases H_2, CO, CO_2, CH_4 and H_2O. However, it was difficult to achieve accurate prediction of highly residence time-dependent values such as tar and char yields using kinetics from literature, which led to the conclusion that the model needs further development, e.g. in form of dedicated char and tar conversion kinetics for steam-oxygen gasification.

A one-dimensional 2-phase model for steam-oxygen gasification of refuse derived fuel (RDF) was published in 2021 [80]. Dedicated thermo-gravimetric analyses of the considered RDF were used to augment the pyrolysis model. Benzene (C_6H_6) and naphthalene ($C_{10}H_8$) were used as tar model species. The simulations were compared with experiments from a pilot plant with 0.25 m diameter. The match between simulation and experiment was good for the main product gases, tar and char. However, only few experimental points were available for comparison.

A review study describes modelling approaches for gasification in the software environment Aspen Plus® [98]. The study points out that thermodynamic equilibrium by the Aspen Plus® built-in "RGibbs"-reactor is part of many modeling approaches. The equilibrium allows to describe the formation of the main product gases well. However, the equilibrium approach is usually complemented by empirical yields for certain products that are provided by literature or dedicated experiments. Furthermore, some models use a temperature restriction of the whole equilibrium or of certain reactions.

Andrés et al. developed an Aspen Plus® model for sewage sludge air and steam-air gasification using a hybrid equilibrium and empirical approach [99]. This comparably simple model allowed fairly accurate description of the gas composition. However, the model had difficulties in describing the carbon conversion accurately, which was attributed to the lack of modeling of char and tar formation. Furthermore, impurity formation was not discussed in detail in the publication. The model was used for comparison with experimental values for different operation parameters, but not to predict application-relevant adiabatic gasifier operation. This reference shows the potential of the hybrid equilibrium and empirical approach for sewage sludge gasifier modeling.

Brachi et al. conducted process simulation with Aspen Plus® for a comprehensive process chain comprising an air-blown fluidized bed gasification of sewage sludge and an internal combustion engine converting the product gas to power and heat [100]. A hybrid equilibrium and empirical

approach is used to model the gasifier which is implemented by the so-called "restricted equilibrium" function. The model described sewage sludge gasification accurately, as comparison with experimental values showed. The study presents variations of n_{O2} and ϑ without sufficiently discussing operation parameters for realistic gasifier operation (e.g. pre-heating of gasification agent, needed n_{O2} for specific ϑ under autothermal conditions). A similar model was used for another study with comparable performance [101].

2.4.8 Process integration of sewage sludge gasification and drying

Brachi et al. studied a comprehensive process chain including air gasification of sewage sludge, power generation from the resulting product gas in an internal combustion engine (ICE) as well as heat integration for sludge drying [83]. The study concludes that around 35 % of the required heat for sludge drying can be supplied from syngas cooling, while another 55 % can be supplied from off-heat of the ICE and the residual 10 % need to be supplied from additional methane (e.g. natural gas or digestion gas).

Another study conducted Aspen Plus® simulations on sewage sludge gasification with syngas conversion to electric energy. It was concluded that 50 % - 57 % of drying heat can be supplied by heat integration [101].

Lumley conducted a process simulation for sewage sludge fixed-bed air gasification with subsequent conversion of the product gas to power in an ICE [102] and calculated a total conversion efficiency of 17 % from sewage sludge lower heating value to electrical energy. Furthermore, the study calculated that the required heat for sludge drying could be almost completely delivered by heat integration from syngas cooling and ICE off-heat. However, the study assumed a dryer efficiency of 100 %, which is considered unrealistic by the author of this thesis since dryer manufacturers specify drier efficiencies between 60 % and 82 %, dependent on the dryer type and temperature [103].

It needs to be noted that much more heat is made available for process chains that aim for the conversion of the syngas to power, e.g. in an ICE, since power production has a comparable low efficiency. A significant fraction of the conversion losses is recoverable as heat for drying. This contrasts with SNG production where the higher conversion efficiencies limit the available excess heat. Since no data was found in literature on heat integration for SNG production from sewage sludge with atmospheric steam-oxygen gasification, a study thereof was conducted by the author and is presented in chapter 6.

2.4.9 SNG production from sewage sludge and biomass

The GoBiGas 20 MW SNG demonstration plant produced SNG from wood pellets by DFB steam gasification and methanation. Cold gas efficiencies of around 65% from wood to SNG were found.

Simulations calculated potentials for increased efficiency through optimization of some of the Go-BiGas' process steps [104].

Another reference studied SNG production using a syngas composition from sewage sludge DFB steam gasification experiments [105]. It was found that 35 % of the carbon from sewage sludge could be converted to SNG. The study fails to include N_2 formed from fuel bound N in the prediction of SNG composition. Also, no heat integration has been studied.

The Res2CNG project simulated the conversion of wood and mixtures of wood, straw and sewage sludge to SNG through a process chain consisting of a pressurized steam-oxygen gasification, a pressurized SOEC and a pressurized methanation [93]. Furthermore, a reference case with atmospheric gasification of wood and electrolysis was studied. The electrolysis was operated to accommodate the H_2 requirement for maximized carbon to CH_4 conversion. High total conversion efficiencies from fuel and electrical power to SNG of 75 % to 80 % were calculated for the pressurized case. The atmospheric case had an efficiency of 65 %. The study showed that the combination of SOEC, steam-oxygen gasification and methanation is a promising concept.

Process simulations were conducted for conversion of municipal solid waste to SNG via steam-oxygen gasification including water electrolysis [92]. Two operation modes of the electrolysis were studied: 1) the electrolysis load was matched to generate the required oxygen for gasification and 2) the electrolysis load was matched to produce sufficient hydrogen for complete syngas methanation. The calculated efficiencies of the two cases were 68 % and 63 %, respectively. The required electrical energy based on the higher heating value of the fuel was 0.36 J J^{-1} and 1.90 J J^{-1}, respectively.

Another numeric analysis of steam-oxygen fixed bed downdraft gasification of mixtures of biomass and sewage sludge coupled with SNG production is available in literature [106]. A four-bed fixed bed methanation was considered. A methane yield of 0.2 kg kg^{-1} based on the biomass feed was found.

2.4.10 Discussion and conclusions state-of-the-art

The results of commercial or experimental operation of sewage sludge fluidized bed gasifiers found in literature can be summarized as following:

- Fluidized bed gasification of sewage sludge with air as gasification agent and sewage sludge ash as bed material as well as limestone as additive for tar and sulfur reduction is already applied commercially to produce heat and power. However, air gasification produces a syngas with high N_2-concentration that is not suitable as feedstock for fuel or chemical synthesis.

- Steam-oxygen gasification of e.g. wood, peat and coal has already been accomplished in pilot scale and produces high-quality syngas suitable for fuel or chemical synthesis.
- Only one research group conducted steam-oxygen gasification of sewage sludge in a laboratory bubbling fluidized bed using olivine as well as dolomite as bed material. The focus of this study was on downstream gas treatment and not on optimizing the gasification step.

Since the goal of this work is to investigate the production of syngas for fuels or chemical synthesis rather than heat and power, a N_2-free syngas needs to be produced. The-state-of-the art shows that steam-oxygen gasification is a suitable technology for that. Whereas it was successfully applied for other fuels like wood up to semi-commercial scale, scarce data is available for sewage sludge. However, to build demonstration plants or commercial plants, a comprehensive understanding of steam-oxygen gasification of sewage sludge is needed. Since there are several degrees of freedom in choosing the operation conditions, insight in the effect of different operation parameters on the gasification performance is needed for process design. In addition, such experiments should be carried out under conditions relevant for industrial application, such as using sewage sludge ash as bed material and limestone as additive. In addition, experimental points should be held as long as possible to get close to steady state conditions. Since this is important for designing downstream gas cleaning equipment, the impurities (e.g. H_2S, COS, NH_3, tar) present in the raw syngas need to be measured. Therefore, the experimental part of this thesis strives to fill this gap.

There are several references for gasifier and process simulations for sewage sludge and other fuels. Simple gasifier models are considered suitable for process simulation by many authors, since they can be implemented easily in process simulation tools like Aspen Plus®. Some references studied the integration of sewage sludge gasification and subsequent power production with sludge drying. Other studies investigated SNG production from sewage sludge derived syngas, however not for atmospheric steam-oxygen fluidized bed gasification. Two references studied the integration of electrolysis with steam-oxygen gasification. The results of these studies provide a frame for this work and can be used for result comparison.

Currently, there is no study for assessing an integrated process chain for SNG production from sewage sludge using atmospheric steam-oxygen gasification, which is another research gap to be closed by this work. Furthermore, this work has the goal of conducting a realistic assessment of the overall conversion efficiency under optimized operation conditions by applying realistic heat integration and including sludge drying which is very important in the context of sewage sludge conversion. Also, the integration of an electrolysis has been put into focus, since promising results were found in literature thereon.

3 Materials and experimental methods

3.1 Fuel and bed materials

The sewage sludge used in this work originated mainly from the municipal wastewater treatment plant Häldenmühle in Marbach am Neckar in south-west Germany. A minor fraction of the sludge (less than 0.2 kg kg^{-1}) came from the municipal wastewater treatment plants "Beilstein" and "Oberes Bottwartal " that are also located in south-west Germany. Those treatment plants delivered their sludge to the drying facility of Bioenergie Bottwartal GmbH & Co. KG, located in the community Großbottwar, where the sludge was dried thermally with hot flue gases from a biogas CHP. The dried sludge was collected in September 2016 from Großbottwar and is therefore in this thesis called "Großbottwar 2016". After drying, the fuel had nominal particle sizes of 5-15 mm. To suit the used experimental facility, the dried sewage sludge was crushed with a beater mill using a 2 mm sieve. Table 3.1 shows the proximate and elemental analysis. The sludge has, compared to wood, high N, S and Cl contents. The ash sums up to almost half of the fuel's dry mass; therefore, the ash itself was used as bed material. The composition of the Großbottwar sewage sludge's organic fraction lies within the ranges reported by literature [41] and different samples from 2013, 2014 and 2017 show comparable composition. Section 2.3 presents a comparison of different sewage sludges.

Limestone without pre-calcination was used as bed additive for some experiments. The calcination took place in the gasifier releasing CO_2. The limestone with origin Messinghausen in Germany was obtained from LHOIST Germany Rheinkalk GmbH. The limestone was delivered as sieve fraction 0.3 mm - 0.7 mm.

Table 3.3 and Figure 3.1 show the particle size distribution of the sewage sludge, and raw limestone as used as well as sewage sludge ash and calcined limestone. The dried sewage sludge had a wide particle size range with $d_{p,50}$ = 1010 µm. During gasification, the sewage sludge particles form sewage sludge ash, the bed material, which has a smaller particle size with $d_{p,50}$ = 520 µm. The used limestone had in its raw state a mean particle size of $d_{p,50}$ = 650 µm. During its residence time in the gasifier the limestone particle size is reduced due to calcination and abrasion. Limestone that was calcined in the 20 kW facility has a mean particle size of $d_{p,50}$ = 370 µm and is thus finer than the sewage sludge ash.

Table 3.2 shows the mineral composition of sewage sludge and limestone. The major elements of sewage sludge are Si, Ca, P, Al and Fe. Heavy metal concentrations in the dry sewage sludge are

presented in Table 4.4. As discussed in section 2.3.2, the mineral composition of this sewage sludge lies in a typical range. Silica and calcium have the highest share in the sewage sludge ash. It is evident from the high iron and alumina content in the analysis that the wastewater treatment plant used iron- and alumina-based phosphorous precipitators. Ash compounds are known to take part in the gasification or combustion process. The high calcium content may lead to self-desulfurization by reaction with gaseous H_2S and COS. The used limestone consists almost only of $CaCO_3$.

Additionally, the BET specific surface area is shown in Table 3.3. It can be seen that the limestone's surface is enhanced during calcination, but still has a comparable low BET surface area.

Table 3.1: Sewage sludge proximate and elemental analysis; au: as used, waf: dry ash free, wf: water free, fc: fixed carbon, vm: volatile matter

proximate analysis				**elemental analysis**						**heating value**		**heat of formation**
y_{H2O}	y_{ash}	y_{fc}	y_{vm}	y_C	y_H	y_O	y_N	y_S	y_{Cl}	Δh_{LHV}	Δh_{HHV}	Δh^0_f
in kg kg^{-1}										in MJ kg^{-1}		
au	wf	waf	waf	waf	waf	waf	waf	waf	waf	waf	waf	waf
0.065	0.476	0.082	0.918	0.510	0.069	0.320	0.075	0.024	0.002	19.523	21.032	5.797

Table 3.2: Mineral composition of sewage sludge ash and limestone

	y_{Al2O3}	y_{CaO}	y_{Fe2O3}	y_{K2O}	y_{MgO}	y_{Na2O}	y_{P2O5}	y_{SO3}	y_{SiO2}	y_{CO2}
	in kg kg^{-1}									
sewage sludge ash	0.129	0.223	0.103	0.017	0.028	0.004	0.162	0.045	0.292	-
limestone	0.001	0.526	0.001	-	0.009	0.001	-	-	0.057	0.405

Table 3.3: Particle sizes, particle density, bulk density and BET surface area of fuel and bed materials

	$d_{p,10}$	$d_{p,50}$	$d_{p,90}$	**BET**	ϱ	ϱ_{bulk}
	in µm			in m^2 g^{-1}	in kg/m^3	
sewage sludge	200	1010	2100	-	1830	810
sewage sludge bed ash	170	520	1700	10.90	2740	820
limestone	300	650	1200	0.26	2710	1513
calcined limestone	165	370	640	8.77	2450	837

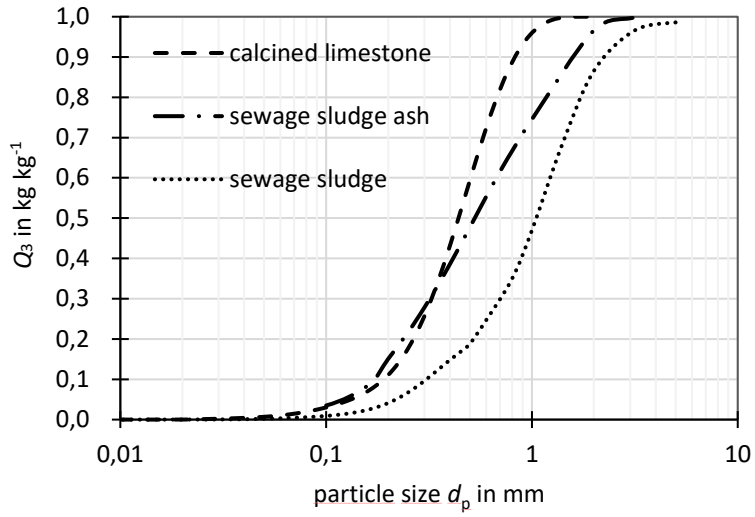

Figure 3.1: Particle size distributions of fuel (sewage sludge), bed material (sewage sludge ash), and limestone after calcination

3.2 Experimental facility

This thesis' experiments were conducted in a 20 kW fuel input fluidized bed facility, which is shown schematically in Figure 3.2. The bubbling fluidized bed reactor is 3.5 m high and has an internal cylindrical cross-section with a diameter of 0.15 m in the gasification zone and 0.2 m in the freeboard above. The reactor wall is made of a high-temperature steel. Electrical heating shells, surrounding the reactor pipe, allow control of the temperature inside the gasifier. The facility is equipped with several thermocouples and pressure transducers at different heights. The gas distributor consists of eight bubble cap nozzles at the bottom of the bed. Preheated steam with a temperature of around 500 °C is injected through six of the nozzles, while oxygen is introduced through two of the nozzles. To prevent overheating of the oxygen nozzles, nitrogen was added to the oxygen stream lowering the oxygen concentration to $y_{O2,nozzle} = 0.75$ m^3 m^{-3}. A gravimetric double screw doser is used to provide a constant mass flow of dried sewage sludge that is introduced into the lower part of the fluidized bed by another screw feeder. The limestone additive is dosed with an additional gravimetric single screw doser through a port slightly above the bed. N_2-purge through both dosing systems is required to prevent backflow of product gas through the dosing systems. Thus, the product gas was in sum (purging of nozzles and solids dosers) diluted with around 0.3 m³ m^{-3} nitrogen. Due to the high ash content in the sewage sludge, the ash itself is used as bed material. Ash is removed during operation by an overflow port to maintain a constant bed height of 0.45 m above the gas distributor. After the gasifier, particles are separated from the product gas by two cyclones and a candle filter, which are heated to 400 °C to prevent tar condensation. The syngas passes a pressure control valve that regulates the pressure to approximately 10 mbar overpressure after the candle filter to avoid false air ingress. The syngas is finally combusted in a flare.

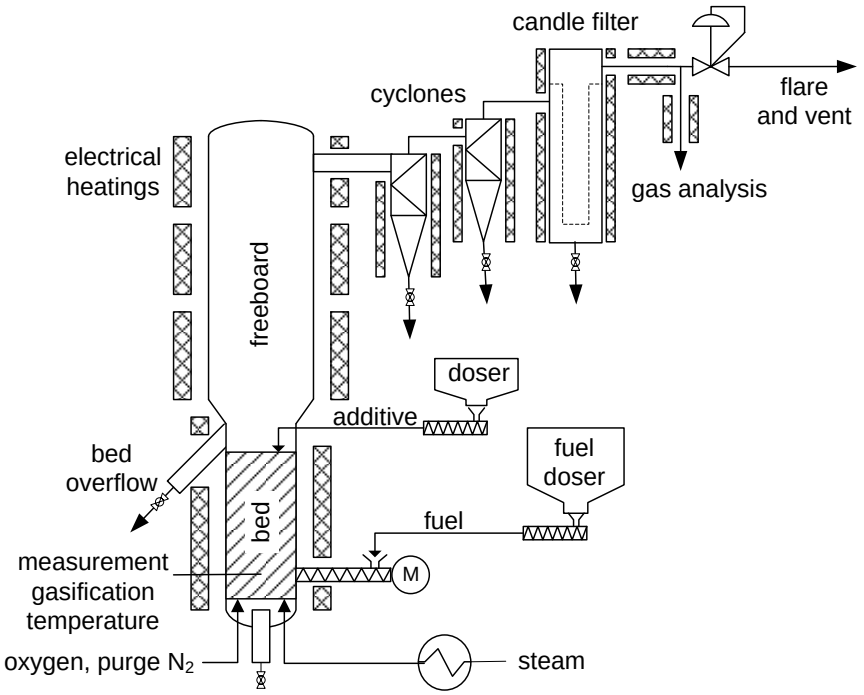

Figure 3.2: 20 kW fluidized bed gasifier at IFK University of Stuttgart utilized for all experiments of this work, total gasifier height 3.5 m, fluidized bed diameter 0.15 m, freeboard diameter 0.2 m, height of overflow over gas distributor 0.45 m

3.3 Experimental procedure

Prior to the experiments, the gasifier was heated to the desired bed temperature with around 7 kg of bed material, consisting of sewage sludge ash. The flows of sewage sludge, steam and oxygen were adjusted according to the desired experimental parameters. When the temperature and gas concentrations were steady, the experimental point commenced. Each experimental point was held in steady state conditions for at least 30 minutes, but for most points over 60 minutes, and mean values were calculated from the continuously recorded data. The tar and NH_3 measurements with durations of 20 minutes each were conducted during steady state operation conditions. For the experiments with limestone as bed additive, a respective batch of limestone was added at least 1 h prior to the start of the experimental point to set up the desired fraction of CaO in the bed. After that, a continuous dosing of limestone with the respective additive ratio n_{CaCO3} (mass limestone per mass of sewage sludge as used) was started. Ash was drained continuously through the overflow.

3.4 Analysis methods

The mass flows of all inlet streams were continuously recorded. For O_2 and purge-N_2, this was achieved with automatic mass flow controllers. For sewage sludge and limestone dosing, the mass

flow signal from the gravimetric screw dosers was logged. The mass of the reservoir for feed water was also continuously logged to calculate the steam mass flow.

Slipstreams of the product gas were extracted through sample lines for gas measurements after the facility's candle filter. H_2, CO, CO_2 and CH_4 were measured continuously in a combined NDIR and thermal conductivity gas analyzer (ABB AO2020), whereas hydrocarbons from C_2 to C_4 (C_xH_y), H_2S and COS were analyzed semi-continuously (every 3 minutes) with a Varian CP-4900 Micro-GC. The measurement gas for these devices went from the gasifier through a heated filter and a heated hose (both 180 °C) directly into a series of 4 chilled impingers (-15 °C), wherein the gas passes through an equal mixture of isopropanol and a 0.3 kg kg^{-1} $H_2SO_{4(aq)}$-solution for tar removal. Afterwards, the gas went through an impinger with a 0.15 kg kg^{-1} $H_2SO_{4(aq)}$-solution at ambient temperature to capture evaporated isopropanol. By these means, tar species are removed to prevent damage to the analytical equipment, but due to the low *p*H value of the solution, H_2S and COS remain in the gas.

The second sample line was used for wet chemical NH_3 measurement according to a modified VDI 3838 [107] guideline: Syngas was sampled over 20 minutes and fed through two impinger bottles to absorb the gaseous ammonia in a 1 mol l^{-1} H_2SO_4-solution. For tar and humidity removal, an isopropanol impinger bottle was arranged before the absorption solution. To avoid NH_3 loss in the isopropanol bottle, the *p*H value was increased by adding NaOH. In total around 50 l (STP) syngas was fed through the setup for each measurement. The liquid samples were analyzed with UV/Vis spectroscopy (Thermo Scientific Genesys 180).

The third sample line was used for tar measurement and is equipped with a heated filter followed by a heated hose maintained at 350 °C. Tar species were measured by extractive sampling and analysis according to the tar protocol CEN/TS 15439 [25]. For this, a quantified volume of the product gas was directed through cooled isopropanol wash bottles, wherein the tar species are dissolved and condensed. The collected isopropanol-tar samples were analyzed by two methods:

1) During *gravimetric analysis*, isopropanol is evaporated from the sample, and the mass of the solvent-free tar residue is used to derive the gravimetric tar concentration. The evaporation procedure was conducted according to CEN/TS 15439 [25]: A rotary evaporator is used with the water bath set to 55 °C. The pressure was ramped down to 100 mbar absolute pressure over a duration of 15 minutes and kept constant at 100 mbar for another 15 minutes. Subsequently, 20 ml of ethanol was added to the sample and the evaporation procedure is repeated. Afterward, the flask was purged with N_2 for 30 minutes at 350 mbar absolute pressure. According to [108], the gravimetric tar concentration includes all tar species with a molar mass over approximately 180 g mol^{-1} (phenanthrene), in the following referred to as "heavy" tar. The detectability of tar species by gravimetric analysis decreases with decreasing molar mass. Tar species with low molar mass, in the

following referred to as "light" tar species, such as benzene, toluene and xylene (BTX), are not detected or only to a small extent by gravimetric analysis. The gravimetric tar concentration is particularly important to assess the amount of tar species with high boiling temperatures that may condense easily on cold facility parts (e.g. gas coolers, valves) and can cause blockage and operation failure. As a novel method, elemental analysis of C, H, N, S, and Cl of the gravimetric tar was conducted to assess its composition.

2) With *gas chromatography (GC) analysis* of the isopropanol-tar sample, actual tar components can be individually identified and quantified. Especially "light" species can be detected very well. These species remain partially present in the gas after cooling, condensation and possibly after gas washing and thus have to be considered for downstream equipment. On the contrary, heavy tar species can only be detected up to a certain molar mass with GC, in this work this was pyrene with 202 g mol^{-1}. For sewage sludge gasification, tar species containing S, N – so-called heterocyclic species - were expected and thus evaluated.

Tar species screening was done by Paul-Scherrer-Institute (PSI) with the following equipment and specifications: HP 6890 gas chromatograph coupled with an HP 5973 mass spectrometer, software HP MSD ChemStation E02.02.1431, column Restek Rxi-17Sil MS Cap (L = 60 m, d = 0.25 mm), temperature program: 5 min at 65 °C, heating rate 15 K min^{-1} to 325 °C, hold 20 min at 325 °C, carrier gas He. This GC was also used coupled with a FID and SCD detector to quantify nitrogen- and sulfur-containing tar species.

Quantification of all other tar species was conducted with GC-FID by the institute of energy and process engineering of FAU (Friedrich Alexander Universität Erlangen-Nuremberg) with the following equipment and specifications: Agilent GC 7890A, column CP Sil 8 CB (L = 25 m, d = 0.25 mm), temperature program: 3 min at 40 °C, heating rate 4.7 K min^{-1} to 300 °C [109].

For simplification, the ECN tar species groups are used [26]. In this work, benzene is considered a tar component despite the fact that it is not named as tar in most literature [108]. Benzene, ECN2 and ENC3 are in the following considered as "light" tar species, whereas ECN4, ECN5 and gravimetric tar are considered as "heavy" tar species.

Elemental and heating value analysis of fuel and gravimetric tar residues were conducted by a CHN analyzer (LECO 628) and combustion in a bomb calorimeter with wet sampling and ion-chromatography of S and Cl. Inorganic elemental analysis of sewage sludge ash and limestone was done using acid digestion with subsequent ICP-MS analysis. Particle size distributions were measured by sieve analysis and with a laser diffraction particle size analyzer (Malvern Mastersizer 3000).

3.5 Equilibrium calculation with FactSage®

The thermochemical equilibrium can be used to calculate the theoretical optimum of the H_2S and COS capture by reaction with CaO during gasification [18, 35, 35]. With the data from Table 3.1 and Table 3.2, the molar ratio of calcium and sulfur, $n_{Ca,S}$, fed into the gasifier by the sewage sludge can be calculated according to equation (2-5). It can be seen that the sewage sludge already has enough CaO in its ash to capture all of the sludge's sulfur. However, sulfur capture can only occur until the equilibrium concentration of H_2S and COS is reached in the syngas. Since also H_2O and CO_2 are part of the relevant chemical reactions (R 11 - R 13) for desulfurization, the total syngas atmosphere influences the equilibrium concentrations of H_2S and COS. Hence, equilibrium calculations of the whole gasification process needed to be performed.

For this, the software FactSage® 7.3, described in [110], with the database FactPS® (pure substances) was used. FactSage's numerical solver then calculated the product composition where the Gibbs energy is at its minimum – the thermodynamic equilibrium:

$$\Delta G_R \overset{!}{=} 0. \tag{3-1}$$

The input masses of fuel, gasification agent and if applicable, limestone additive were entered into the FactSage® solver. The gasification temperature was set. All calculations were done for ambient pressure of 1 bar. FactSage® then returned the equilibrium product masses including the permanent gases like H_2, CO, CO_2 as well as H_2S and COS. From this result, the equilibrium concentrations of H_2S and COS were calculated as volume fraction based on the water free syngas.

4 Experimental results and discussion

This chapter presents the results of experiments investigating the influence of operation parameters on sewage sludge steam-oxygen gasification in a 20 kW fluidized bed facility. The shown data is published by this author in [19, 20]. For reference and comparison, also gasification of wood pellets and wheat straw pellets was conducted with comparable operation conditions. These results are not included in this thesis but are published in [10].

The operation conditions for the experimental runs are summarized in Table 4.1. The parameters n_{O2}, n_{SC}, ϑ, n_{WHSV} and n_{CaCO3} were varied and the runs are labeled according to the respective parameter variation (e.g. O1…O4 for the points of n_{O2}-variation). All other operation parameters were kept as constant as possible at a reference value while one parameter was varied. Most experimental points resembled steady states of over one hour. Only for few points, shorter steady state durations of around 30 minutes were evaluated.

First, this section discusses the effect of operation parameter variation on the syngas, namely permanent gas yields and concentrations, tar species concentrations, H_2S and COS concentrations as well as NH_3 concentrations. Furthermore, the generated amount and composition of bed ash and fly ash is shown. The chapter closes with a carbon balance of steam-oxygen gasification of sewage sludge and a field report on the behavior of the sewage sludge ash as bed material.

Table 4.1: List of all experimental points of this thesis with respective operation conditions

variation	run	ϑ	n_{SC}	n_{O2}	n_{WHSV}	$\dot{m}_{fuel}$	m_{bed}	n_{CaCO3}	u_0	$u_0\ u_{mf}^{-1}$
		°C	mol mol^{-1}	mol mol^{-1}	h^{-1}	kg h^{-1}	kg	kg kg^{-1}	m s^{-1}	-
n_{O2}	O1	848	1.03	0.20	0.49	7.2	6.1	0	0.34	4.5
	O2/ref	842	1.05	0.25	0.44	7.1	7.8	0	0.36	4.7
	O3	842	1.01	0.27	0.41	7.2	7.6	0	0.36	4.8
	O4	852	1.04	0.28	0.49	7.2	7.2	0	0.37	5.0
n_{SC}	S1	852	0.59	0.24	0.52	11.3	7.4	0	0.37	5.0
	S2/ref	842	1.05	0.25	0.44	7.1	7.8	0	0.36	4.7
	S3	839	1.48	0.25	0.43	7.2	8.2	0	0.47	6.3
	S4	849	1.98	0.26	0.54	7.0	6.8	0	0.60	8.0
ϑ	ϑ1	659	1.03	0.26	0.54	7.0	6.8	0	0.29	3.9
	ϑ2	778	0.97	0.26	0.53	7.1	7.1	0	0.32	4.2
	ϑ3/ref	842	1.05	0.25	0.47	7.1	7.8	0	0.36	4.7
	ϑ4	894	1.03	0.25	0.50	7.0	7.3	0	0.37	4.9
ϑ with $CaCO_3$ additive	ϑCa1	655	1.01	0.25	0.48	6.9	5.8	0.25	0.28	3.8
	ϑCa2	708	1.04	0.26	0.26	6.9	7.6	0.25	0.31	4.1
	ϑCa3	770	1.06	0.26	0.29	6.8	7.4	0.25	0.33	4.3
	ϑCa4	798	1.12	0.28	0.40	6.4	7.9	0.25	0.33	4.5
	ϑCa5	844	1.08	0.27	0.38	6.6	8.4	0.25	0.35	4.6
	ϑCa6	897	1.26	0.26	0.48	7.0	7.1	0.25	0.43	5.7
n_{WHSV}	W1	848	1.21	0.25	0.27	7.2	12.9	0	0.41	5.4
	W2/ref	842	1.05	0.25	0.44	7.1	7.8	0	0.36	4.7
	W3	829	1.02	0.26	0.71	13.6	9.4	0	0.67	9.0
	W4	849	0.99	0.26	1.19	7.0	2.9	0	0.34	4.5
	W5	846	0.95	0.26	1.29	13.9	5.3	0	0.65	8.7
n_{CaCO3}	C1/ref	842	1.05	0.25	0.44	7.1	7.8	0	0.36	4.7
	C2	850	1.09	0.26	0.47	6.7	7.0	0.06	0.33	4.44
	C3	847	1.05	0.25	0.48	7.1	7.2	0.13	0.33	4.46
	C4	856	0.00	0.25	0.42	7.1	8.3	0.18	0.34	4.50

4.1.1 Variation of oxygen ratio n_{O2}

Figure 4.1 shows the influence of the oxygen ratio n_{O2} on the permanent gases at constant temperature ϑ. With increasing oxygen ratio, the H_2 concentration decreased and the CO_2 and H_2O concentrations increased. In addition, a slight decrease in CO was observed. This reflects the increased combustion of H_2 and CO to H_2O and CO_2, respectively, due to the higher oxygen supply. The CH_4 and C_yH_y concentrations were not influenced by the oxygen ratio in the investigated range. The gas yield is slightly increasing with rising n_{O2}.

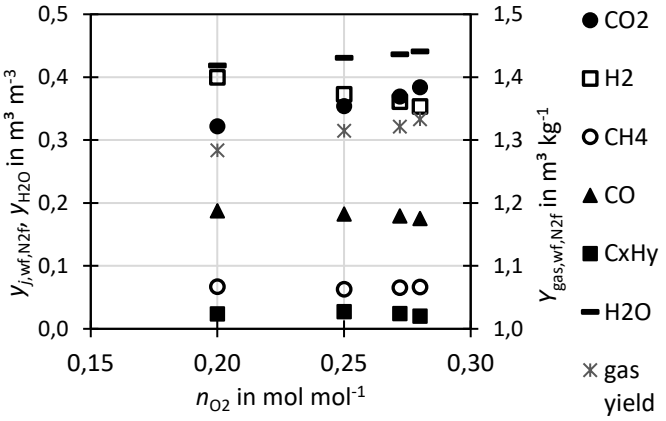

Figure 4.1: Permanent gas concentrations on water and N_2-free basis, H_2O concentration on N_2-free basis, as well as permanent gas yield per water and ash free sewage sludge for different n_{O2}

A comparison with experimental results from literature was conducted. In most experiments found in literature, also other parameters such as temperature were changed when different n_{O2} were investigated; therefore it is difficult to compare the trends [44, 79, 111, 112]. However, some studies also used electrically heated facilities to maintain constant temperature during n_{O2} variation. One study varied n_{O2} for steam-air co-gasification of sewage sludge and straw pellets, and similar trends to this study were reported [78]; experiments were also conducted at even higher n_{O2} of up to 0.58, while the trends in gas concentrations remained. Comparable trends were also reported for air gasification of sewage sludge in a laboratory bubbling fluidized bed [64]. For coal gasification in a steam-oxygen blown slightly pressurized spouting bed at 940 °C [113], n_{O2} variation also showed increasing CO_2 concentration whereas H_2 and CO were increasing until n_{O2}=0.35 but then decreased with increasing n_{O2}. The cited study connects this to increasing gas yield and carbon conversion up to n_{O2} = 0.35. Overall, the results of this thesis are in good agreement with literature.

4.1.2 Variation of temperature ϑ

Figure 4.2 shows the influence of the gasification temperature ϑ on the permanent gases for a constant n_{O2}. It was aimed to investigate temperatures from 650 °C to 900 °C, however, the most

relevant temperature range for industrial application is between 800 °C and 900 °C. The electrical heating of the facility enabled a uniform temperature profile over the reactor height.

With increasing temperature, the gas yield increased due to higher carbon conversion to permanent gases, as can also be seen in the decreased tar concentration in the syngas (see section 4.2.4) and carbon content of the bed material and the fly ash (see section 4.5).

Regarding the syngas composition, the H_2 and CO concentration increased and the CO_2 and H_2O concentration decreased with increasing temperature. The enhanced formation of H_2 and CO can be attributed to the enhanced fuel conversion. The reduced steam concentration is attributed to conversion of steam through gasification reactions into H_2 and CO, but also to a dilution effect, since the permanent gas yield is enhanced with temperature. The decreasing CO_2 concentrations are caused by dilution due to enhanced H_2 and CO formation as well as the water-gas shift equilibrium that is moving away from CO_2-production for rising temperatures. The temperature variation exhibited little change and no specific trend for CH_4 and C_xH_y concentrations.

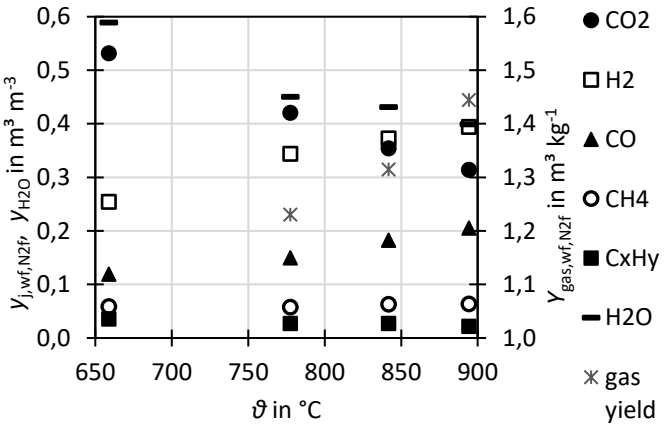

Figure 4.2: Permanent gas concentrations on water and N_2-free basis, H_2O concentration on N_2-free basis, as well as permanent gas yield per water and ash free sewage sludge for different ϑ at constant n_{O2}

Similar trends regarding increasing gas yield and H_2 and CO concentration, were found for steam-air gasification of sewage sludge [15, 27] and corn straw [114], also, when calculated to N_2-free basis, similar gas concentrations of all permanent gases were reported. Additionally, the temperature influence in steam-oxygen gasification of wood is reported in literature [79] and shows similar trends compared to this study concerning H_2, CO_2 and gas yield. However, differences were reported in the trend of the CO, CH_4 and C_xH_y concentrations, which decreased slightly with temperature in the reference whereas in this study they increased (CO) or stayed almost constant (CH_4, C_xH_y). Similar trends to this study were also obtained by steam gasification of sewage sludge in the same gasifier operated in DFB mode [68].

4.1.3 Variation of steam to carbon ratio n_{SC}

Figure 4.3 shows the influence of the steam to carbon ratio n_{SC} on the permanent gases. The n_{SC} had a strong influence on the permanent gas composition, since H_2 and CO_2 strongly increased and CO decreased with n_{SC}. This was due to the water gas shift reaction (R 11) that was driven to H_2-production by adding steam. Also, the dry gas yield rose since water was converted to H_2 through WGS. The CH_4 and C_xH_y concentrations showed a slight decrease with increasing n_{SC}. Naturally, the H_2O concentration increased with n_{SC} due to the increased steam input.

These results indicate that through higher n_{SC}, increased conversion of CO to H_2 and CO_2 can be achieved to improve the H_2-yield or to adjust the H_2/CO-ratio. However, higher n_{SC} requires more energy-intensive steam production, so that in practice it needs to be considered if a higher n_{SC} or a downstream catalytic WGS unit, which are currently developed for raw syngas [115], is preferred.

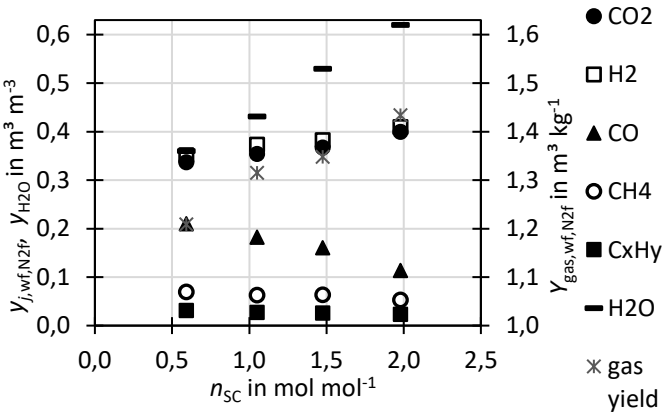

Figure 4.3: Permanent gas concentrations on water and N_2-free basis, H_2O concentration on N_2-free basis, as well as permanent gas yield per water and ash free sewage sludge for different n_{SC}

Variation of n_{SC} was conducted in literature for steam-oxygen gasification of wood [79], air-steam gasification of sewage sludge [27] and corn straw [114], where similar trends for H_2, CO, CO_2 and H_2O were found, but in contrast to this thesis, a more pronounced decrease of CH_4 and C_xH_y was reported with increasing n_{SC}. High CO and lower H_2 and CO_2 concentrations at low n_{SC} as in this work were also reported by [78]. For steam-air gasification of refuse-derived fuel in a rotary kiln also a rise in gas yield with n_{SC} was reported [116].

4.1.4 Variation of weight hourly space velocity n_{WHSV}

Figure 4.4 shows the influence of the weight hourly space velocity, n_{WHSV}, calculated as quotient of the mass flow of dry ash-free sewage sludge and bed inventory mass, on the permanent gases. It has to be mentioned that n_{WHSV} was changed, both, by variation of fuel feed and bed inventory as can be seen in Table 4.1. For the gases CO, CO_2, CH_4 and C_xH_y no clear trend was observed for

different n_{WHSV}. A slight decrease for the H_2 concentration with increased n_{WHSV} was present, which could be related to less CO-shifting through WGS due to the decreasing residence time of the gas.

Similar behavior was reported for sewage sludge steam-air gasification [11], where for higher turnover rates, respective higher n_{WHSV}, lower H_2 concentrations and no or only little change in the other permanent gas concentrations were found.

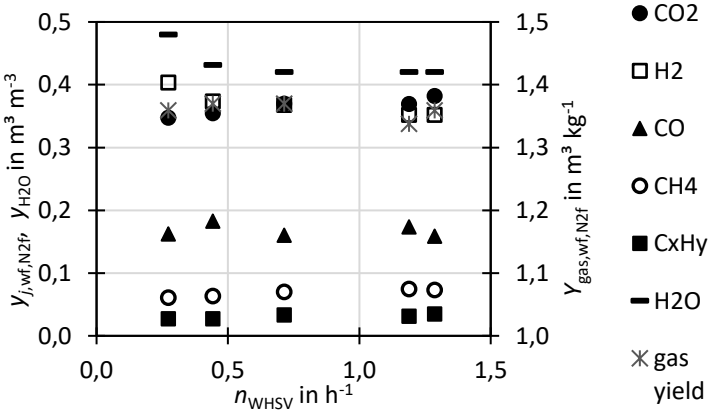

Figure 4.4: Permanent gas concentrations on water and N_2-free basis, H_2O concentration on N_2-free basis, as well as permanent gas yield per water and ash free sewage sludge for different n_{WHSV}i

4.1.5 Variation of fuel

Results on the steam-oxygen gasification of wood and straw pellets in comparison to sewage sludge were published by the author [10]. It was found that the permanent gas yields and concentrations are similar for wood pellets, straw pellets and sewage sludge gasification. Another reference is available for steam-oxygen gasification of wood [78], which is in good agreement with this work.

4.2 Tar concentration

To determine the concentrations of tar species in the syngas, tar sampling was conducted wet chemically whereas each sample was analyzed by two methods: GC analysis and gravimetric analysis (see section 3.4). The specific results of both analysis methods are discussed in detail in the sections 4.2.1 and 4.2.2. The sections 4.2.3 to 4.2.8 show the impact of the operation parameters n_{O2}, ϑ, n_{SC}, n_{WHSV} and n_{CaCO3} on the tar concentration.

4.2.1 GC tar species screening and analysis

GC-MS tar species screenings were conducted to get on overview of the tar species. Figure 4.5 depicts this GC-MS screening for the reference experimental run "ref". The peaks of all identified species are labelled with the respective species names. Most of the identified species were quantified

by GC-FID analysis by the FAU lab (black label) or PSI lab (grey label). Blue italic labels refer to only identified but not quantified species.

The number of peaks reflects the vast number of hydrocarbons and aromatic species that are generated during gasification. Aromatic and polyaromatic components, known from wood gasification [108], such as toluene and naphthalene are present with very high peaks. The benzene peak was not captured by this analysis due to the GC-MS setup, but was later on quantified by GC-FID. In addition, heterocyclic aromatic species containing nitrogen, such as pyridine, benzonitrile and dimethylhydantoin and species containing sulfur like thiophene and benzothiophene were found. From those species, pyridine and dimethylhydantoin had the highest peaks. Styrol, methylpyridine and quinoline, could be identified with medium-sized peaks but were not quantified. Also, further small-sized to medium-sized peaks were detected, but no species could be assigned to the respective elutriation times. It can be concluded that the majority of the high peaks could be quantified, and therefore the sum of GC detectable tars as used in the following sections reflects the total tar concentration to a considerable extent for species up to the molar mass of 202 g mol^{-1} (pyrene).

Figure 4.6 shows the tar concentration for the reference run, quantified by GC-FID analysis from two labs. All tar species concentrations are shown as tar mass per volume of dry and N_2-free syngas in STP conditions. The tar yields can be calculated by multiplying the tar concentration with the gas yields shown in section 4.1. The main analysis was conducted by the FAU lab and included 16 tar species that are depicted in black in Figure 4.6. This analysis was accomplished for all samples shown in this thesis. For the points C1/ref, C2, C3, C4, additional GC-MS analyses of heterocyclic tar species were conducted by the PSI laboratory (depicted in grey).

The majority of the GC-detectable tars were found to be benzene, toluene, xylene (BTX). While toluene and xylene are included in ECN3, benzene is considered independently of the ECN classes. Also, considerable amounts of heterocyclic species belonging to the ECN2 class, mainly pyridine but also benzothiophene, carbazole, dimethylhydantoin, benzonitrile, pyrrole and others were found. Furthermore, considerable concentration of tar species of ECN4 were found with naphtalene and indene being the most dominant. The cumulated concentration of ECN5 tars is below 0.2 g m^{-3}, however due to the high boiling point of these species, this can cause blockages already at temperatures below 400 °C (e.g. in syngas coolers).

The additional species quantified by the PSI lab sum up to around 0.06 kg kg^{-1} of the total GC tar concentration. The FAU analysis is therefore sufficient to assess the total tar concentration and its trends for different gasification operation parameters, while the PSI analysis provide additional information on tar species of the more water-soluble ECN2 species, which is important for the design of downstream scrubbers for tar removal. For future experiments, it is, however, advised to add pyridine as mandatory specie for analysis as it has a comparably high concentration.

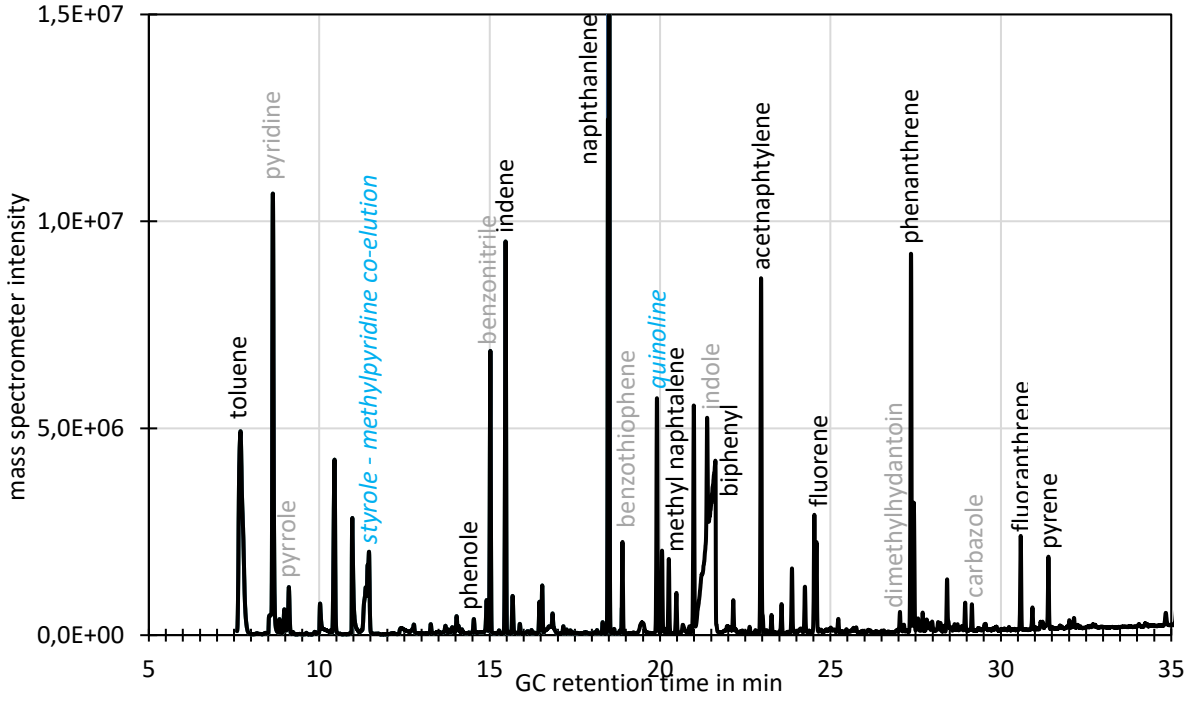

Figure 4.5: GC-MS screening measurement of experimental reference point "ref", black components: quantified with GC-FID (FAU lab), grey components: quantified with GC-FID (PSI lab), both see Figure 4.6, blue italic components: not quantified

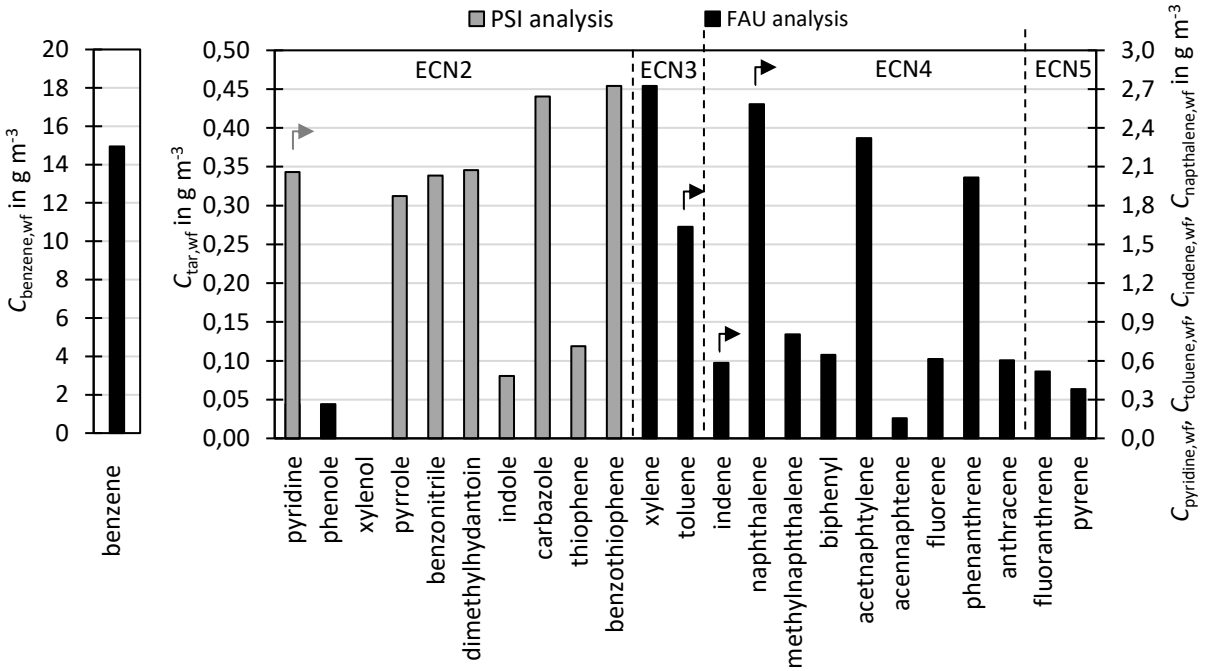

Figure 4.6: GC-FID analysis of tar species concentrations of experimental reference point "ref", black components: quantified with GC-FID (FAU lab), grey components: quantified with GC-FID (PSI lab)

4.2.2 Gravimetric tar composition

For some runs, the tar sample was retrieved after gravimetric analysis and an elemental analysis was performed. Figure 4.7 shows the elemental composition of the retrieved gravimetric tar samples. It can be seen that the carbon mass fraction for all samples is only around 0.5 kg kg^{-1} compared to up to 0.9 kg kg^{-1} for tar from wood, as published by the author in [10]. In addition, significant amounts of S, N and Cl were found in sewage sludge gravimetric tar.

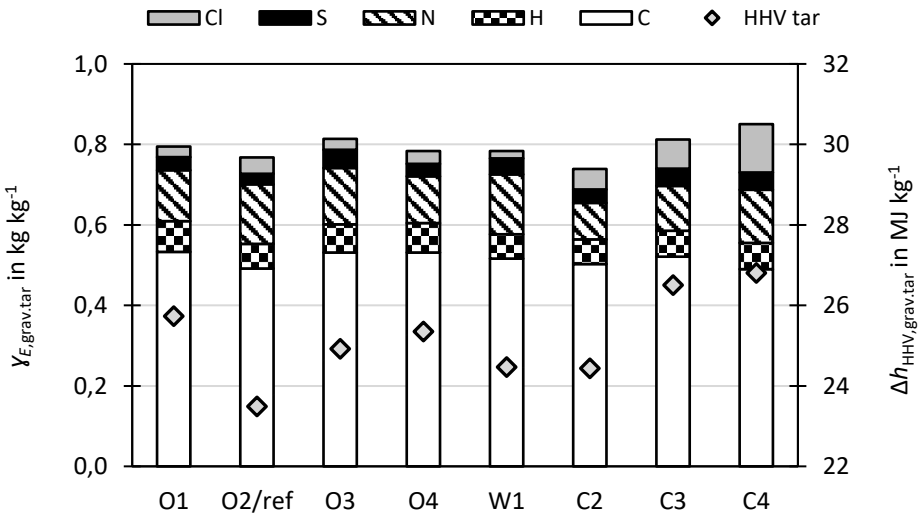

Figure 4.7: Elemental analysis and heating values of gravimetric tars

The elements N, S and Cl are present in heterocyclic tar species as shown in section 4.2.1; however, their concentration found in gravimetric tar goes well beyond the concentration of these elements in heterocyclic tar species. In addition, heterocyclic tar species have significant higher carbon concentration than the gravimetric tar. It is therefore assumed that the gravimetric analysis does not only sample typical tar species (e.g. PAH) when applied to sewage sludge derived syngas, but also salts like NH_4Cl, $(NH_4)_2CO_3$, $(NH_4)_2SO_4$ and others that are e.g. formed from NH_3, HCl and H_2S, which are present in high concentrations in the syngas. This hypothesis is supported by the following two observations: First, the measured higher heating value of the gravimetric tars, which were found to be around 25 MJ kg^{-1} are thus by around 40% below the heating value of a typical gravimetric tar species (e.g. naphthalene 40 MJ kg^{-1}) implying the presence of incombustible (e.g. inorganic) compounds. Second, it was noticed during the tar sampling that the isopropanol-tar samples contained a white precipitate. The visible fraction of this precipitate was separated from the sample via centrifugation before the gravimetric analysis procedure as proposed by the tar protocol. Thereby, a clear sample was obtained. The separated precipitate was found to be volatile at ambient temperature and therefore difficult to analyze. Thus, its composition is not definitely known, but an odor testing suggested that this precipitate contained ammonium.

It can be concluded that gravimetric tar from sewage sludge has a different composition than gravimetric tar from wood gasification and contains substantially less carbon and hydrogen, but considerable amounts of S, N and Cl instead. Nevertheless, the gravimetric analyses were conducted according to CEN/TS 15439 and thus deliver tar concentrations according to the standard. However, as a consequence of this work, an elemental analysis of gravimetric tars is recommended for a better assessment of the tar concentration in syngas from gasification of sewage sludge and other feedstock containing considerable amounts of S, N and Cl.

4.2.3 Variation of oxygen ratio n_{O2}

Figure 4.8 shows the influence of the oxygen ratio n_{O2} on the tar concentration. The gravimetric tar concentration is dropping slightly with increasing oxygen ratio. This could be related to enhanced tar oxidation. The GC tar concentration was determined only by the FAU lab (see 4.2.1). Since due to technical reasons only one GC analysis was performed for this parameter variation, no trend can be observed for GC tars.

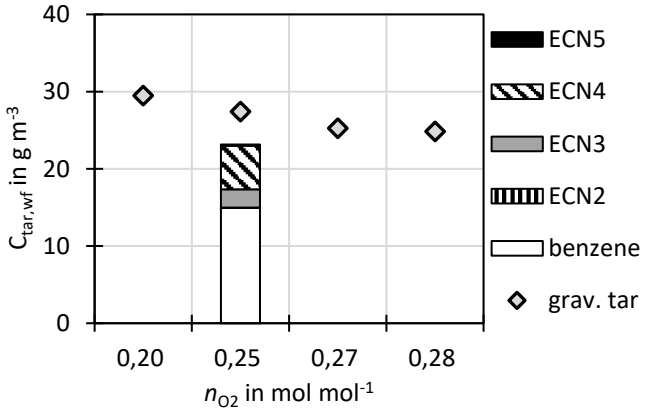

Figure 4.8: Gravimetric and GC (only FAU analysis) tar concentrations on water free, N_2-free and STP basis at different oxygen ratios n_{O2}

Manya et al [64] conducted an n_{O2}-variation for steam-air gasification of sewage sludge and found no clear trend of the tar concentrations. Although n_{O2} was varied by several other researchers [44, 79, 111, 112], other significant parameters such as temperature were altered as well in most references. Therefore, no further exclusive variation of n_{O2} was found in literature.

4.2.4 Variation of temperature ϑ

Figure 4.9 shows the tar concentration at different gasification temperatures ϑ. At 659 °C, a very high gravimetric tar concentration of 98 g m^{-3} was measured. When the temperature was increased to 778 °C, the concentration drastically dropped to 31 g m^{-3}. With further temperature increase, the gravimetric tar concentration steadily dropped to 27 g m^{-3} and 23 g m^{-3} at 842 °C and 894 °C, respectively. As known [23], at low gasification temperatures considerable fractions of the fuel are

not converted into small molecules, but form large tar molecules which are detected well by gravimetric analysis. At higher temperatures, those gravimetric tars are cracked or reformed into smaller tar species or into permanent gases.

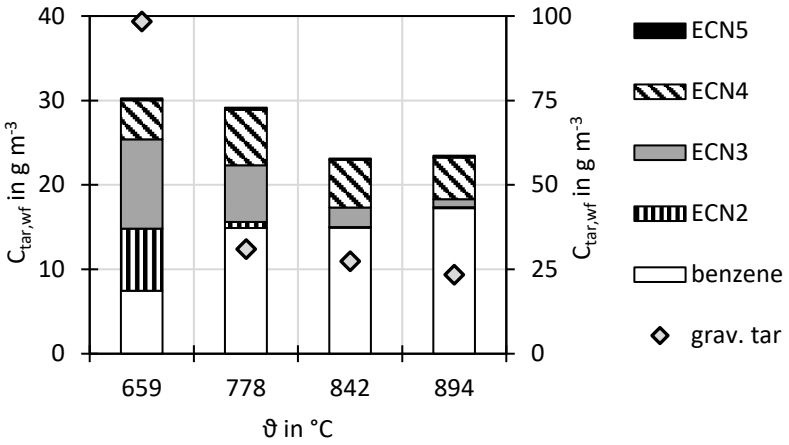

Figure 4.9: Gravimetric and GC (only FAU analysis) tar concentrations on water free, N_2-free and STP basis at different ϑ

The total GC tar concentration, as measured by the FAU lab, was 31g m^{-3} at 659 °C. When the temperature was increased, the GC tars were found to be decreasing slightly but steadily to 23 g m^{-3} at 894 °C. It has to be noted that the concentration of tar species from ECN2 and ECN3 classes decreased severely with temperature, while benzene is increasing. Similar behavior is reported in literature [68, 79, 111, 117–120].

4.2.5 Variation of steam to carbon ratio n_{SC}

Figure 4.10 shows the tar concentrations against steam to carbon ratio $n_{SC,}$ where a decrease of the gravimetric tar concentration with increasing n_{SC} was observed. This could be due to the known [23, 121] effect of higher steam concentrations on reforming of gravimetric tars. The GC tars stayed rather constant over variation of n_{SC}. This corresponds well to other gasification experiments where higher steam concentrations also reduced tar concentrations [15, 38, 79, 121].

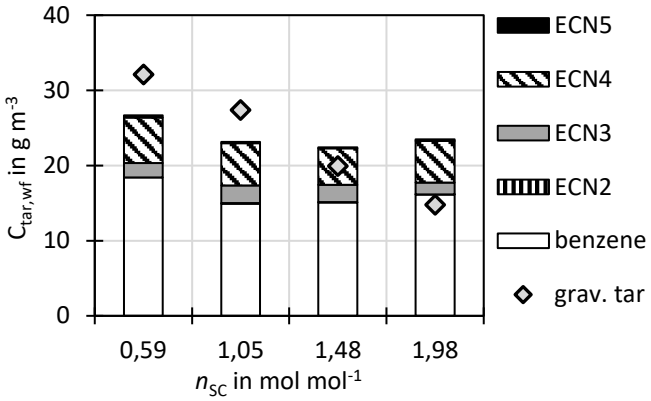

Figure 4.10: Gravimetric and GC (only FAU analysis) tar concentrations on water free, N_2-free and STP basis at different n_{SC}

4.2.6 Variation of weight hourly space velocity n_{WHSV}

Figure 4.11 shows the tar concentration against the weight hourly space velocity n_{WHSV}. It has to be noted that the point at n_{WHSV}=1.29 h^{-1} was conducted with a higher fuel mass flow of around 14 kg h^{-1} compared to around 7 kg h^{-1} (see Table 4.1) for the other points. Despite that, the tar concentration for the points at n_{WHSV} = 1.19 h^{-1} and 1.29 h^{-1} were found to be similar. Decreasing tar concentrations can be seen when comparing the two runs at lower n_{WHSV} with the two at higher n_{WHSV}. A trend of increasing GC tar concentration with rising n_{WHSV} may be visible.

For a constant gasifier cross section, rising n_{WHSV} lead to decreasing gas residence times, which, in theory, should lead to less contact of gas with active bed resulting in increasing tar concentrations. The measured GC tar concentration seems to lightly follow this trend but not the gravimetric one. It can be concluded that it is not possible to deduct a clear assessment of the influence of n_{WHSV} on tar concentration with the obtained results. A more comprehensive study is needed.

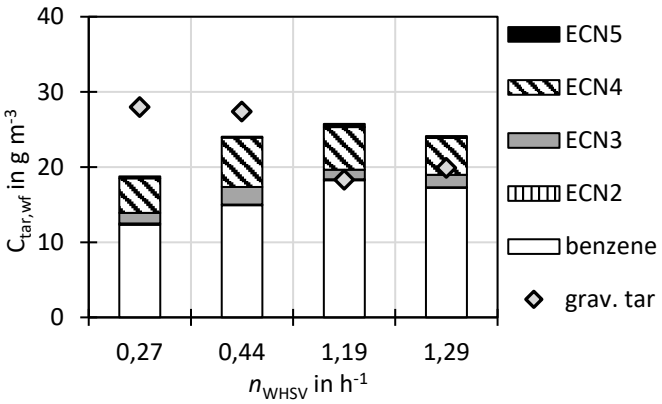

Figure 4.11: Gravimetric and GC (only FAU analysis) tar concentrations on water free, N_2-free and STP basis at different n_{WHSV}

It was reported in literature [11] that for steam-air gasification the tar concentration slightly increasees with higher "turnover rate" respective higher n_{WHSV}. For steam gasification of wood [117], slightly decreasing gravimetric tar yields, but constant GC tar yields were reported for increasing n_{WHSV} which is consistent with this work.

4.2.7 Variation of limestone additive ratio n_{CaCO3}

The gravimetric and GC tar concentrations are depicted in Figure 4.12. For these runs, GC analyses from FAU and PSI were conducted, however, to assure comparability to the results in 4.2.3 to 4.2.6, only analyses from FAU are presented here. The results of the PSI analysis as well as the concentrations of each evaluated tar species are published by the author in [20].

The gravimetric tar concentration for the run C1 without additive was around 27 g m^{-3}. With increasing additive ratio, the gravimetric tar concentration dropped substantially to around 7 g m^{-3} for run C4 with 0.18 kg kg^{-1} additive ratio. This drop was most pronounced between run C1 (without additive) and run C2 (low additive ratio of 0.06 kg kg^{-1}). This indicates that very little addition of limestone is needed to achieve substantial reduction of gravimetric tar.

The concentrations of GC detectable tar species were less affected by limestone than those of gravimetric tars. It can be concluded that limestone is much less active in cracking light aromatic and polyaromatic GC-tar species than in cracking heavy gravimetric tars. With further increasing additive ratios in run C3 and run C4, a noticeable concentration decrease in the majority of the GC tar species and subsequently also the sum of all GC tars was observed in comparison to run C1. It needs to be noted that the cracking of gravimetric tars may have produced GC detectable tars, which could be overlaying the actual trend of light tar conversion.

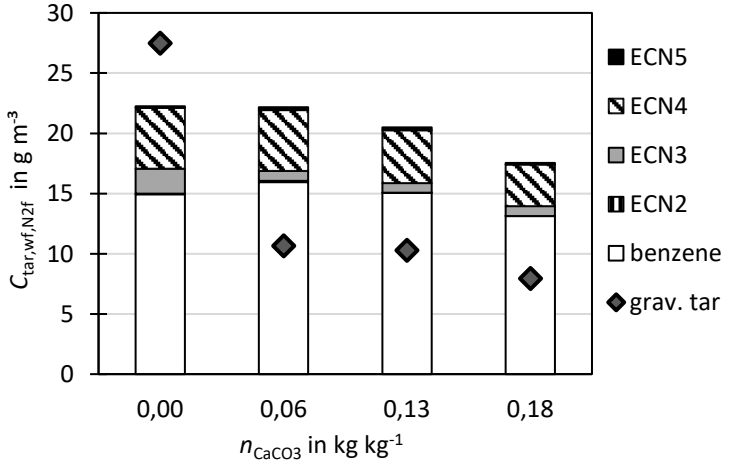

Figure 4.12: Gravimetric and GC (only FAU analysis) tar concentrations on water free, N_2-free and STP basis at different n_{CaCO3}

Since the catalytic activity of CaO for cracking of heavy tars was also observed in literature [15, 18, 68, 122] for various fluidized bed gasification processes and fuels, this work's results can be transferred to other gasification applications. In this respect, considerably lower additive ratios, and hence only very small amounts of limestone, are required to mitigate tar problems in the case of fuels with a lower ash content, such as woody biomass.

Figure 4.13 depicts the concentration of tar species with and without methyl groups. Benzene and naphthalene, both species without methyl groups, are first increasing from run C1 without additive and C2 with 0.06 kg kg^{-1} additive ratio and then decreasing at run C3 and C4 with further increasing additive ratio. Toluene, xylene and methylnahpthalene have methyl groups and are decreased distinctly from run C1 to run C2. This suggests that limestone catalyzes the separation of methyl groups, so that toluene, xylene methylnaphthalene are converted into benzene and naphthalene, which is also supported by lab experiments [33].

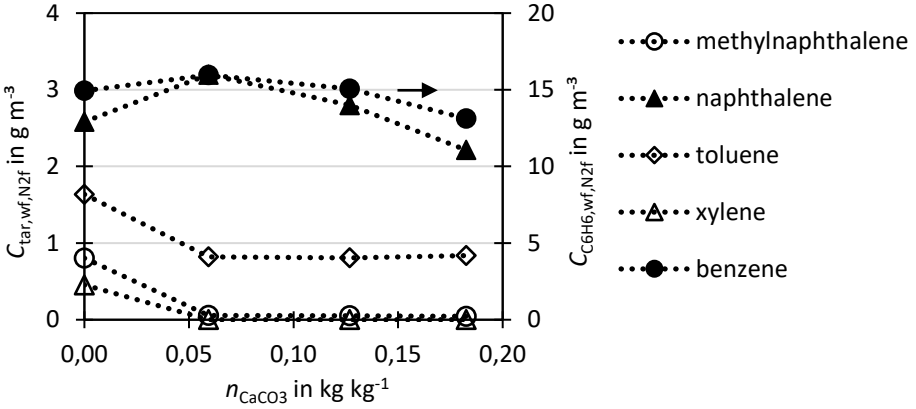

Figure 4.13: De-methylation of tar species with increasing n_{CaCO3}: water free and N_2-free concentration of tar species with methyl groups (unfilled symbols), toluene, xylene and methylnaphthalene, and without methyl groups (filled symbols), benzene, naphthalene

4.2.8 Variation of fuel

This author also conducted measurements of tar concentrations for steam-oxygen gasification of wood pellets and straw pellets that are published in [10]. The tar concentrations for wood, straw and sewage sludge were in the same value range. However, the gravimetric tar concentration for sewage sludge was, for the run without limestone additive, higher than for wood and straw whereas for GC tars the opposite was observed. The composition of gravimetric tar differed remarkably from wood and straw to sewage sludge. The carbon content in gravimetric tars from wood pellets, straw pellets and sewage sludge gasification was 0.87 kg kg^{-1}, 0.77 kg kg^{-1} and 0.52 kg kg^{-1}, respectively. Possible reasons for this are discussed in section 4.2.2.

4.3 H_2S and COS concentration

In this chapter, the concentrations of the gaseous sulfur species H_2S and COS are discussed.

4.3.1 Variation of oxygen ratio n_{O2}

Figure 4.14 shows the measured H_2S and COS concentrations as well as the equilibrium concentrations, calculated with FactSage® (see section 3.5), over the oxygen ratio n_{O2}. For oxygen ratios from 0.20 to 0.28, H_2S concentrations between $1900 \cdot 10^{-6}$ m³ m^{-3} and $2700 \cdot 10^{-6}$ m³ m^{-3} were measured at the respective conditions of 847±5 °C. From the measurements of this work, it is hard to deduct a specific trend for H_2S, but it can be noted that the two points at higher n_{O2} show slightly higher concentrations. For COS only one measurement was conducted of $59 \cdot 10^{-6}$ m³ m^{-3} at n_{O2} = 0.2 mol mol^{-1}. The equilibrium, calculated by the software FactSage®, predicts a slight increase of H_2S and COS concentration with n_{O2}. This is related to an increased feed of oxygen to the gasifier at higher n_{O2}, leading to the formation of H_2O and CO_2 driving R 13 and R 14 away from sulfur capture following Le Chatelier's principle. The equilibrium concentrations are significantly lower than the experimental values, which suggests that equilibrium conditions were not reached in the experiments.

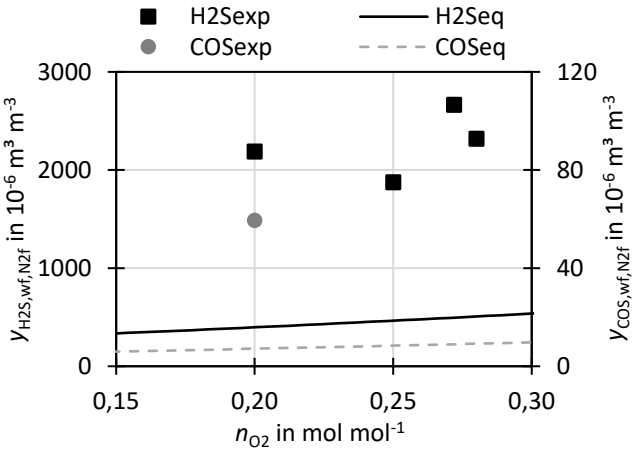

Figure 4.14: Measured and equilibrium H_2S and COS concentrations on water free and N_2-free basis at n_{O2}

4.3.2 Variation of temperature ϑ

Figure 4.15 shows the H_2S concentration and Figure 4.16 the COS concentration at different temperatures for cases with the reference bed material, sewage sludge ash, but also for runs with limestone additive. Additionally, the H_2S and COS concentrations of the thermochemical equilibrium are shown.

A strong dependence of the concentration of the two sulfur species on the temperature could be observed in the experiment as well as in the equilibrium calculations. At low temperatures, high

concentrations of up to $7653 \cdot 10^{-6}$ m³ m^{-3} for H_2S and up to $215 \cdot 10^{-6}$ m³ m^{-3} for COS were measured with sewage sludge ash as bed material. With increasing temperatures, the H_2S and COS concentrations decreased until a minimum was reached before the concentration increased again at higher temperatures. This is related to the facts that sewage sludge ash contains CaO that can capture sulfur through reactions R 13 and R 14, which are exothermic and therefore favored at lower temperatures. However, the calcination reaction R 12 is favored at higher temperatures. The overlay of calcination and sulfur capture leads to the observed temperature dependency. For the case with limestone additive, a similar trend was observed but consequently lower concentrations were measured. The lowest measured concentration without limestone additive was $1855 \cdot 10^{-6}$ m³ m^{-3} at 778 °C and with limestone additive, the lowest concentration was $624 \cdot 10^{-6}$ m³ m^{-3} at 770 °C. With the limestone additive, the H_2S concentration could thus be reduced by around factor 3 at these temperatures.

The equilibrium has a similar trend as the experiments but shows for all cases lower concentrations, which is in agreement with the fact that the equilibrium predicts optimal sulfur capture and thus the lowest possible concentration. The minimum H_2S equilibrium concentration was calculated for 740 °C with $243 \cdot 10^{-6}$ m³ m^{-3}. For COS similar behavior was observed, at 770 °C-778 °C the concentration for sewage sludge ash bed is $40 \cdot 10^{-6}$ m³ m^{-3}, with limestone additive it is reduced to $13 \cdot 10^{-6}$ m³ m^{-3}, also by around factor 3. The COS minimum equilibrium concentration was calculated for 740 °C with $6 \cdot 10^{-6}$ m³ m^{-3}.

As discussed, with further increasing temperatures the measured and equilibrium H_2S and COS concentrations are rising again. At the reference temperature of 840 °C, which is also a very common temperature to operate sewage sludge incinerators and gasifiers [123], slightly higher concentrations of H_2S with $1873 \cdot 10^{-6}$ m³ m^{-3} and COS of $59 \cdot 10^{-6}$ m³ m^{-3} were observed without additive. Again, the limestone additive brings a reduction. It was noticed that with limestone additive the COS concentrations can be brought very close to the equilibrium for all investigated temperatures above 750 °C while for H_2S the concentrations with additive still are further away from the equilibrium.

In literature [18, 35], similar trends of H_2S concentrations over temperature in the presence of CaO were reported in experiments and equilibrium calculations.

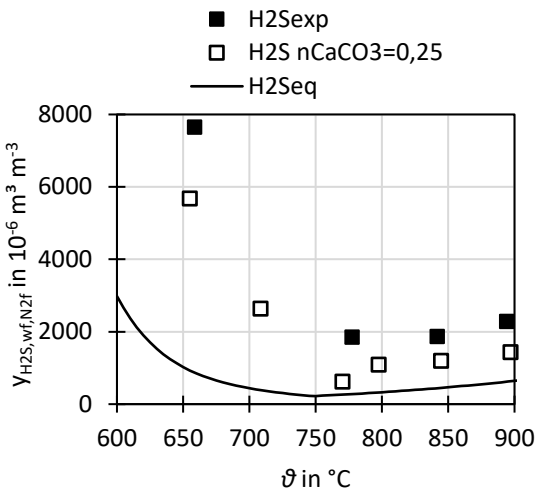

Figure 4.15: Measured and equilibrium H_2S concentration on water free and N_2-free basis at different ϑ

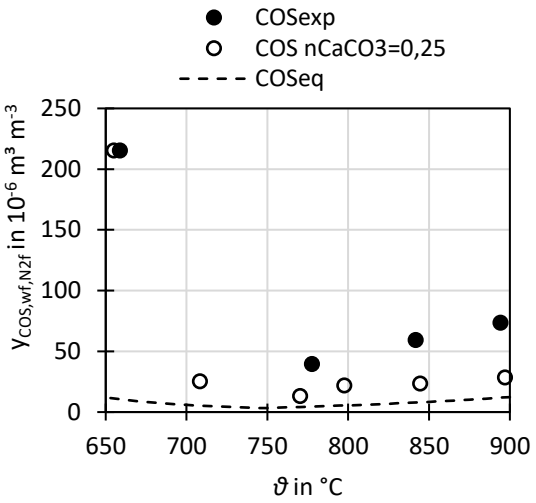

Figure 4.16: Measured and equilibrium COS concentration on water free and N_2-free basis at different ϑ

4.3.3 Variation of steam to carbon ratio n_{SC}

Figure 4.17 shows the H_2S and COS concentrations for different steam to carbon ratios n_{SC} at a gasification temperature of around 850 °C. The measured H_2S concentrations increased with n_{SC}. The lowest n_{SC} tested was 0.6 mol mol^{-1}, which lowered the H_2S concentration to 1340·10^{-6} m³ m^{-3}. A similar trend was found by [35]. This follows well the trend of the equilibrium where the H_2S concentrations are increasing with n_{SC} following Le Chatelier's principle: With higher n_{SC} more steam is introduced into the gasifier, driving R 13 to the left towards less H_2S capture.

The measured COS concentration stayed at the same level throughout the n_{SC} variation, whereas the equilibrium predicts a very small increase. Since steam does not participate in R 14, n_{SC} has no direct effect on COS capture. However, through the water gas shift reaction, steam addition can also produce more CO_2 influencing the COS capture.

Additionally, the equilibrium for 750 °C is shown since sulfur capture is maximized at this temperature. It can be seen that very low concentrations are achievable at operation conditions of 750 °C and low n_{SC} according to the equilibrium.

In literature [18, 35], similar trends of H_2S concentrations over n_{SC} in the presence of CaO were reported in experiments and equilibrium calculations.

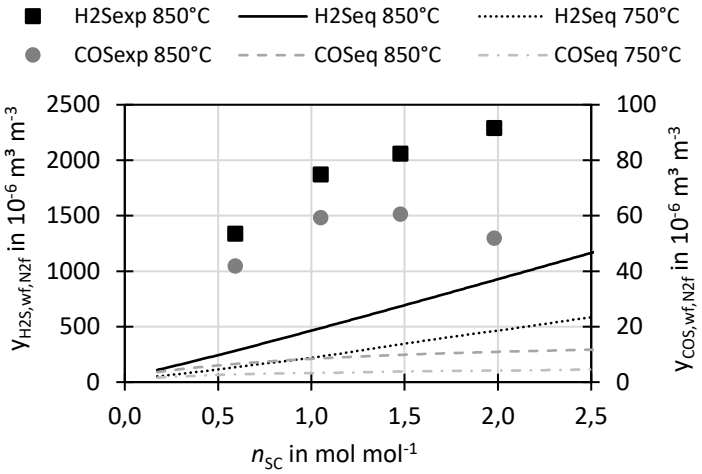

Figure 4.17: Measured and equilibrium H_2S and COS concentration on water free and N_2-free basis at different n_{SC} at 850 °C, additionally equilibrium calculations for ϑ = 750 °C showing optimal sulfur capture

4.3.4 Variation of weight hourly space velocity n_{WHSV}

Figure 4.18 shows the H_2S and COS concentration at different space velocities n_{WHSV}. For the measured values, no specific trend could be observed. This is not as expected, since for a given reactor cross section, n_{WHSV} is correlated to the gas residence time in the bed; therefore, lower n_{WHSV} should lead to a better sulfur capture. Further experiments are needed to investigate this interrelation. It would be of further interest to vary n_{WHSV} for experiments with limestone additive.

Since the equilibrium already assumes infinite residence time of the fuel, it cannot produce trends of the space velocity and thus a constant equilibrium concentration is shown.

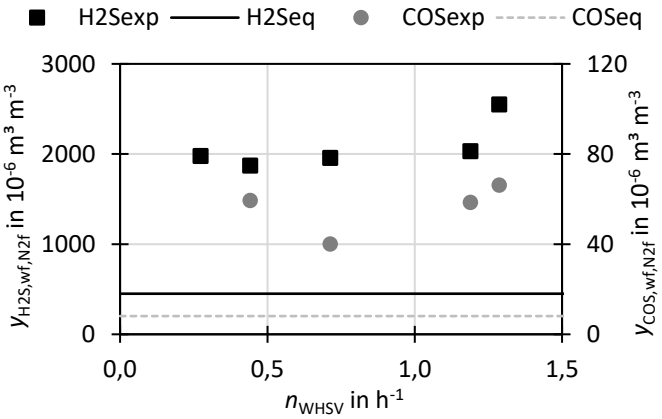

Figure 4.18: Measured and equilibrium H_2S and COS concentration on water free and N_2-free basis at different n_{WHSV}

4.3.5 Variation of limestone additive n_{CaCO3}

The measured H_2S and COS concentrations as well as the calculated equilibrium concentrations are shown in Figure 4.19 and Figure 4.20. For a better assessment of the sulfur capture efficiency, the additive ratio is correlated to the Ca/S ratio ($n_{Ca,S}$) on the secondary horizontal axis, considering the calcium in the sewage sludge and the calcium introduced by the limestone additive.

For the run without additive, the highest H_2S and COS concentrations of $1823 \cdot 10^{-6}$ m³ m^{-3} and $58 \cdot 10^{-6}$ m³ m^{-3}, respectively, were present. This corresponds to an elemental yield of fuel-S forming H_2S and COS of $S_{H2S,S} = 0.14$ and $S_{COS,S} = 0.005$, respectively, indicating that the majority of the sulfur stayed in the ash, most probably in CaS and FeS formations.

The measured H_2S and COS concentrations decreased with increasing additive ratio, showing clearly the sulfur capture activity of the additive. For a high additive ratio, the concentrations come close to the equilibrium concentration. For COS a higher relative reduction could be achieved.

It can be concluded that sulfur capture takes place for both species, H_2S and COS, but an excess of Ca is needed for a substantial effectivity as also observed in literature [35]. At the investigated conditions, equilibrium is not favorable for complete sulfur capture, in-situ desulfurization thus can only be a pre-capture step requiring an additional downstream desulfurization step. If a higher in-situ sulfur capture with Ca is intended, the thermodynamically optimized temperature of 740 °C and a low steam-to-carbon ratio should be used.

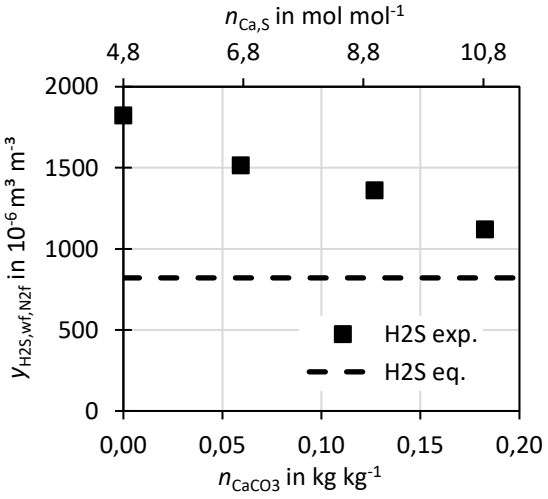

Figure 4.19: Measured and equilibrium H_2S concentration on water free and N_2-free basis at different additive ratios n_{CaCO3}

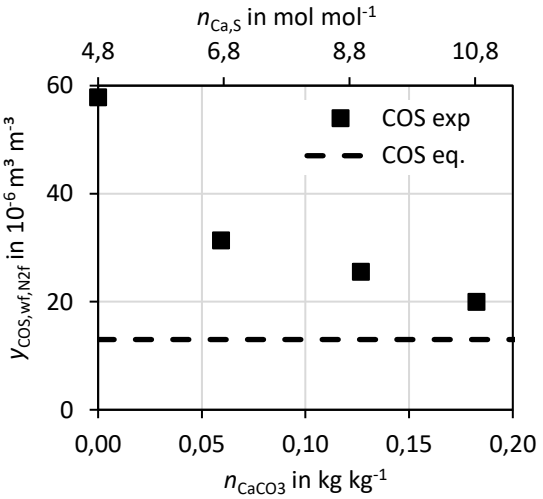

Figure 4.20: Measured and equilibrium COS concentration on water free and N_2-free basis at different additive ratios n_{CaCO3}

4.3.6 Variation of fuel

For straw pellets steam-oxygen gasification, H_2S concentrations of $1240 \cdot 10^{-6}$ m³ m^{-3} were measured as published by the author in [10], which is about half of the concentration measured for sewage

sludge gasification at comparable conditions. However, the sulfur content in straw pellets was with 0.002 kg kg^{-1} one magnitude lower than that in sewage sludge. For sewage sludge there is thus a significant lower elemental yield of fuel S in H_2S observed than for straw pellets. This is probably attributed to the previously discussed self-desulfurization of sewage sludge due to its calcium-rich ash.

4.4 NH_3 concentration

Figure 4.21 to Figure 4.24 show the measured NH_3 concentrations in the syngas with respect to different operation conditions. As indicated above, NH_3 was measured wet chemically and was not measured for every experimental point. For most runs, the NH_3 concentrations were between $4000 \cdot 10^{-6}$ m³ m^{-3} and $8000 \cdot 10^{-6}$ m³ m^{-3}. However, for runs with lower ϑ or with higher n_{SC} higher NH_3 concentrations of up to $15500 \cdot 10^{-6}$ m³ m^{-3} were measured.

Figure 4.21 shows the temperature variation. While the NH_3 concentration for the two lower temperatures 659 °C and 778 °C, are around $15000 \cdot 10^{-6}$ m³ m^{-3}. Significant lower concentrations of $3894 \cdot 10^{-6}$ m³ m^{-3} and $5941 \cdot 10^{-6}$ m³ m^{-3} were measured for the higher temperatures 842 °C and 894 °C, respectively. It can be concluded that NH_3 formation is enhanced at lower temperatures.

For n_{SC} variation three measurements are available (Figure 4.22). While for n_{SC} = 1.05 and n_{SC} = 1.48 NH_3 concentrations of around $4000 \cdot 10^{-6}$ m³ m^{-3}, respectively, were measured, the point at n_{SC}=1.98 showed a significant higher concentration of $13053 \cdot 10^{-6}$ m³ m^{-3}. There is thus an implication that the NH_3 concentration rises with increasing n_{SC}. However, due to the limited number of measurements, no clear trend can be determined. No data was found in literature on the trend of NH_3 concentrations for n_{SC} variation.

For variation of n_{O2}, no clear trend was observed (Figure 4.23), while a constant trend was visible for variation of n_{CaCO3} (Figure 4.24).

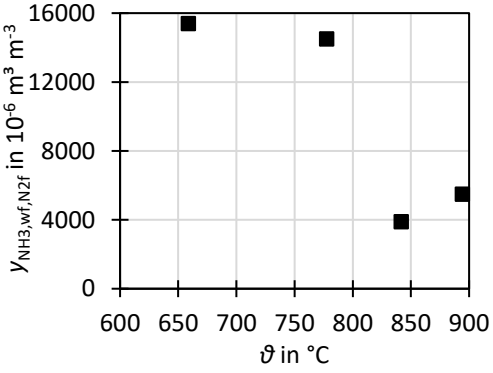

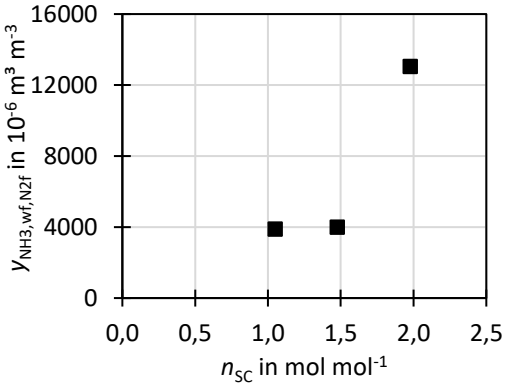

Figure 4.21: NH_3 concentration on water free and N_2-free basis at different temperatures ϑ

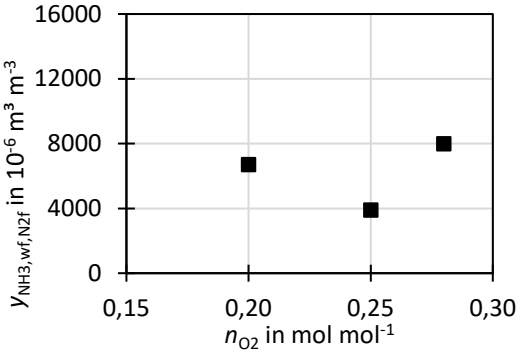

Figure 4.22: NH_3 concentration on water free and N_2-free basis at different steam to carbon ratios n_{SC}

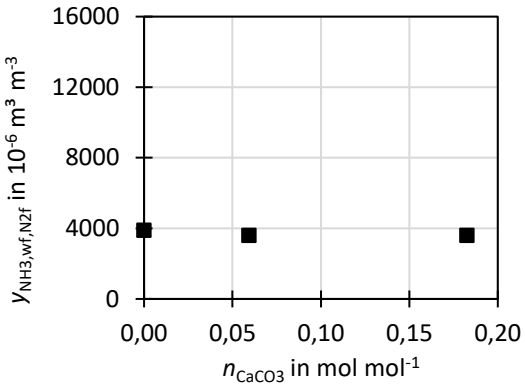

Figure 4.23: NH_3 concentration on water free and N_2-free basis at different steam to carbon ratios n_{O2}

Figure 4.24: NH_3 concentration on water free and N_2-free basis at different additive ratios n_{CaCO3}

It can be concluded that NH_3 is occurring in considerable concentrations in sewage sludge derived syngas, which is clearly related to the high nitrogen content in the fuel. Other research also shows high NH_3 concentrations for high N-containing fuels such as sewage sludge [10, 68], manure [68], peat [84] or coal [124]. It has to be noted that steam-oxygen gasification seams to show considerably lower NH_3 concentration than steam gasification [68] in the same facility at IFK. This is an indication that the presence of oxygen reduces the NH_3 formation. Literature also reports decreasing NH_3 concentrations with increasing temperature for air-steam gasification [45, 62] and for steam gasification of other fuels [125] which is in line with this study. The author of this thesis conducted steam-oxygen gasification of straw pellets at 850 °C and n_{SC} = 1 mol mol^{-1} and found a NH_3 concentration of $1810 \cdot 10^{-6}$ NH_3 [10].

4.5 Ash yields and carbon contents

Ash streams are divided into bed ash and fly ash (see section 2.2.1). Carbon contained in ash streams leaves the reactor unreacted and therefore reduces the conversion efficiency of fuel to syngas. In this work, the yield and composition of fly ash streams could be determined only if the gasification process was stopped before and after an experimental point to measure the amount of fly ashes from the cyclones and the candle filters. This was done only for the experimental runs shown in Table 4.2. Whereas for all other experiments, two or more runs were conducted on one day while only measuring the amount of fly ashes at the end of the day.

4.5.1 Bed ash

Bed ash was the main ash stream in the experiments. The bed ash serves also as bed material and is discharged continuously through an overflow. The bed ash yield per water free sewage sludge was 0.41 kg kg^{-1} as calculated from the difference of the fuel's ash content (proximate analysis Table 3.1) and the measured fly ash yields (Table 4.2). The carbon content of the bed material after discharge from the reactor was around 0.017 kg kg^{-1} for the reference run (gasification temperature of 842 °C); however, for lower temperature the carbon content was found to be higher, up to 0.04 kg kg^{-1} at 668 °C.

4.5.2 Fly ash

Small fuel particles, dust produced by bed attrition or soot formed by fuel conversion are entrained from the fluidized bed and are considered fly ash. In the used experimental facility, fly ash is captured by a primary cyclone, a secondary cyclone and a ceramic candle filter. The yields of the respective fly ash for the reference run are $Y_{ash,prim.cyclone,SSwf}$ = 0.051 kg kg^{-1}, $Y_{ash,sec.cyclone,SSwf}$ = 0.008 kg kg^{-1} and $Y_{ash,filter,SSwf}$ = 0.003 kg kg^{-1}, based on water free sewage sludge. It can be seen that the majority of the fly ash is separated by the primary cyclone. In Table 4.2, the fly ash yield and the carbon mass fraction are shown for different runs, wherein all respective fly ash fractions (prim. cyclone, sec. cyclone, filter) are cumulated. It can be seen that the fly ash yield is for all presented runs between 0.059 kg kg^{-1} and 0.072 kg kg^{-1}. The carbon mass fraction of the fly ash varied between 0.047 kg kg^{-1} and 0.110 kg kg^{-1} and was found to be dependent on gasification temperature.

Table 4.2: Fly ash and bed ash yields per water free sewage sludge and carbon content for experimental reference point

run	ϑ	n_{SC}	n_{O2}	n_{WHSV}	$Y_{flyash,SSwf}$	$Y_{bedash,SSwf}$	$y_{C,flyash}$	$y_{C,bedash}$
unit	°C	mol mol^{-1}	mol mol^{-1}	h^{-1}	kg kg^{-1}	kg kg^{-1}	kg kg^{-1}	kg kg^{-1}
ϑ1	659	1.03	0.259	0.54	0.072	0.404	0.110	0.045
ϑ2	778	0.97	0.256	0.53	0.063	0.413	0.092	0.031
ref	842	1.05	0.250	0.47	0.062	0.414	0.085	0.017
ϑ4	894	1.03	0.254	0.51	0.059	0.417	0.047	0.006
W1	848	1.21	0.252	0.27	0.065	0.411	0.066	0.016
SC4	849	1.98	0.256	0.54	0.070	0.406	0.055	0.014

4.6 Ash mineral composition

4.6.1 Main elements

Table 4.3 shows the main elemental analysis of the ash fractions of the reference run. The major components of the ash were calcium, silica, phosphorous, aluminum and iron. These elements originated from the mineral content of wastewater and additives for phosphorous precipitation. Due to the high phosphorous content, the ash can be used as fertilizer if it fulfills the respective regulations or as raw material for industrial fertilizer production. There was no considerable difference in the elemental composition of bed ash, primary cyclone, secondary cyclone and candle filter.

4.6.2 Heavy metals

Table 4.4 shows the heavy metal concentrations of water free sewage sludge and the ash streams from the gasification experiments. Furthermore, the German legal limits for fertilizers [49] in general and specifically for the deployment of sewage sludge as fertilizer [5] are given. It can be seen that the used dry sewage sludge already fulfills the legal limits for all components except of thallium. Depending on the species, the concentrations of the heavy metals in the ashes are different from those of the sewage sludge. For more volatile elements such as Hg, Cd, Pb and Tl, the concentrations in the bed ash is reduced compared to the sewage sludge, while these elements are found again in the fly ashes with increased concentrations. The bed ash fulfills all legal limits except of Nickel. However, the high Ni concentrations of the bed ash are assumed to originate from the high-temperature steel pipe of the reactor and are not attributed to the Ni present in the sewage sludge. Since industrial plants are refractory lined, the ash is expected to meet the Ni limits. The bed ash is only slightly below the Cu limit. The concentrations of zinc in the ash streams suggest that most of it stayed in the bed ash, however, according to the mass balance, some Zn seems to be evaporated and partially condensed in the secondary cyclone.

It has to be noted that in this study only the total value of chrome was measured, but not Cr^{VI} for which strict limits are imposed [49]. However, heavy metal concentrations of the bed ash from a commercial air-blown sewage sludge fluidized bed gasifier were reported in literature, and the Cr^{VI} concentration was below 0.5 mg kg^{-1}, which is below the legal limit [123]. From this commercial facility, also very low concentrations of Cd, Hg and Tl were reported, each below 0.2 mg kg^{-1}, 0.05 mg kg^{-1} and 0.5 mg kg^{-1}, respectively, and Pb was reported with 20 mg kg^{-1}. These values correspond well to the findings of this thesis. The Ni concentration was reported to be much lower in the commercial gasifier, underlining the above stated hypothesis that in this thesis the Ni content of the ash came from the high-temperature steel of the reactor pipe. Arsenic was with 3 mg kg^{-1} reported to be much lower in the commercial gasifier compared to this study, however there could also be differences in the sewage sludge composition, which is not given in [123].

Table 4.3: Main elemental analysis of ash fractions from experimental reference point

	bed ash	**fly ash**		
sampling position	overflow	primary cyclone	secondary cyclone	filter
	in kg kg^{-1}			
γ_{Al2O3}	0.105	0.105	0.107	0.108
γ_{BaO}	0.001	0.001	0.001	0.001
γ_{CaO}	0.235	0.252	0.302	0.335
γ_{Fe2O3}	0.098	0.095	0.115	0.108
γ_{K2O}	0.015	0.017	0.014	0.011
γ_{MgO}	0.025	0.029	0.031	0.031
γ_{MnO2}	0.003	0.002	0.003	0.002
γ_{Na2O}	0.004	0.004	0.004	0.003
γ_{P2O5}	0.141	0.128	0.137	0.135
γ_{SO3}	0.040	0.033	0.033	0.028
γ_{SiO2}	0.307	0.267	0.228	0.228
γ_{SrO}	0.001	0.001	0.001	0.001
γ_{TiO2}	0.005	0.006	0.006	0.006

Table 4.4: Heavy metal concentration in water free sewage sludge and in ash fractions from experimental reference point (ref). German legal limit is given as comparison. [a]German fertilizer law (DüMV), [b]German sewage sludge treatment law (AbfklärV2017), [c]for dry sewage sludge with 8% P_2O_5, for ash with 12% P_2O_5, [e]stricter limits for Cr^{VI}: 2 mg kg^{-1}

	sewage sludge	**bed ash**	**fly ash**			**German legal limit**
sampling position	-	overflow	primary cyclone	secondary cyclone	filter	
			in mg kg^{-1}			
γ_{As}	10	38	40	86	38	40[a]
γ_{Be}	1	1	1	1	1	-
γ_{Cd}	1.7	0.2	3.3	29	0.0	4[a,c]/6[a,d]
γ_{Co}	3	29	29	41	29	-
γ_{Cr}	377	828	1018	1939	828	900[a]/2[e]
γ_{Cu}	515	865	946	1552	865	900[b]
γ_{Hg}	0.4	0.0	0.1	0.5	0.0	1[a]
γ_{Mo}	7	25	36	81	25	-
γ_{Ni}	25	592	4639	6338	592	80[a]
γ_{Pb}	60	134	219	710	134	150[a]
γ_{Sb}	2	15	12	23	15	-
γ_{Se}	13	43	103	217	43	-
γ_{Sn}	134	75	122	195	75	-
γ_{Tl}	3	<0.3	<0.3	<0.3	<0.3	1[a]
γ_{V}	31	52	53	64	52	-
γ_{Zn}	1010	1607	1589	2291	1607	4000[b]

4.7 Elemental balances

This chapter discusses on the one hand the distribution of the fuel's carbon in the different product species for different temperatures and on the other hand the total retrieval of the main elements carbon, hydrogen and oxygen in all product species to assess the quality and plausibility of the experiments.

4.7.1 Carbon distribution for temperature variation

Figure 4.25 shows the elemental carbon yields for different gasifier temperatures. On the left y-axis, the carbon yield in tars, in bed ash and in fly ash is shown. On the right y-axis, the carbon yield in the syngas main components (CO, CO_2, CH_4, C_xH_y) as well as the total retrieval of carbon in all measured product species.

The carbon yield in tars was calculated as sum of carbon in gravimetric tars as measured from gravimetric tar concentration (section 4.2.4) and its elemental analysis (see section 4.2.2) as well as the carbon in benzene, toluene and xylene (benzene and ECN3) taken from the GC tar analysis. This approach adds the light tars to the gravimetric tars to represent a total tar amount.

The carbon yield in tars decreased with temperature, since the tars are thermally cracked at higher temperatures. The carbon yield in bed ash and fly ash decreased with increasing temperature since more char was gasified e.g. by the water-gas reaction at higher temperatures due to faster reaction rates.

The carbon yield in the syngas main components increased with temperature, since at higher temperature more char and tar is converted to gases such as CO, CO_2, and CH_4. The total carbon yield sum for all shown runs are close to 1 kg kg^{-1}, which means that approximately the same amount of carbon was found in the products as introduced with the sewage sludge.

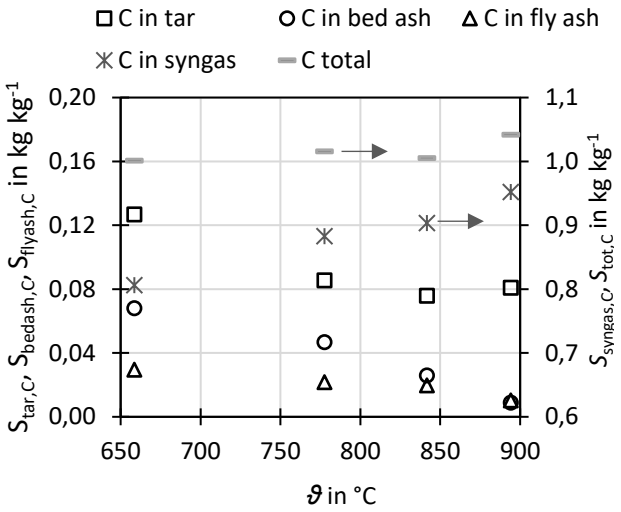

Figure 4.25: Carbon balance: Yield of carbon in syngas, tar, bed ash, fly ash and total sum for different gasifier temperatures

4.7.2 Retrieval of carbon, hydrogen and oxygen

This section discusses the balances for the three main elements carbon, hydrogen and oxygen in order to assess the quality of the measurements. The retrieval of these elements in the products were calculated by

$$E_{\mathrm{E}} = \frac{\sum_j x_{E,j}\, \dot{M}_j^{\mathrm{prod}}}{\sum_k x_{E,k}\, \dot{M}_k^{\mathrm{ed}}}, \quad \text{for } E\text{=C, H, O,} \tag{4-1}$$

wherein $\dot{M}_j^{\mathrm{prod}}$ and $\dot{M}_k^{\mathrm{ed}}$ are the mass flows of all relevant product species *j* and educt species *k* and $x_{E,j}$ and $x_{E,k}$ represent the mass fractions of the respective element in the product or educt species. The considered product and educt species are summarized in Table 4.5

Table 4.5: Considered product and educt species for calculation of elemental retrieval

	j	***k***
E_{C}	CO, CO_2, CH_4, C_xH_y, tar, fly ash, bed ash	fuel
E_{H}	H_2O, H_2, CH_4, C_xH_y, tar	fuel, steam
E_{O}	H_2O, CO, CO_2	fuel, steam, oxygen

It has to be noted that the yield and composition of fly ashes were not determined for all experimental points, due to the complicated sampling procedure. Therefore, the fly ash yield and composition of the reference point was used for the points where no data was available to enable the calculation of the carbon retrieval.

Figure 4.26 shows the carbon retrieval, which shows values between 0.90 and 1.05 for all experimental runs and for the majority between 0.95 and 1.05, thus within ±5 %. The carbon retrieval was thus very good. This attests that the results are of high quality and plausibility, since carbon is the most important indicator to assess the fuel conversion.

Figure 4.27 depicts the retrieval of hydrogen, which is between 0.94 and 1.06 for all runs excluding the run S4 with 1.18. The hydrogen retrieval can thus still be assessed as good (±6 % with one exception), however, not as good as the carbon retrieval.

Figure 4.28 shows that oxygen retrieval is for all runs between 1.03 and 1.26 with a mean value of 1.11. This means that for all runs, more oxygen was found in the products as introduced with the educts, which suggests systematic measurement errors. There are different possible error sources. According to the author's opinion, it is most important that the product species H_2O in the syngas has a considerable influence on the calculation of the O_2 retrieval due to its oxygen mass fraction of 0.89 kg kg^{-1} and the high quantity of H_2O present in the syngas. Furthermore, the measurement technique used to measure the H_2O concentration in the syngas (impact jet hygrometer) has higher inaccuracies than e.g. measurements methods used for permanent gases (e.g. NDIR). It could be possible that the H_2O concentration was always overestimated by the measurements. Another possible source of inaccuracies could be the sewage sludge analysis (oxygen is not measured but calculated as difference), errors in the syngas volume flow measurement or measurements of oxygen-containing permanent gases (CO_2, CO). However, the deviation of on average +11% is still acceptable for experimental work in 20 kW scale, but the over-retrieval of oxygen needs to be kept in mind when discussing or applying the experimental results of this work. It is suggested to improve H_2O concentration measurement in the syngas and syngas volume flow measurement for further studies.

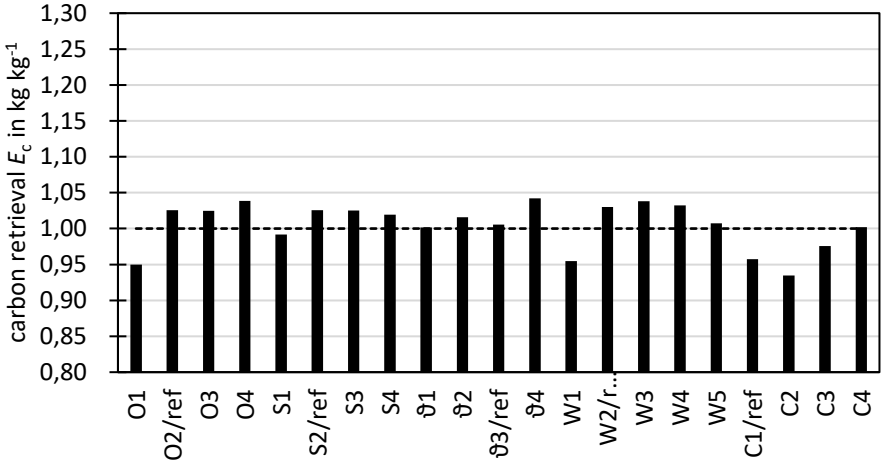

Figure 4.26: Retrieval of carbon as quotient of cumulative carbon in products and educts.

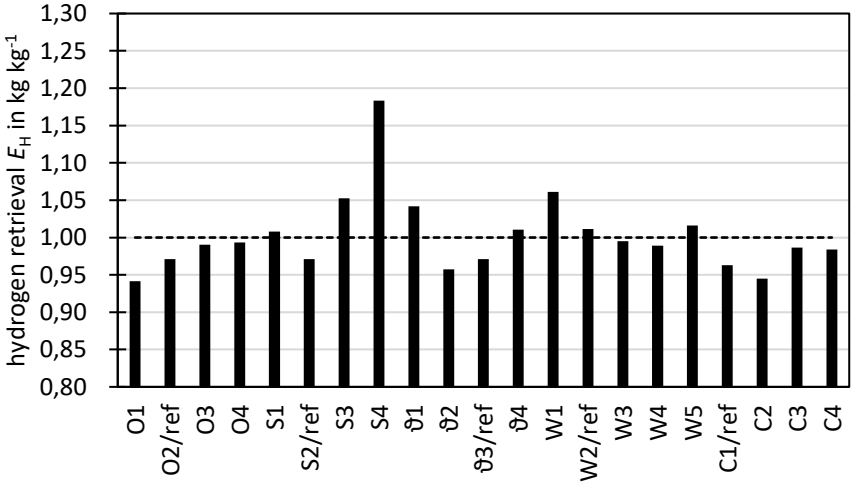

Figure 4.27: Retrieval of hydrogen as quotient of cumulative hydrogen in products and educts.

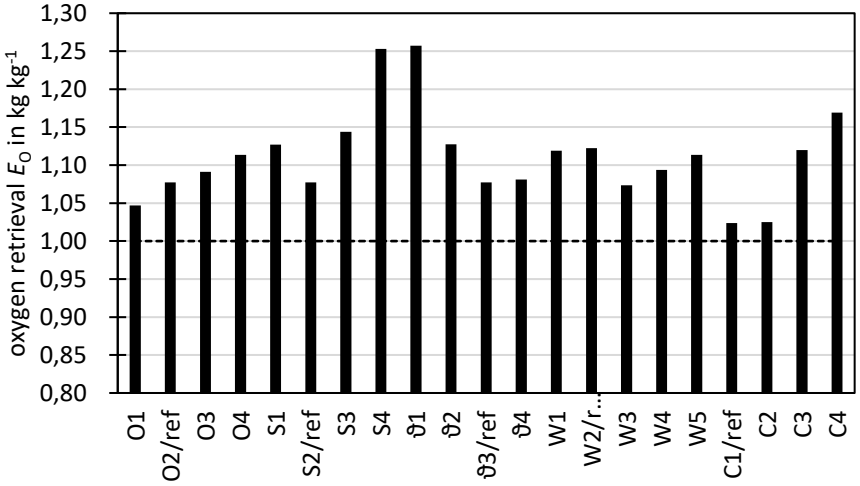

Figure 4.28: Retrieval of oxygen as quotient of cumulative oxygen in products and educts.

4.8 Behavior of sewage sludge ash as bed material

The fluidization behavior of the bed material during the experiments was good. The facility was in operation with sewage sludge for over 25 trial days with each a gasification operation of 4 h to 8 h. In most cases, the experimental conditions were varied several times per day to investigate different experimental points. Stable hydrodynamical conditions were reached quickly during the majority of the experiments, visible by a constant pressure drop over the fluidized bed.

However, bed melting and agglomeration have been observed on few occasions for operation points with low fluidization velocity of $u_0 < 0.2$ m s^{-1} (superficial velocity) corresponding to $u_0\ u_{mf}^{-1}\ (d_{p,50}) < 3$ and temperatures over 850 °C. In these cases, stable condition could be reached at the beginning of the experiments, but then a rapid temperature rise accompanied by partial bed material melting and agglomeration was triggered assumingly by a short interruption of the fuel supply. After that, fluidization was not possible anymore and the agglomerated bed material needed to be removed from the reactor. Short fuel supply interruptions also occurred at other operation points with higher fluidization velocity, but no negative effect was observed. Leading to the explanation that after the fuel supply interruption the endothermic effect of the fuel conversion ceased and the further supplied oxygen could exothermally oxidize char and metals (e.g. FeO) in the bed, additionally the electric heating supplied heat through the reactor's wall. Due to the low fluidization velocity, the bed was poorly mixed and therefore the temperature could rise above the ash melting temperature locally at the gasifier bottom. The author therefore advises to always ensure a good bed material mixing by maintaining sufficient fluidization velocity of $u_0\ u_{mf}^{-1}\ (d_{p,50}) > 3$ and temperatures below the shrinkage starting temperature for reducing conditions (see 2.3.3).

4.9 Discussion and conclusion experiments

It was shown that steam-oxygen fluidized gasification of sewage sludge works reliably in the investigated 20 kW scale and that the syngas contained high H_2 and CO concentrations and is thus suitable for synthesis of fuels and chemicals. The experimental results can be utilized for process design and to set up and validate a gasifier model, as accomplished in chapter 5, since the yields of product gas, char, tar and impurities as well as their dependencies on the operation conditions are presented. The distribution of carbon in syngas, bed ash and fly ash as well as tar was highly temperature dependend. For the reference run at 842 °C, the loss of carbon in tar and char was 0.04 kg kg^{-1} and 0.05 kg kg^{-1}, respectively.

It was found that steam-oxygen gasification of sewage sludge exhibited similar gas yield and gas composition, considering main species H_2, CO, CO_2, CH_4 and C_xH_y, as steam-oxygen gasification

of other biogenic fuels like wood or straw. However, syngas from sewage sludge contained significantly higher concentrations of H_2S, COS and NH_3 than syngas from wood gasification. While the tar concentrations were in the same range, the composition of tars differs between wood and sewage sludge gasification. GC analysis of sewage sludge tars revealed the presence of heterocyclic species of which pyridine had the highest concentration. This thesis used elemental analyses of gravimetric tars as a novel method, which disclosed that sewage sludge derived gravimetric tars have a carbon content of only around 0.5 kg kg^{-1} (compared to 0.9 kg kg^{-1} carbon for wood tar). The cause of that was suspected to be salts formed by NH_3, H_2S, carbonates and other syngas components during tar sampling and only to a lower extent heterocyclic tar species. It is therefore highly recommended to conduct an elemental analysis when using gravimetric tar analysis for gasification of sewage sludge and other fuels with high N and S content. When using GC analysis, it is recommended to quantify the tar species pyridine on top of the commonly analyzed species due to its high concentrations.

The temperature variation experiments indicated that the gas yield was enhanced and the tar yield decreased with increasing gasification temperature. It can therefore be concluded that the gasification temperature should be chosen as high as practically feasible (i.e., 850 °C to 900 °C) while staying below the shrinkage starting temperature (IDT), which can be lower under reducing conditions than under oxidizing conditions, to prevent bed agglomeration.

It was further found that the H_2/CO-ratio can be controlled efficiently by altering the steam to carbon ratio n_{SC}, as steam promotes the water gas shift reaction. Furthermore, it could be shown that the H_2/CO-ratio could be tailored to 2 (e.g., for methanol or DME-production) or 3 (for methanation) within a reasonable range of n_{SC}.

Since the sewage sludge ash contains calcium, the majority of the sludge's sulfur is bound in the bed ash. By adding limestone ($CaCO_3$) to the gasifier, this sulfur capture is enhanced and the H_2S and COS concentrations in the syngas are lowered, but due to equilibrium limitations, no complete capture could be obtained. Lowest H_2S and COS concentrations were found at a gasification temperature of around 750 °C, due to the overlapping temperature-dependent equilibriums of calcination and sulfur capture. In addition, low n_{SC} increased sulfur capture.

Tar concentrations, especially gravimetric tar and GC tar species with methyl groups, are reduced by addition of limestone as bed additive. The smallest tested additive ratio of 0.06 kg kg^{-1} already achieved significant reduction in gravimetric tars that are the main contributors to gas clogging of high temperature facility parts (e.g. gas cooler), whereas higher additive ratios yielded comparably smaller additional gravimetric tar reductions. Therefore, considering cost of limestone as well as the energetic penalty and CO_2-emission caused through in-situ calcination of limestone, additive ratios of 0.06 kg kg^{-1} or even lower are recommended.

In the experiments, the majority of the ash is received as bed ash. Hazardous cadmium, mercury and thallium contained in the sewage sludge were transferred into the gas phase; therefore the bed ash was found to be free of or very lean in those elements, which is beneficial for the ash's application for fertilizer production. These elements were found in higher concentrations in the cyclone and filter ash. Less volatile heavy metals, such as Zn, Cu, Pb and Cr, stayed mostly in the bed ash.

Overall, the steam-oxygen gasification proved to be an efficient and technically feasible process for sewage sludge treatment. The process can play a role in closing the loop for carbon by converting the organic fraction of sewage sludge or other fuels to carbon-containing biofuels or chemicals as well as in closing the loop for phosphorous that can be recovered from the ash.

Some important aspects of steam-oxygen gasification of sewage sludge were not or insufficiently covered by this thesis and are therefore suggested to be part of further studies. These points are discussed in the following.

In this thesis, variation of n_{WHSV}, which is correlated to the residence time of the solids in the bed, showed no clear trends, however, only few experimental points were conducted. Since n_{WHSV} is an important parameter for reactor design, further investigations should be done. In addition, dedicated investigations of gas residence times in the bed and the freeboard would generate valuable information for reactor design.

It is known from literature that syngas from sewage sludge contains further impurities that were not measured in this work. One example is hydrogen cyanide (HCN) which was found in considerable concentrations in literature [126]. HCN is poisonous and water-soluble and thus makes treatment of wastewater from syngas scrubbers necessary. Furthermore, HCl is formed during sewage sludge gasification [68]. However, it is very difficult to measure HCl accurately in a tar-loaded syngas. Therefore, the HCl content of the syngas was not further studied in this work. A further field of interest is assessing the corrosion potential of the syngas due to the content of alkali, chlorine and lead.

This thesis had its focus on the gas composition and only few solid samples were collected and evaluated. Future work should focus more on the behavior of solids such as char conversion dependent on reactor design and solid residence time. Also, different sewage sludges show a different behavior in respect to attrition, which could lead to a higher fly ash fraction. It would thus be interesting to correlate the waste water treatment process (e.g. utilized phosphorous precipitation additive), the drying process (dryer technology type) with the mechanic and thermochemical behavior of the sewage sludge in the gasifier. Also, analysis methods such as SEM microscopy and XRD mineral phase analysis could enhance the knowledge on the physical and chemical conversion

of the solids during gasification. These insights are also important to optimize the ash for phosphorous extraction or direct fertilizer production from ash. Furthermore, bed additives could be studied to improve the fertilizer performance of sewage sludge ash during gasification.

In the used electrically heated facility, n_{O2} was disconnected from the actual energy demand of the gasification. Due to the high and unknown heat losses of the facility, it was not possible to conduct an energy balance, so the actual energy demand of the gasification could not be determined. It was thus not possible to calculate a process efficiency. Chapter 5 of this work uses simulation as a tool to calculate the process performance and efficiency for adiabatic conditions.

5 Gasifier modeling and simulation

This chapter describes the development of a process model for the steam-oxygen gasification of sewage sludge, followed by a simulative sensitivity analysis of the gasification process focusing on the actual oxygen requirement for autothermal gasification and the resulting cold gas efficiency and gas compositions, which could not be determined in the experiments due to the electrically heated facility. Further simulations were conducted to determine optimized gasifier operation conditions.

5.1 Gasifier model requirements and method selection

The following requirements were set for the gasifier model:

1. calculating the steady state energy balance to determine the needed oxygen ratio for autothermal gasification
2. describing the steady state yields of the most relevant products of the gasification and their sensitivity to the operation parameters in accordance with the experimental data
3. short calculation time
4. ability to include the gasifier model in a larger process simulation e.g. for assessing production chains of synthetic biofuels or biochemicals

To satisfy requirement 1, the model needs to be able to calculate the mass and energy balance of the gasification process for a specified gasifier temperature. In the steam-oxygen gasification, the gasifier is heated by feeding oxygen, which in turn changes the mass balance through oxidation reactions. Therefore, the mass and energy balances need to be solved in one equation system or iteratively in series. For this, the model has to describe the influence of the oxygen ratio n_{O2} on the product composition accurately.

To satisfy requirement 2, different model approaches are possible. The simplest way would be to deduce strictly empirical functions from the experimental product yields in dependence of all relevant parameters. Such an empirical model typically allows simulation results with good agreement to the experimental data and has very short calculation times. However, the model would not be capable of any extrapolation beyond the experimental data. It would also be hardly possible to use this model if the process is altered in any manner, e.g., for slightly altered fuel elemental analyses.

The other extreme would be a rigorous model where a detailed 3-D fluid dynamic model for gases and solids is used together with a detailed set of chemical reactions with the respective reaction kinetics. Such models can allow a very accurate description of the process including extrapolation

outside the experimental data that were used to evaluate the model. However, very high efforts are required to develop and validate such a model. In addition, the calculation time is typically several days on a personal computer for low detail simulations whereas for very detailed simulations typically a supercomputer is necessary, which is contradicting requirement 3. Also, the integration in a larger process simulation is typically difficult, which is contradicting requirement 4.

An approach between these two extremes is needed, aiming at reducing calculation time and modeling effort but at the same time maintaining some extrapolation capability. For fluidized bed gasification, the author has already co-developed and used a 1-D fluidized bed model with a simplified kinetic reaction model [94, 95]. This model had short calculation times and proved a good agreement with experimental data for some parameters while for other it was poorer than a much simpler equilibrium calculation. The main challenge was the development of adequate kinetic models for the relevant pyrolysis and gasification. From this previous experience it was concluded that the still high development and validation efforts that are needed to enable a 1-D model to be superior to a simpler 0-D model are not justified for the specific application of this thesis.

An even simpler but powerful approach for reaction simulation is the thermochemical equilibrium calculation using commercially available tools (e.g. FactSage®, AspenPlus®). These calculators enable a basic description of the product yields and their dependencies on the operation conditions of most chemical reaction systems without requiring any specific model development. The drawback is that for fluidized bed gasification, some reactions such as tar and char formation are not in equilibrium and therefore cannot be correctly described. In addition, an equilibrium calculation is independent of the reactants' residence time, and therefore kinetic effects cannot be included in that model.

To decide whether kinetics should be included in the gasifier model, the experimental data, shown in chapter 4, were analyzed: Varying n_{WHSV}, and with that, the gas and fuel residence time, had no specific effect on the gasification products, e.g. permanent gas yield, tar yield and impurity yield. This means either that the gasification product yields are little influenced by fuel and gas residence times, or that the used experimental methods were incapable of detecting this influence. In any case, a validation of a kinetic fuel conversion model would not be possible with the experimental data of this thesis due to the lack of sensitivity on residence times.

Taking into account all discussed points, it is concluded that an equilibrium model can adequately describe the product yields of the permanent gases. To describe the yields of char, tar and other impurities, the equilibrium model needs to be complemented with empirical yield functions for these species derived from the experimental results. With such a model, all set requirements can be met.

The model can be conveniently realized with the software package AspenPlus®, which already has built-in tools for iterative calculation of mass and energy balances and for equilibrium calculations. In addition, customized code can be used to add the empirical models. It is further possible to incorporate the gasifier model into a larger AspenPlus® process model. The following sections describe the model in detail.

5.2 Gasifier model description

The core of the gasifier model is the Aspen Plus® "RGibbs" equilibrium calculator. This calculator comprises a thermodynamic database containing correlations on the Gibbs energy of various chemical substances in dependency of temperature and pressure and a numerical solver that calculates the product composition for minimized Gibbs energy. The equilibrium calculator needs the following input: mass flow of the chemical elements of the educts, temperature and pressure. The equilibrium model is then able to predict the main products of the gasification (H_2, CO, CO_2, H_2O, ash species) and their dependency on operation parameters (such as ϑ, n_{SC}, n_{O2}) assuming the reaction to be in equilibrium state. As some reactions do not reach thermochemical equilibrium in a fluidized bed gasifier, the equilibrium model can be complemented by other modeling approaches as explained in the following.

5.2.1 Gasifier model in Aspen Plus

For the gasifier model, the feed streams are sewage sludge, steam, oxygen and optional limestone as additive. The gasification temperature ϑ needs to be specified. Aspen Plus® is able to calculate the required oxygen amount to achieve the specified gasification temperature for adiabatic conditions with the built-in iterative method "design spec". Since the model is only foreseen to simulate atmospheric gasification, the pressure was always set to 1 bar absolute pressure.

The fuel conversion in fluidized bed gasification is, to a considerable extent, determined by the fuel pyrolysis [24, 127]. In pyrolysis, the large solid fuel molecules are broken down into smaller molecules by thermal cracking of chemical bonds (see section 2.1.1). Pyrolysis products contain tar species, hydrocarbons (C_xH_y) and CH_4 as well as impurities such as NH_3, H_2S, COS and HCl [128]. After pyrolysis, these products undergo further gasification reactions but are partially still present in the product gas since the residence time in the fluidized bed is too short for these gases to reach the thermochemical equilibrium. In particular CH_4 and C_2-, C_3- and C_4-hydrocarbons represent approximately 0.2 J J^{-1} to 0.3 J J^{-1} of the higher heating value of the product gas [19, 20, 129–131]. These species must therefore not be neglected, but their formation cannot be predicted with the thermochemical equilibrium. To overcome this, empirical correlations have been implemented in

this model to calculate the yields of these so-called non-equilibrium species. The empirical models were parametrized by the experiments of this thesis.

The combination of equilibrium model and empirical model was realized as shown in Figure 5.1. A part of the sewage sludge stream is converted into non-equilibrium species in a separate block using empirical correlations. The reaction enthalpy of this conversion, ΔH_R, is conveyed into the RGibbs reactor to allow the isothermal operation of the non-equilibrium block. The residual elements of the sewage sludge as well as steam and oxygen are fed into the RGibbs reactor. The products of both reactors are then mixed to form the gasification products syngas, char and ash. To compare simulation and experiment, it is also possible to run the gasifier simulation with a fixed n_{O2} at isothermal non-adiabatic conditions.

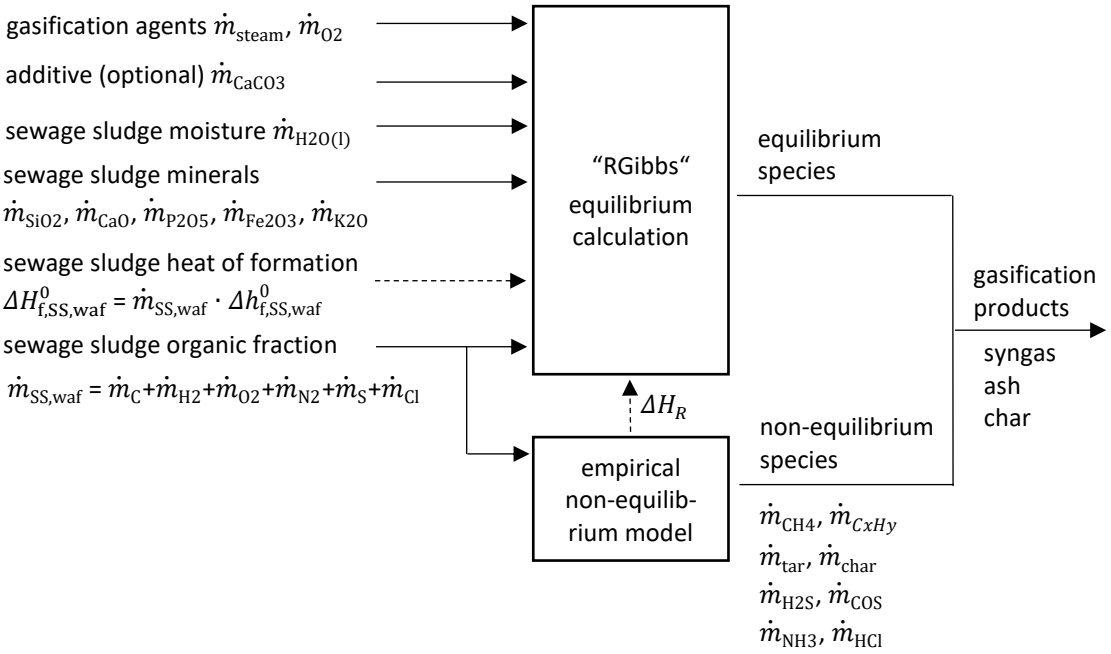

Figure 5.1: Gasifier model in Aspen Plus®

5.2.2 Modeling of educt and product species

The organic fraction of sewage sludge was modeled as a material stream consisting of the components C, H_2, O_2, N_2, S and Cl_2 according to the fuel elemental analysis (Table 3.1) and an energy stream $\Delta H^0_{f,SS,waf}$ which was calculated as product of the heat of formation (see section 2.2.3) and the mass flow of the sewage sludge. The inorganic fraction of the sewage sludge was modeled by a stream comprised of the major ash species according to the sewage sludge ash analysis (Table 3.2).

The Aspen Plus model considers the following chemical species to describe the syngas: H_2O, N_2, H_2, CO, CO_2, CH_4, H_2S, COS, NH_3, HCl as well as further hydrocarbons and tar species that were summarized by the three model compounds C_2H_4 (ethene), C_6H_6 (benzene), $C_{10}H_8$ (naphthalene)

as described in Table 5.1. Another product stream is the ash for which the following components are considered in the equilibrium reactor: Fe, FeO, CaO, $CaCO_3$, CaS, SiO_2, Fe_2O_3, Fe_3O_4, MgO, Al_2O_3, K_2O, KCl, $CaCl_2$, P_2O_5.

Table 5.1: Model compounds in AspenPlus® for hydrocarbons and tar species

Gasification product from experiment	**model compound in AspenPlus®**	**modeling approach to describe experimental data**
hydrocarbons C_xH_y (C_2H_4, C_2H_6, C_3H_6, C_3H_8, C_4H_{10})	C_2H_4 (ethene)	The total carbon mass contained in the species C_2H_4 in the simulation was set to equal the cumulative carbon mass of all GC-measured hydrocarbons C_xH_y in the experiment: $m_{C,C2H4,sim} = m_{C,CxHy,exp}$.
gravimetric tar (ECN1)	$C_{10}H_8$ (naphthalene)	Carbon amount of $C_{10}H_8$ in the model was set to equal the carbon amount in measured gravimetric tar.
GC tar (only benzene and ECN3 tar species)	C_6H_6 (benzene)	Carbon amount of C_6H_6 in the model was set to equal the carbon amount of measured benzene and ECN3 tar species (toluene and xylene). Further GC tar components were omitted to avoid overlapping with gravimetric tars [108]. By this approach, the model is able to describe the total tar amount in the syngas sufficiently while still differentiating between gravimetric and GC tars.

5.3 Parameterization of non-equilibrium species

As described above, most of the gasification product species can be described adequately with the thermochemical equilibrium. However, for some product species, the so-called non-equilibrium species, the concentrations measured in experiments vary considerable from the thermochemical equilibrium. The experimental elemental yields of these non-equilibrium species $S_{i,E}$ are thus parameterized from experimental data by using equation (2-18).

The evaluation of the experimental data showed that the elemental yields of CH_4, C_2H_4, C_6H_6 (GC tar) and NH_3 were almost constant for all experiments of this study (see section 4). Therefore, these species were modeled with constant yields, deducted from the experimental reference point.

The species $C_{10}H_8$ (gravimetric tar), carbon in fly ash, carbon in bed ash, H_2S and COS showed to be dependent on at least one experimental parameter. This was modeled by first deducting a yield for the reference point with the index "ref". Additional parameterization was done subsequently

by using the relative yield $\xi_{j,E}$ to parameterize the deviation of the elemental yield from the reference point as function of relevant operation parameters:

$$\xi_{j,E}(\vartheta, n_{SC}, n_{CaCo3}) = \frac{S_{j,E}(\vartheta, n_{SC}, n_{CaCo3})}{S_{j,E,ref}} \,. \tag{5-1}$$

In return, the Aspen Plus® non-equilibrium model uses the equation (5-1) resolved to $S_{j,E}$ to calculate the elemental yield:

$$S_{j,E}(\vartheta, n_{SC}, n_{CaCo3}) = S_{j,E,ref} \cdot \xi_{j,E}(\vartheta, n_{SC}, n_{CaCo3}) \,. \tag{5-2}$$

5.3.1 Non-equilibrium species yields at reference point

In a first step, the model has been parameterized with the yields of the non-equilibrium species with data from the experimental reference point (ϑ = 842 °C, n_{SC} = 1.05 mol mol^{-1}, n_{O2} = 0.25 mol mol^{-1}) as shown in Table 5.2. As no experimental data for HCl is available in this thesis, the yield $S_{HCl,C}$ = 0.5 was deducted from experimental findings in literature [68]. As mentioned above, the yields of CH_4, C_2H_4, C_6H_6 (GC tar) and NH_3, are directly used as constants while the yields of $C_{10}H_8$ (gravimetric tar), carbon in fly ash, carbon in bed ash, H_2S and COS that have the index "ref", are later on used in equation (5-2) to account for operation parameter sensitivity.

Table 5.2: Non-equilibrium yields calculated from experimental reference point of this work, HCl yield from literature [68]

$S_{CH4,C}$	$S_{C2H4,C}$	$S_{C6H6,C,ref}$	$S_{C10H8,C,ref}$	$S_{flyash,C,ref}$	$S_{bedash,C,ref}$	$S_{NH3,N}$	$S_{HCl,Cl}$
		in kg_C kg_C^{-1}				in kg_N kg_N^{-1}	in kg_{Cl} kg_{Cl}^{-1}
0.0881	0.0757	0.0423	0.0368	0.0197	0.0260	0.0890	0.5000

Table 5.3 shows the elemental yields for H_2S and COS. It has to be noted that these species are already formed by the equilibrium model. However, additional formation of these species in the non-equilibrium model are needed to match the experimental yields. Therefore, the non-equilibrium yields have been calculated as the difference between the experimental yield and the yield from the "RGibbs" equilibrium reactor at the operation conditions of the experimental reference point:

$$S_{j,S,ref} = S_{j,S,exp,ref} - S_{j,S,eq,ref}, \quad \text{for } j = H_2S, \text{ COS}. \tag{5-3}$$

Table 5.3: Experimental H_2S and COS elemental yields at reference point $S_{j,S,exp,ref}$, Aspen Plus® equilibrium elemental yields $S_{j,S,eq,ref}$ at conditions of reference point, and non-equilibrium elemental yields $S_{j,E,ref}$ calculated as difference between experimental and equilibrium yield

$S_{H2S,S,exp,ref}$	$S_{H2S,S,eq,ref}$	$S_{H2S,S,ref}$	$S_{COS,S,exp,ref}$	$S_{COS,S,eq,ref}$	$S_{COS,S,ref}$
0.1555	0.0929	0.0626	0.0050	0.0021	0.0029

5.3.2 Sensitivity of non-equilibrium species to ϑ

The yields of gravimetric tars, carbon in bed ash and carbon in fly ash were in the experiments identified to decline noticeably with rising gasification temperature ϑ (see chapter 4). Figure 5.2 to Figure 5.5 show the elemental yields $S_{j,C}$ calculated from the experiments as well as the regression functions for yield deviation $\xi_{j,E}$ in respect to the reference point (ϑ = 842 °C).

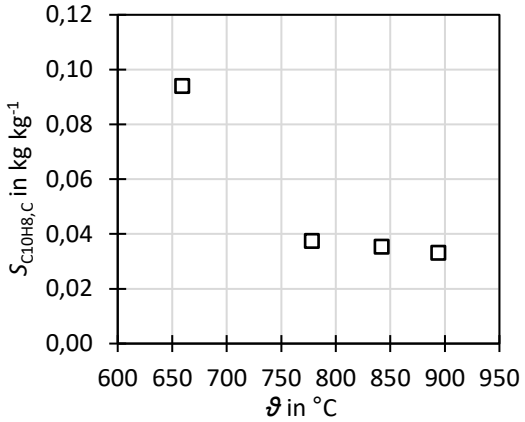

Figure 5.2: Experimental elemental yield of gravimetric tar, $S_{C10H8,C}$, based on sewage sludge carbon content at different ϑ

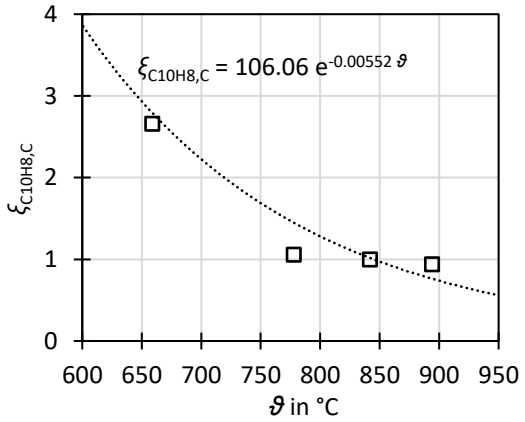

Figure 5.3: Relative yield $\xi_{C10H8,C}$, expressing deviation from reference point at different ϑ and regression function for the non-equilibrium model

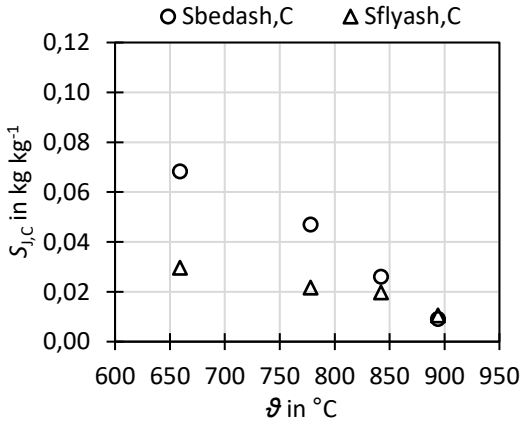

Figure 5.4: Experimental elemental yield of carbon in bed ash and carbon in fly ash, $S_{bedash,C}$ and $S_{flyash,C}$, based on sewage sludge carbon content at different ϑ

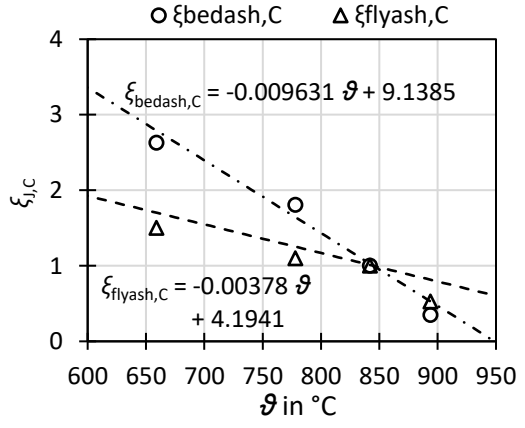

Figure 5.5: Relative yield $\xi_{bedash,C}$ and $\xi_{flyash,C}$ expressing deviation from reference point at different ϑ and regression function for the non-equilibrium model

The regression functions of $\xi_{bedash,C}$ and $\xi_{flyash,C}$ become negative at high temperatures which is futile for the model. Therefore, these functions were implemented into Aspen Plus® using an if-cause that does not allow the function value to become negative, but sets it to zero instead.

5.3.3 Modeling of non-equilibrium species sensitive to n_{SC}

In the experiments (see section 4.2.5), the gravimetric tar yield was found to be dependent on the steam-to-carbon ratio. This behavior is explained in literature [132, 133] with steam being a reactant promoting tar reforming (R 10). This dependency is shown in Figure 5.6 and could be derived from the measured tar concentration (Figure 4.10). To incorporate this dependency in the model, the relative yield of gravimetric tar expressing deviation from the reference point (n_{SC} = 1.05 mol mol^{-1}) was used to calculate a regression function for the model (Figure 5.7).

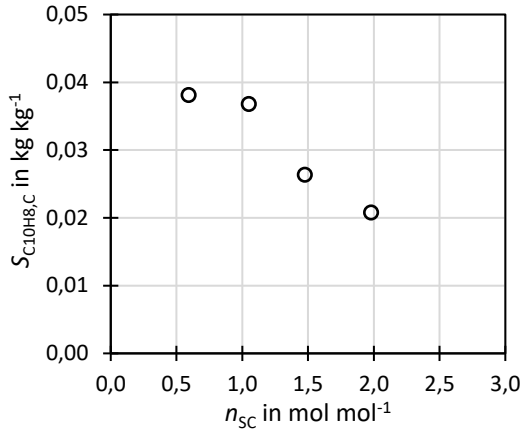

Figure 5.6: Experimental elemental yield of gravimetric tar, $S_{C10H8,C}$, based on sewage sludge carbon content at different n_{SC}

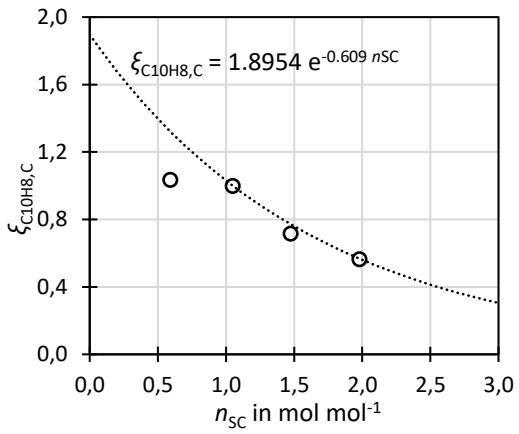

Figure 5.7: Relative yield $\xi_{C10H8,C}$ expressing deviation from reference point at different n_{SC} and regression function for the non-equilibrium model

5.3.4 Modeling of non-equilibrium species sensitive to n_{CaCO3}

Gravimetric tar yield

In the experiments, the gravimetric tars were found to be dependent on the limestone additive ratio since limestone is catalytically active for the cracking of gravimetric tars. This dependency could be derived from the experiments and the elemental yields of gravimetric tars (model component $C_{10}H_8$) as shown in Figure 5.8, while Figure 5.9 shows the derivation from the experimental reference point (n_{CaCO3} = 0).

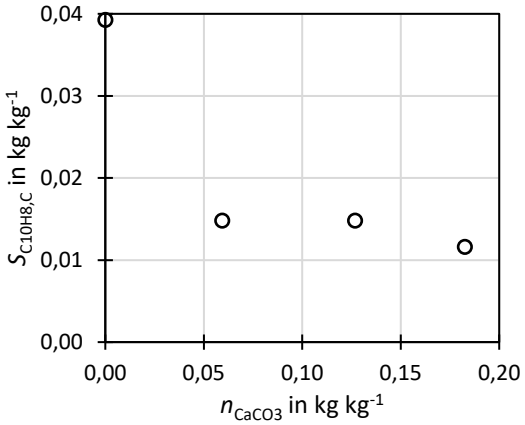

Figure 5.8: Experimental elemental yield of gravimetric tar, $S_{C10H8,C}$, based on sewage sludge carbon content at different n_{CaCO3}

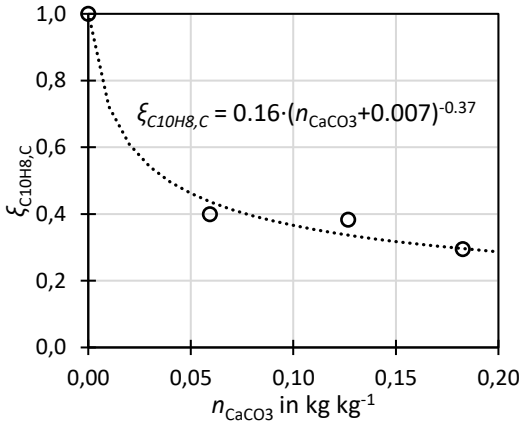

Figure 5.9: Relative yield $\xi_{C10H8,C}$ expressing deviation from reference point at different n_{CaCO3} and regression function for the non-equilibrium model

H_2S and COS yield

Also, H_2S and COS yields are dependent on the limestone additive ratio since the sulfur is captured as CaS by equilibrium reactions. However, in the experiments (see section 4.3) the equilibrium was not reached and the total yields of H_2S and COS were found to be higher than those from the equilibrium. Therefore, additional regression functions for non-equilibrium yields are used in this model. The non-equilibrium elemental yields of H_2S and COS are calculated as the difference between the experimental elemental yields and the equilibrium elemental yields and are shown in Figure 5.10 and Figure 5.12 over the limestone additive ratio. In other words: The RGibbs reactor of Aspen Plus® already accounts for sulfur capture in CaS in equilibrium state. The non-equilibrium yields, $S_{H2S,S}$ and $S_{COS,S}$ account for additional H_2S and COS contents in the syngas that go beyond the equilibrium state. The regression functions used for the non-equilibrium model are shown in Figure 5.11 and Figure 5.13.

It has to be noted that the results of Aspen Plus® RGibbs reactor model were found to be slightly different from those of FactSage® (see section 4.3.5); however, the H_2S and COS concentrations are in the same range. This behavior could origin from different databases or calculation algorithms. The COS yields of the experimental point for n_{CaCO3} = 0.18 kg kg^{-1} is slightly below the Aspen Plus® equilibrium whereas it is slightly above the FactSage® equilibrium. This point is thus not used for calculation of the regression function $\xi_{COS,S}$.

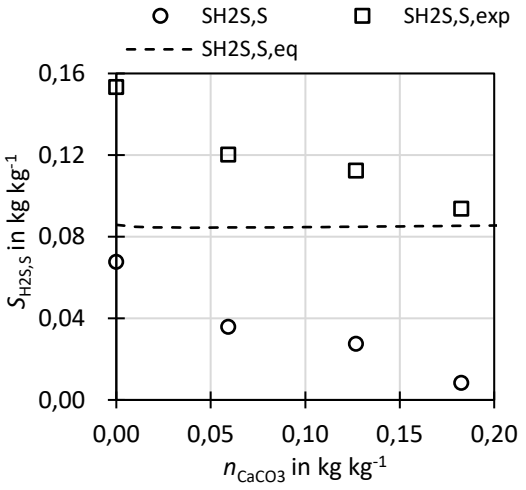

Figure 5.10: H_2S elemental yield from Aspen Plus® RGibbs reactor, $S_{H2S,S,eq}$, from the experiments, $S_{H2S,S,exp}$, non-equilibrium elemental yield, $S_{H2S,S}$, as difference of experiment and equilibrium at different n_{CaCO3}

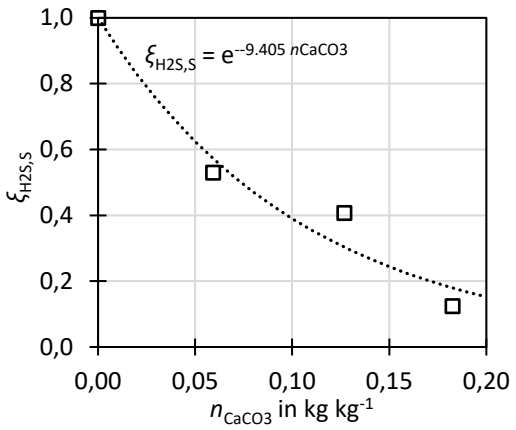

Figure 5.11: Relative yield $\xi_{H2S,S}$ expressing deviation from reference point for different n_{CaCO3} and regression function for the non-equilibrium model

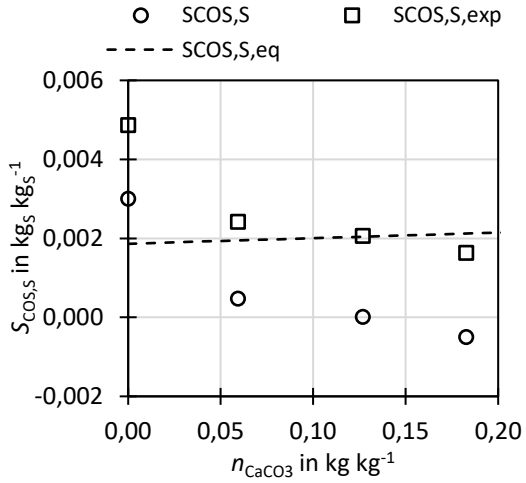

Figure 5.12: COS elemental yield from Aspen Plus® RGibbs reactor, $S_{COS,S,eq}$, from experiments, $S_{COS,S,exp}$, non-equilibrium elemental yield, $S_{COS,S}$, as difference of experiment and equilibrium at different n_{CaCO3}

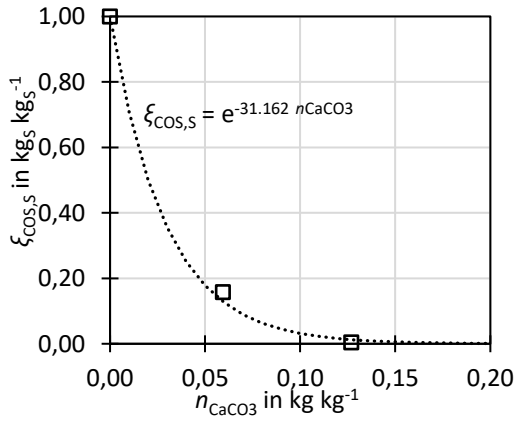

Figure 5.13: Relative yield $\xi_{COS,S}$ expressing deviation from reference point at different n_{CaCO3} and regression function for the non-equilibrium model

5.4 Comparison of simulation and experiment

This section compares the simulation results with the experiments to verify the accuracy of the model. For this, simulations with similar operation conditions as the experiments were conducted as summarized in Table 5.4.

Table 5.4: Operation conditions of simulations for comparison with experiments

		variation of			
		ϑ	n_{SC}	n_{O2}	n_{CaCO3}
ϑ	°C	600 - 950	850	850	850
n_{SC}	mol mol^{-1}	1.0	0.5 - 2.8	1.0	1.0
n_{O2}	mol mol^{-1}	0.25	0.25	0.1 - 0.5	0.25
n_{CaCO3}	kg kg^{-1}	0	0	0	0 - 0.25

5.4.1 Permanent gases and H_2O

This section compares permanent gas and steam concentrations of simulation and experiment.

Temperature variation

Figure 5.14 and Figure 5.15 show comparisons of simulation results with the experimental data for syngas composition and gas yield for variation of gasification temperature.

A very good agreement between simulation and experiment was found for concentrations of CO, CH_4, C_xH_y and H_2O (except for 650 °C). For H_2 and CO_2 the trends are in agreement, however, the simulation shows higher H_2 and lower CO_2 concentrations. The higher H_2 prediction of the model is related to the equilibrium assumption for the water gas shift (WGS) reaction R 11 where H_2 is formed. However, WGS cannot be the only influencing factor since the simulation has lower CO_2 but higher H_2 concentrations than the experiment and matching CO and H_2O prediction. Other influences contributing to this deviation could be inaccuracies in the measurements of concentrations and gas yields. By looking at the elemental balances of the experiments, it can be seen that the retrieval (input/output balance) of carbon and hydrogen fits very well for almost all experimental points (see section 4.7.2), whereas for all cases more oxygen was detected in the output streams than introduced with the input streams. Possible measurement errors that could result in this imbalance for oxygen are overestimation of H_2O and CO_2 concentration, which would be in line with the simulation results. For the experimental point at 650 °C, it is expected that due to the low-temperature a high amount of tar species and other hydrocarbons are formed that could not be measured.

The dry and N_2-free gas yield shows a good agreement, attesting a successful parameterization of the char and tar yield, which are directly influencing the permanent gas yield.

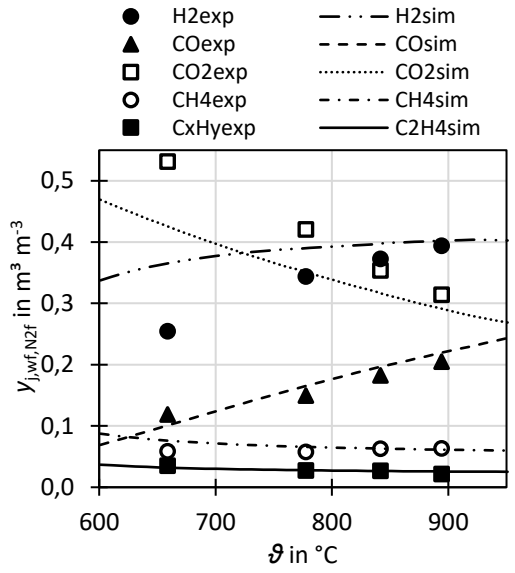

Figure 5.14: Comparison of simulation and experiment for permanent gas concentrations on water free and N_2-free basis for different ϑ

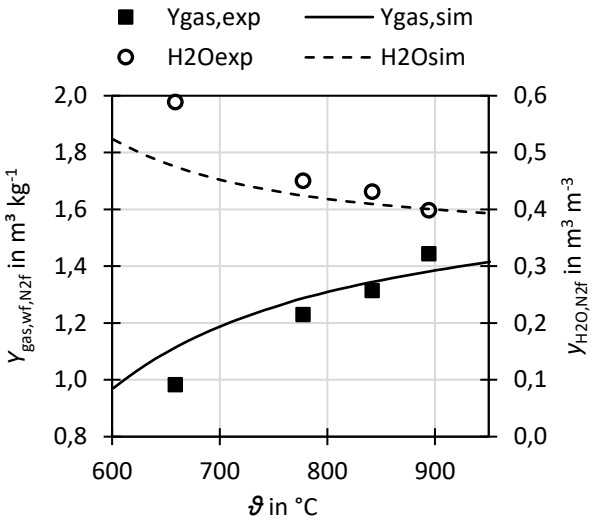

Figure 5.15: Comparison of simulation and experiment for H_2O (steam) concentrations on N_2-free basis as well as N_2-free, water free gas yield per water ash free sewage sludge for different ϑ

Oxygen ratio variation

Figure 5.14 and Figure 5.15 show variation of the oxygen ratio n_{O2}. Experiments are available for n_{O2} = 0.2 – 0.28. In this range, the gas concentration trends of the simulation are very similar to the experiment. Similarly to the above shown ϑ-variation, the values for CO_2 and H_2 differ slightly between simulation and experiment, which is acceptable. As already described in chapter 4, higher n_{O2} leads to combustion of H_2 and CO and thus formation of CO_2 and H_2O. This reaction is described well by the used equilibrium approach.

For the water free and N_2-free gas yield, the simulation shows a decreasing trend with the oxygen ratio, which is related to the combustion of H_2 to H_2O since H_2O is not considered in the permanent gas yield. The agreement for the gas yield is very good for $n_{O2} > 0.25$. The experimental point at $n_{O2} = 0.2$ does not match to the simulations trend. A reason for that could be a decreased char conversion through oxidation in the experiment for lower oxygen ratios. Due to the limited experimental points and lack of data on char conversion behavior in dependency to n_{O2}, it was decided to not parameterize the model in this respect. Also, for achieving relevant gasification temperatures of 750 °C - 900 °C, typically $n_{O2} > 0.25$ is required. The overall agreement of simulation and experiment is considered sufficient to describe the gasification for process simulation.

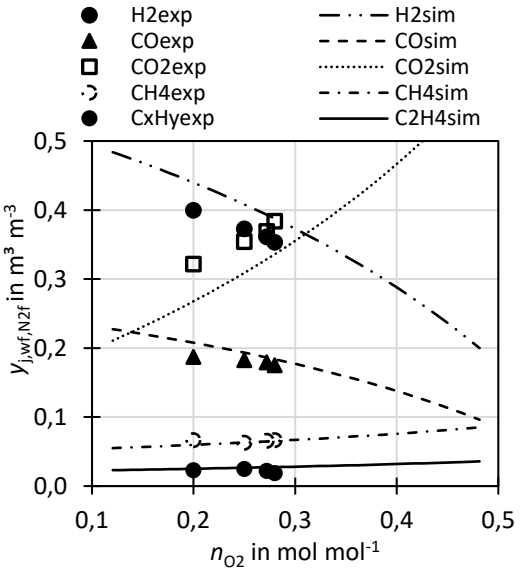

Figure 5.16: Comparison of simulation and experiment for permanent gas concentrations on water free and N_2-free basis for different n_{O2}

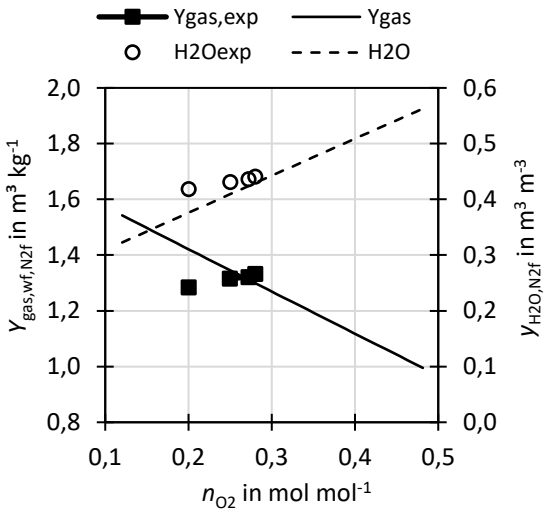

Figure 5.17: Comparison of simulation and experiment for H_2O (steam) concentrations on N_2-free basis as well as N_2-free, water free gas yield per water and ash free sewage sludge for different n_{O2}

Steam to carbon ratio variation

Figure 5.18 and Figure 5.19 show the permanent gases for variation of n_{SC}. The dominating effect is the water gas shift reaction R 11 causing decreasing CO concentrations and increasing H_2 and CO_2 concentrations for increasing n_{SC}. The equilibrium approach of the model describes this well. Consequently, the experimental and simulative concentration trends are in good agreement. Similar to the other variations, namely variation of ϑ and n_{O2}, the values for CO_2 and H_2 differ slightly between simulation and experiment within an acceptable range. The permanent gas yield is increasing since through water gas shift reaction, H_2O is converted into permanent gases H_2 and CO_2 but also due to enhanced tar reforming which has been empirically modeled as described above.

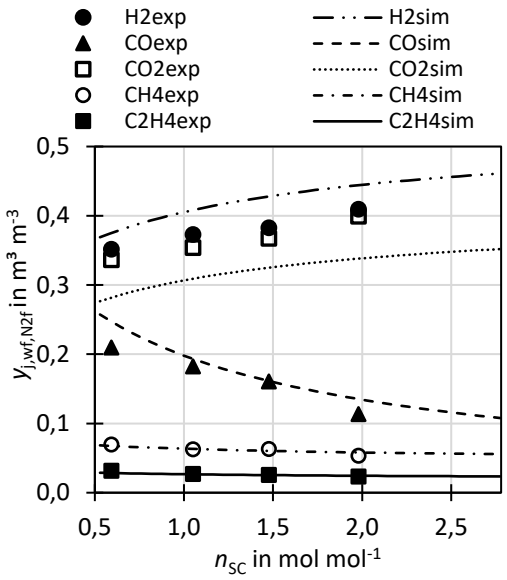

Figure 5.18: Comparison of simulation and experiment for permanent gas concentrations on water free and N_2-free basis for different n_{SC}

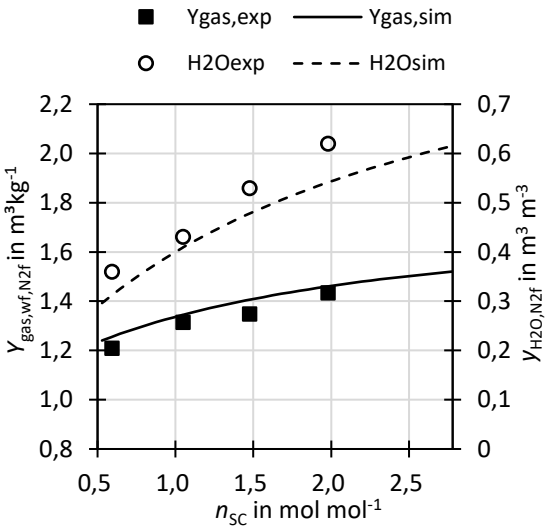

Figure 5.19: Comparison of simulation and experiment for H_2O (steam) concentrations on N_2-free basis as well as N_2-free, water free gas yield per water and ash free sewage sludge for different n_{SC}

5.4.2 Tar concentration

Figure 5.20, Figure 5.21 and Figure 5.22 compare the tar concentration of measurements and simulation for different ϑ, n_{SC} and n_{CaCO3}, respectively. As explained above, the model uses two tar species, benzene (C_6H_6) and naphthalene ($C_{10}H_8$). With C_6H_6 being the model component of light GC tars considering only the species benzene and those of ECN3 group (toluene, xylene) to avoid overlapping with gravimetric tars. The simulation result of the model species C_6H_6 is thus compared to the sum of the measured benzene and ECN3. The second tar model component, $C_{10}H_8$, is representing gravimetric tar and is thus compared to measured gravimetric tar. As mentioned in section 4.2.2, the standardized gravimetric tar measurement captures not only tar species, but also other precipitation. To overcome this and to enable a suitable comparison of model tar components and measurement, the tar concentration is shown in tar-bound carbon mass per dry STP volume of syngas. The achieved agreement between simulation and experiment is very good, showing that the used fixed parametrization of C_6H_6 and the parameterization for $C_{10}H_8$, dependent on ϑ, n_{SC} and n_{CaCO3}, was successful.

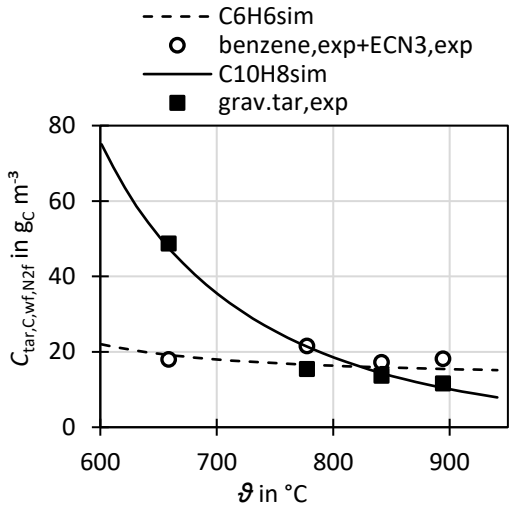

Figure 5.20: Comparison of simulation and experiment for tar carbon concentrations for ϑ variation

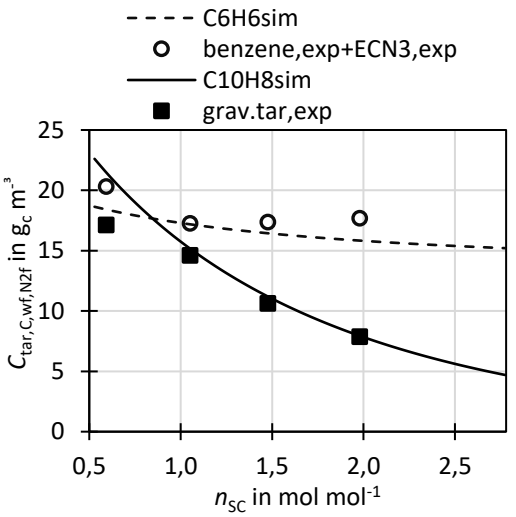

Figure 5.21: Comparison of simulation and experiment for tar carbon concentrations for n_{SC} variation

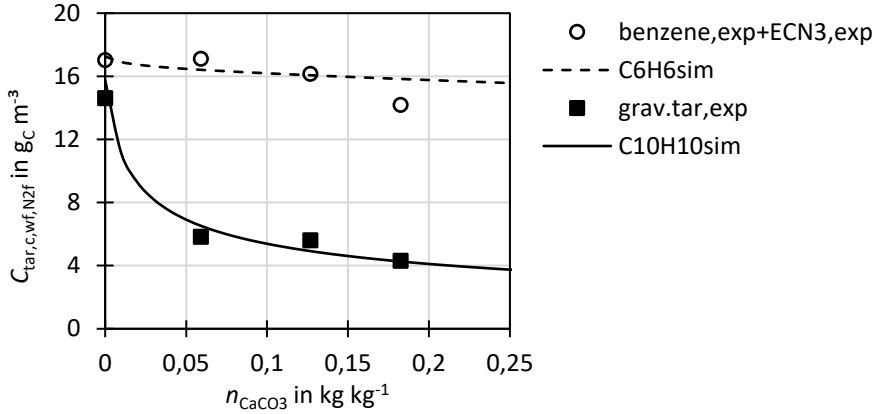

Figure 5.22: Comparison of simulation and experiment for tar carbon concentrations for n_{CaCO3} variation

5.4.3 Impurity concentrations H_2S, COS, NH_3, HCl

Figure 5.23, Figure 5.24 and Figure 5.25 compare simulations and experiments for the concentrations of impurities at different operation conditions.

The NH_3 concentration was modeled with the constant yields of the reference point, which resulted in a good agreement for the reference point, but in a considerable difference for other temperatures. However, this match was regarded acceptable for the purpose of this work.

A good agreement between simulation and experiment was achieved for H_2S and COS for all experimental points except of the one at 649 °C. The dependencies of H_2S and COS on ϑ and n_{SC}

were predicted well by the equilibrium approach; therefore, no n_{SC} and ϑ-dependent parameterization was needed. The n_{CaCO3}-dependent parameterization was thus successful.

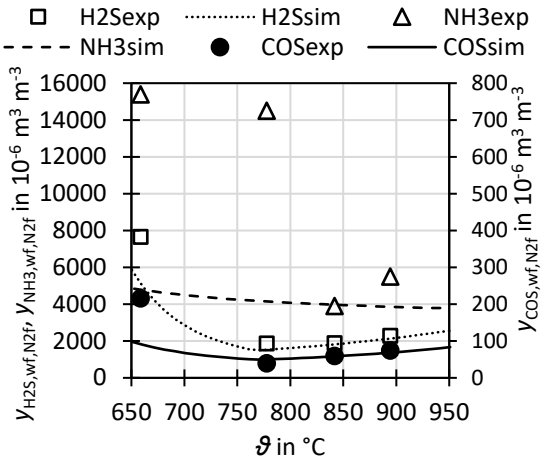

Figure 5.23: Comparison of impurity concentrations between simulation and experiment for different ϑ

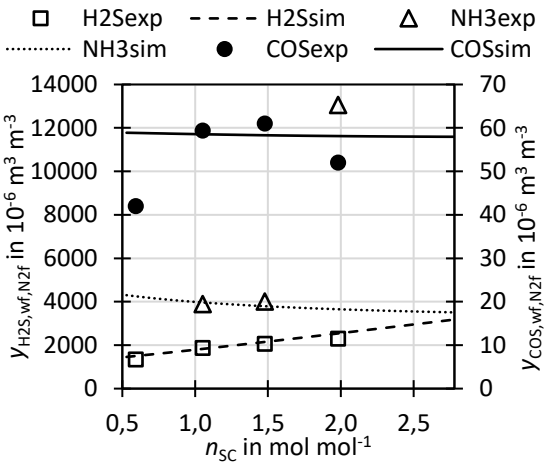

Figure 5.24: Comparison of impurity concentrations between simulation and experiment for different n_{SC}

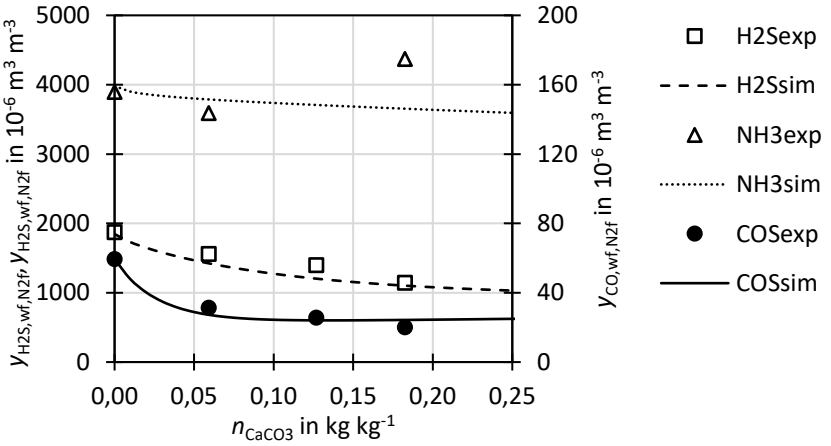

Figure 5.25: Comparison of impurity concentrations between simulation and experiment for different n_{CaCO3}

5.5 Results of adiabatic gasifier simulations

The experiments conducted in this work were not adiabatic since the used gasifier was electrically heated. Therefore, simulations are used to calculate the oxygen ratio n_{O2} required for adiabatic sewage sludge gasification and the cold gas efficiency η_{CGE}. The energy requirement of the gasifier and hence the oxygen ratio are dependent on various parameters. The most influential are gasifier temperature ϑ, steam to carbon ratio n_{SC}, feed temperature of steam ϑ_{steam}, feed temperature of oxygen ϑ_{O2}, fuel moisture $\gamma_{H2O,au}$, fuel enthalpy of formation $\Delta h^0_{f,waf}$ (calculated from elemental anal-

ysis and higher heating value), and additive ratio n_{CaCO3}. A sensitivity study was conducted as summarized in Table 5.5. The oxygen preheating temperature was kept constant at 450 °C for all calculations.

Table 5.5: Operation conditions of comparison simulations

		variation of				
		ϑ	n_{sc}	$\gamma_{H2O,au}$	$\Delta h^0_{f,waf}$	n_{CaCO3}
ϑ	°C	600 - 950	850	850	850	0
ϑ_{steam}	°C	450	200, 450, 600	450	450	0
n_{sc}	mol mol^{-1}	1	0.5 - 2.8	1 - 7	1	0
$\gamma_{H2O,au}$	kg kg^{-1}	0.1	0.1	0 - 0.75	0.1	0
$\Delta h^0_{f,waf}$	MJ kg^{-1}	-5.7	-5.7	-5.7	-7.5 - 4.2	0
n_{CaCO3}	kg kg^{-1}	0	0	0	0	0 - 0.2

5.5.1 Oxygen ratio and cold gas efficiency

Increased n_{O2} always results in the oxidation of a larger fraction of H_2 and CO to CO_2 and H_2O, reducing the heating value of the syngas and consequently reducing the cold gas efficiency. The results are presented and discussed in the following.

Influence of ϑ

Figure 5.26 depicts the required n_{O2} for different gasification temperatures where a steep increase of n_{O2} with temperature is visible. While a n_{O2} = 0.23 mol mol^{-1} is required to achieve a gasification temperature of 600 °C, n_{O2} = 0.37 is necessary to heat the gasifier up to 950 °C. This shows that the oxygen requirement can be drastically reduced by lowering the gasification temperature. However, lower gasification temperature also results in less complete fuel conversion causing higher tar yield and char yield reducing the cold gas efficiency. This makes the cold gas efficiency dependent on both effects, n_{O2} and fuel conversion. However, the increasing fuel conversion with temperatures has in this work the dominant impact as can be seen by the monotonous increase of η_{CGE} with temperature (Figure 5.27).

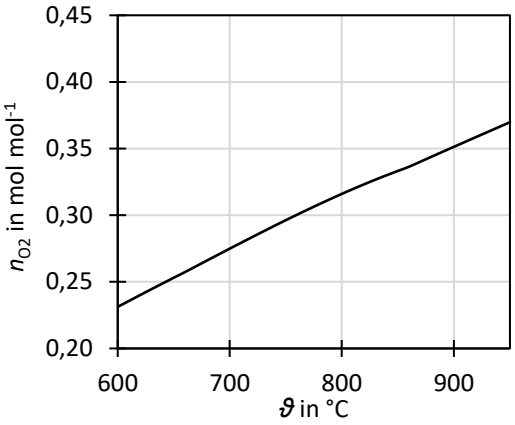

Figure 5.26: Oxygen ratio n_{O2} for adiabatic gasifier simulation at different temperatures

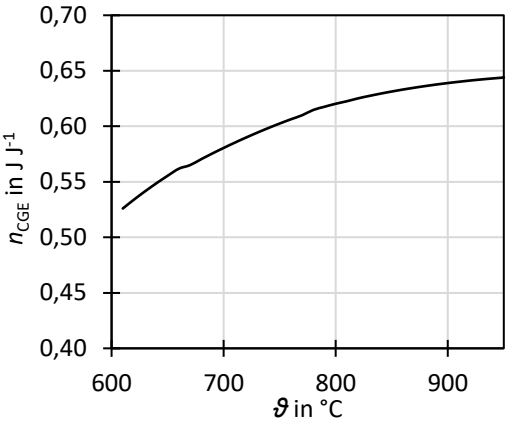

Figure 5.27: Cold gas efficiency η_{CGE} for adiabatic gasifier simulation at different temperatures

Influence of n_{SC}

The effect of n_{SC} on the required oxygen ratio is depicted in Figure 5.28 for different steam feeding temperatures. Higher n_{SC} results in higher steam feeding rates into the gasifier requiring more heat and thus higher n_{O2} to obtain the respective gasification temperature. For a steam temperature of 600 °C, only slight increase of n_{O2} with rising n_{SC} is visible. However, for a low steam temperature of 200 °C, a steep increase of n_{O2} with rising n_{SC} can be seen. The reference steam temperature in this section is 450 °C, which shows a moderate increase of n_{O2} with n_{SC}. The cold gas efficiency is reduced with increasing n_{SC} due to the increased partial combustion while lower steam pre-heating temperatures enhance the effect as shown in Figure 5.29.

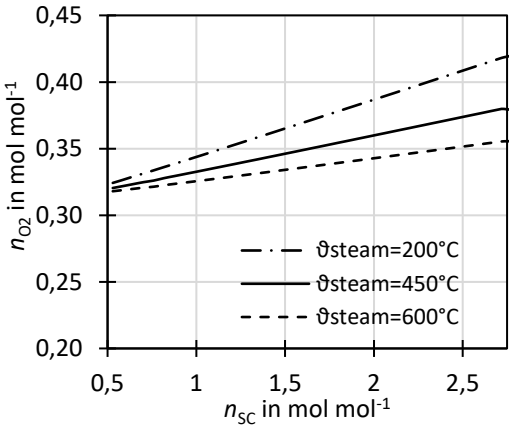

Figure 5.28: Oxygen ratio n_{O2} for adiabatic gasifier simulation at different steam to carbon ratios

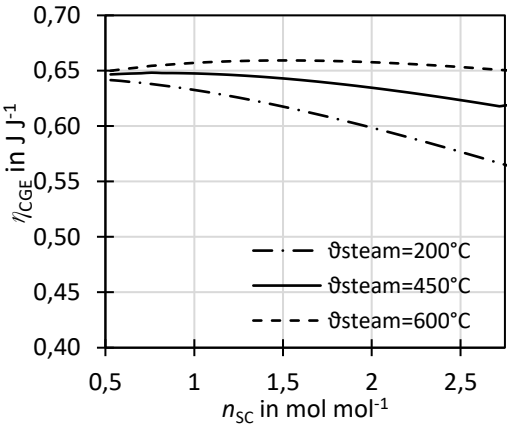

Figure 5.29: Cold gas efficiency η_{CGE} for adiabatic gasifier simulation at different steam to carbon ratios

Influence of sewage sludge moisture γ_{H2O}

Figure 5.30 shows the variation of the sewage sludge moisture content γ_{H2O}. The required n_{O2} is drastically increasing with increasing γ_{H2O} due to the heat of evaporation. Also, n_{SC} is depicted, which was kept constant at $n_{SC} = 1$ for rising γ_{H2O} as far as possible, resulting in consecutive decrease of the fluidization steam. In this hypothetical setup, the fuel moisture is sufficient to provide $n_{SC} = 1$ until $\gamma_{H2O} \approx 0.3$ completely replacing all of the fluidization steam. Further moisture increase leads to $n_{SC} > 1$. It further needs to be noted that a asifier being fluidized by only or mostly vapor from fuel drying would be something entirely new and its technical feasibility is still yet to be confirmed.

The cold gas efficiency as depicted in Figure 5.31 is for rising γ_{H2O} significantly decreasing with rising fuel moisture, resulting in a cold gas efficiency of only $\eta_{CGE} = 0.3$ for sewage sludge with a moisture content of $\gamma_{H2O} = 0.5$ kg kg^{-1}.

It can be concluded that the moisture content has a considerable effect, since increasing moisture leads to decreasing efficiency and increasing oxygen demand. The author recommends to dry sewage sludge as well as possible to achieve high process efficiencies.

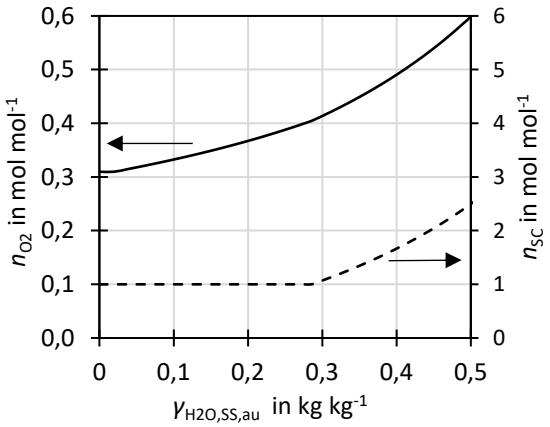

Figure 5.30: Oxygen ratio n_{O2} and steam to carbon ratio n_{SC} for adiabatic gasifier simulation at different sewage sludge moisture contents

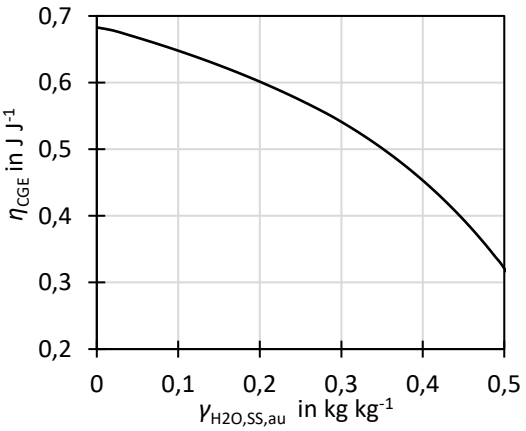

Figure 5.31: Cold gas efficiency η_{CGE} for adiabatic gasifier simulation at different sewage sludge moisture contents

Influence of sewage sludge enthalpy of formation

Figure 5.32 and Figure 5.33 show the effect of the water and ash free fuel's enthalpy of formation, $\Delta h^0_{f,SS,waf}$. With increasing $\Delta h^0_{f,SS,waf}$, n_{O2} is steeply increasing and, as a result thereof, η_{CGE} is steeply decreasing. Thus, $\Delta h^0_{f,SS,waf}$ has a considerable effect on the energy demand of the process. As shown in Figure 5.34, slight changes or errors in the fuel analysis can have a considerable influence on $\Delta h^0_{f,SS,waf}$ and thus on the n_{O2} and η_{CGE} prediction of the model.

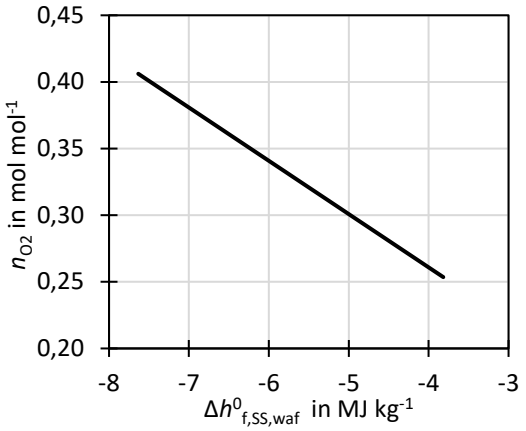

Figure 5.32: Oxygen ratio n_{O2} for adiabatic gasifier simulation at different fuel enthalpy of formation $\Delta h^0_{f,SS,waf}$

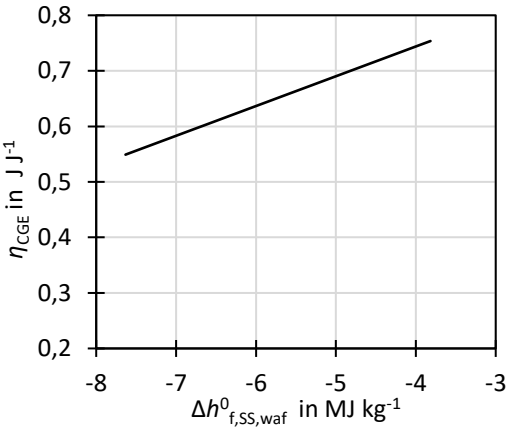

Figure 5.33: Cold gas efficiency η_{CGE} for adiabatic gasifier simulation at different fuel enthalpy of formation $\Delta h^0_{f,SS,waf}$

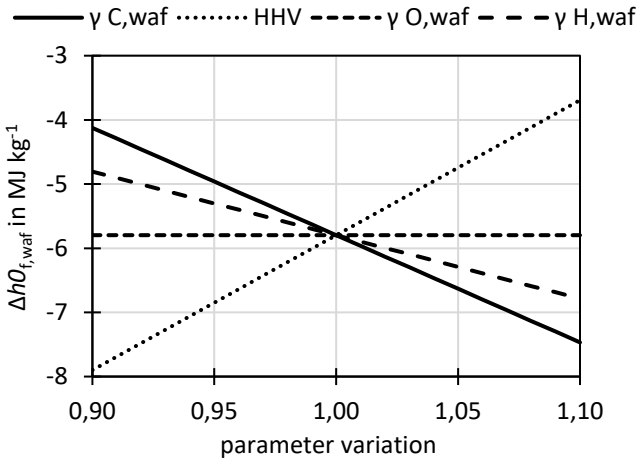

Figure 5.34: Enthalpy of formation $\Delta h^0_{f,SS,waf}$ for variations in fuel composition and higher heating value. Abscissa value 1 represents the sewage sludge analysis of this work.

5.5.2 Adjustability of syngas composition and stoichiometry

The syngas stoichiometry is important for downstream synthesis processes. With the assumption that CO_2 is completely removed, the H_2/CO ratio, $\alpha_{H2,CO}$, is a suitable indicator for syngas stoichiometry. For methanation $\alpha_{H2,CO} = 3$ is needed while Fischer-Tropsch or methanol synthesis requires $\alpha_{H2,CO}=2$. The state of the art for industrial facilities is the utilization of a dedicated catalytic water gas shift unit downstream of the gasifier to adjust $\alpha_{H2,CO}$ as required by the synthesis process. However, it was observed in the experiments of this work that water gas shift also occurred extensively in the gasifier, thus enabling adjustment of $\alpha_{H2,CO}$ by altering n_{SC} in-situ.

Figure 5.35 shows the gas composition for n_{SC} variation. It can be seen that with increasing n_{SC}, H_2O, H_2 and CO_2 concentrations are increasing, while the CO concentration is decreasing. The added steam drives the water gas shift reaction towards H_2 and CO_2 formation, changing $\alpha_{H2,CO}$. The shown concentrations also include N_2, whereas in the experimental section the concentrations were always calculated to N_2-free state. The N_2 concentration is constant at $y_{N2,wf} \approx 0.04$ m^3 m^{-3} and originated from fuel-bound nitrogen.

The results in Figure 5.36 show that $\alpha_{H2,CO}$ can be adjusted well by n_{SC} variation, since it is possible to achieve $\alpha_{H2,CO} = 2 – 4$ with $n_{SC} = 1.0 – 2.7$. It is thus technically feasible to use n_{SC} to tailor the syngas composition for the desired synthesis product. However, the economic trade-off between the disadvantages of adding additional steam (e.g. higher energy demand for steam generation) and the CAPEX advantage of not needing a dedicated water gas shift unit needs to be assessed in further studies. It also needs to be taken into account when choosing the target $\alpha_{H2,CO}$ in the raw syngas that reforming of tar species, hydrocarbons or CH_4 in or before the synthesis can influence the effective stoichiometry of the synthesis process.

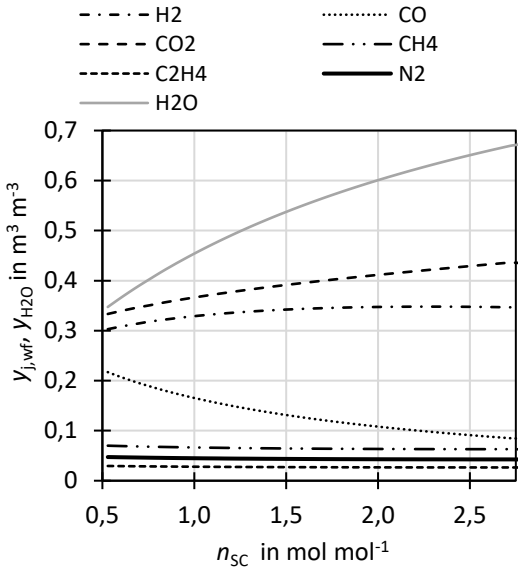

Figure 5.35: Gas concentration for adiabatic gasifier simulation at different steam to carbon ratios

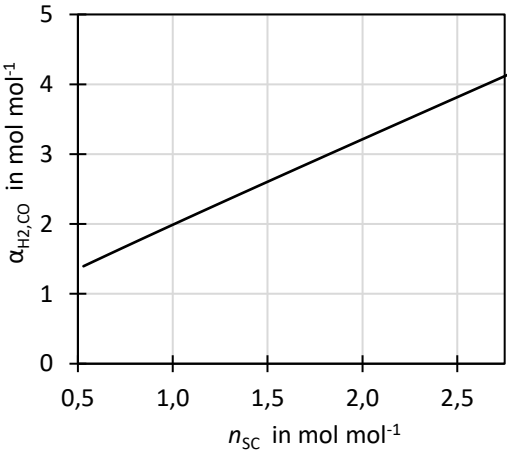

Figure 5.36: H_2 to CO ratio for adiabatic gasifier simulation at different steam to carbon ratios

5.5.3 Syngas heating value

Figure 5.37 shows that the higher heating value of the wet syngas is strongly decreasing with rising n_{SC} due to the dilution with steam. With n_{SC} of below 1 mol mol^{-1} a heating value of the wet syngas of approximately 6 MJ kg^{-1} can be achieved. For high n_{SC}, it can drop to 3 MJ kg^{-1} which is below the heating value of syngas from air gasification [9]. The heating value of water free syngas is approximately 9 MJ kg^{-1} and is almost independent of n_{SC}. It can be concluded that for applications where steam is not condensed (e.g. direct hot application of syngas), the reduced heating value by steam dilution needs to be considered. After condensation of steam, the heating value is comparably high for syngas produced via biomass gasification, but is still only one fourth of the heating value of natural gas.

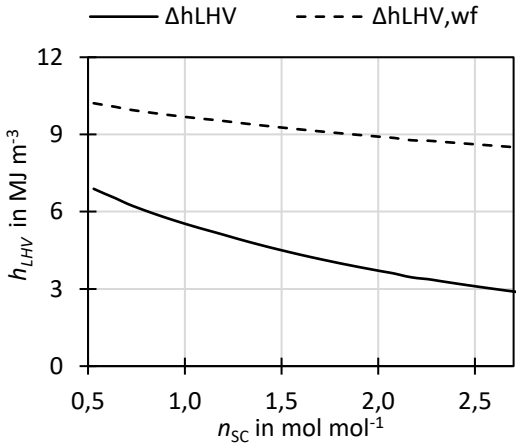

Figure 5.37: Syngas heating value on wet basis as well as on water free basis for different n_{SC} for the integrated process chain

5.5.4 Oxygen inlet concentration

Figure 5.38 shows the oxygen concentration in the oxygen-steam mixture of the gasification agent. The oxygen concentration can reach up to 0.6 m^3 m^{-3} for very low n_{SC} of 0.5 mol mol^{-1} while it is strongly decreasing for higher n_{SC}. It can be concluded that for very low n_{SC}, special attention needs to be drawn on possible hot spots near the gas distributors that can cause slagging and agglomeration of the sewage sludge ash.

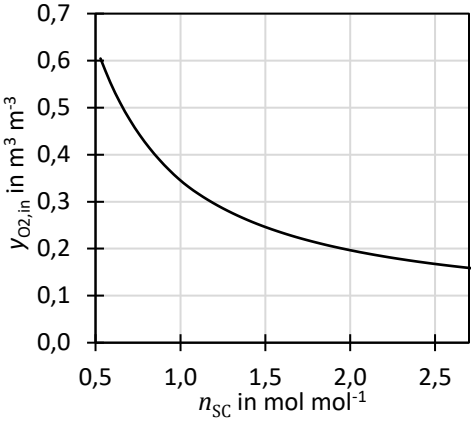

Figure 5.38: Oxygen inlet concentration for different n_{SC}

5.5.5 Impurity reduction with limestone additive

The effects of limestone addition into the gasifier were studied experimentally in section 4. The model was parameterized to describe these effects sufficiently. The simulations now allow to assess the benefits of limestone addition on H_2S, COS and gravimetric tar (model component $C_{10}H_8$) reduction but also its effect on permanent gas composition and cold gas efficiency.

Figure 5.39 shows the reduction of H_2S and COS due to sulfur capture with increasing limestone additive ratio. It can be seen that H_2S concentrations are monotonously decreasing with increasing additive ratio in the observed value range whereas for COS, at first, a steep decline followed by an almost constant trend for $n_{CaCO3} > 0.05$ kg kg^{-1} is observed. Figure 5.40 shows the concentration of $C_{10}H_8$ that is decreasing with increasing n_{CaCO3} due to catalytic tar cracking. However, the steepest decrease takes place in the range $n_{CaCO3} = 0$ - 0.05 kg kg^{-1}.

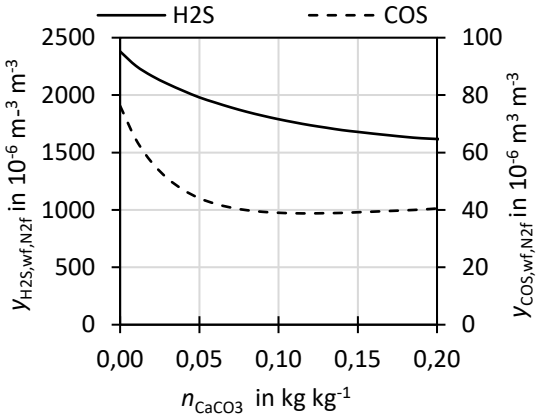

Figure 5.39: H_2S and COS concentration at different limestone additive ratios

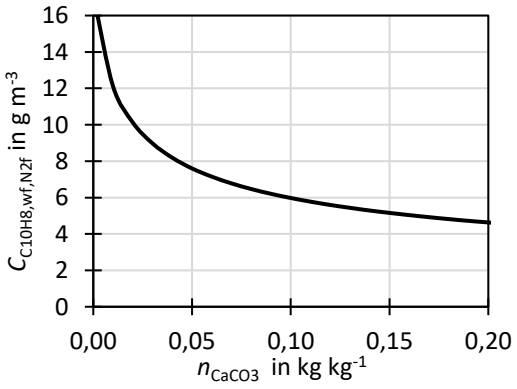

Figure 5.40: Carbon concentration of gravimetric tar, $C_{10}H_8$, at different limestone additive ratios

The oxygen ratio rises with n_{CaO3} due the heat requirement for calcination. For increasing additive ratio, the cold gas efficiency, as depicted in Figure 5.42, first increases until $n_{CaCO3} \approx 0.03$ kg kg^{-1}, followed by a decreasing trend. The initial increase is due to gravimetric tar conversion to burnable permanent gases that contribute to the cold gas efficiency. The subsequent decrease is attributed to enhanced heat demand for limestone calcination resulting in higher n_{O2} and thus lower η_{CGE}.

The conclusion is drawn that the most beneficial effect can be achieved with a small amount of limestone additive between 0 kg kg^{-1} and 0.05 kg kg^{-1}, as COS and $C_{10}H_8$ have steep decreases in this range. Higher limestone additive ratios are not recommended due to the efficiency loss and the additional CO_2-production. The cold gas efficiency has its maximum at n_{CaCO3}=0.03 kg kg^{-1}, it is therefore suggested to take this as the optimal limestone additive ratio.

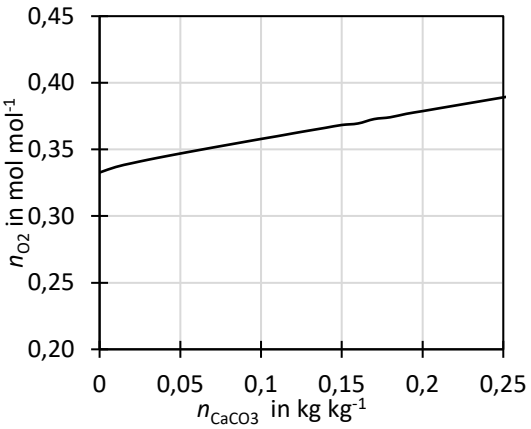

Figure 5.41: Oxygen ratio at different limestone additive ratios

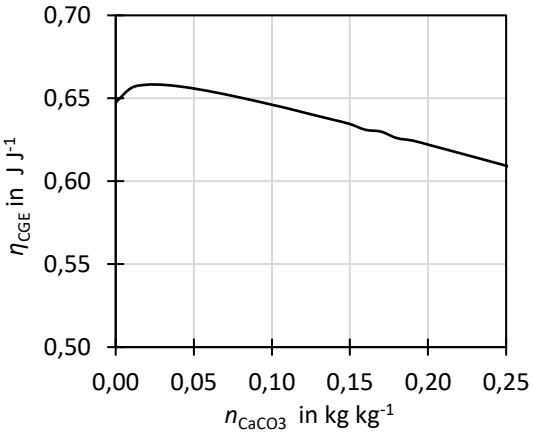

Figure 5.42: Cold gas efficiency η_{CGE} at different limestone additive ratios

5.6 Conclusions gasifier simulations

A gasifier model combining equilibrium and empirical approaches was set up. The equilibrium approach allows the model to describe the main gasification products, i.e. H_2, CO, CO_2, H_2O and their sensitivity to relevant operation parameters without parameterization from experimental data. The yield of the non-equilibrium species CH_4 and C_2H_4 could be parametrized by a simple zero-dimensional fit to one experimental point. The yields of char, tar, H_2S and COS were parameterized in dependency of gasifier operation parameters according to experimental data. A comparison of the model-predicted gas concentrations and –yields with experimental data showed sufficient accuracy to describe the sewage sludge steam-oxygen gasification for process simulation. The model has short calculation times with around 5 seconds for a steady state operation point. It is possible to include the simulation in a larger process simulation in AspenPlus®.

Adiabatic simulations allowed investigating the oxygen requirement and cold gas efficiency of the process, which was not possible by the experiments in the electrically heated facility. In addition,

key performance indicators such as the H_2/CO-ratio, $a_{H2,CO}$, and impurity concentrations were analyzed and optimized. The main conclusions of the adiabatic simulations are:

Increasing gasifier temperature ϑ leads to increasing $n_{O2.}$ As a result of this, decreasing η_{CGE} would be expected. However, it was found that η_{CGE} is monotonously increasing with rising ϑ in the relevant range due to improved tar and char conversion. To obtain a gasifier temperature of 850 °C, as common for industrial gasifiers, n_{O2} = 0.33 and n_{CGE}=0.63 were calculated.

Syngas stoichiometry can be adjusted well by n_{SC}. To obtain $a_{H2,CO} \approx 3$ mol mol^{-1} as needed for CO-methanation $n_{SC}\approx1.7$ is required. However, higher values of $a_{H2,CO} \approx 3.5$ mol mol^{-1} may be required in practice to also enable methanation of all hydrocarbons (e.g. after a re-forming or pre-methanation step) resulting in $n_{SC}\approx2.3$.

If steam is pre-heated to temperatures of 450 °C or preferably higher, rising n_{SC} leads only to a small increase of n_{O2} and small decrease of η_{CGE}. However, utilization of low-grade steam (e.g. 200 °C) considerably increases n_{O2} and decreases cold gas efficiency with increasing n_{SC}. The energy requirement of steam production needs to be considered as well when choosing the design value of n_{SC}.

The simulations predicted an N_2 concentration in the water free syngas of 0.04 m^3 m^{-3}, which is thus not completely N_2-free. The N_2 was formed from fuel-bound N. This needs to be considered for the downstream syngas application (e.g. SNG synthesis).

Cold gas efficiency, η_{CGE}, is dropping significantly with increased sewage sludge moisture content; therefore, it is recommended to dry the sludge as good as possible before gasification.

Addition of limestone into the gasifier reduces tar, H_2S and COS concentration of the syngas. Small amounts of limestone additive even increased the cold gas efficiency due to tar reforming, while higher amounts decreased the efficiency considerably. An additive ratio of n_{CaCO3} = 0.03 was found to be the optimum in respect of tar and sulfur reduction and cold gas efficiency.

6 Simulation of SNG production chain

The syngas produced via steam-oxygen gasification of sewage sludge can be used to synthesize various products such as substitute natural gas (SNG), gasoline, diesel, kerosene, dimethyl-ether (DME), methanol, ethanol and plastic monomers. In the scope of this work, the production of SNG was assessed as exemplary pathway from sewage sludge to synthetic fuel. SNG was selected for the following reasons:

The sewage sludge derived product gas already contains around 0.07 m^3 m^{-3} CH_4 reducing the methanation effort. Whereas synthesis processes other than methanation would require an additional catalytic reforming step to convert CH_4 to CO and H_2 upstream of the synthesis, adding CAPEX and OPEX to the process chain.

Europe currently consumes almost 14 EJ a^{-1} of natural gas [134], which is used mainly in domestic heating, (back-up) power generation, industrial furnaces and as educt material in the chemical industry. The infrastructure and technology of natural gas storage, transportation as well as utilization for heat and power generation and transport already exist. Even if a very fast conversion of our economy to renewable energy is accomplished, it is still very likely that we will need natural gas in the next decades.

Moreover, a sewage sludge conversion plant is most likely situated at a large wastewater treatment plant and operated by a municipal utilities operator. In some cases, the operators are experienced in handling natural gas since the municipality runs its own local distribution grid in which the SNG could be fed. While for other possible synthesis products, a distribution chain must be created from scratch. Additionally, synergies with SNG production through upgrading of digestion gas from the WWTP could be beneficial.

The following sections describe how the sewage sludge to SNG process chain was modelled and present the simulation results. The goals of this chapter are:

- determining complete mass and energy balance and composition of all relevant streams
- determining total energy efficiency of sewage sludge to SNG conversion, considering also practical heat integration and electrical energy consumption
- determine the amount of sewage sludge that can be dried with excess heat from the conversion process
- assess the integration of an electrolysis for power-to-gas operation

6.1 Process chain model description

This subsection describes how the process chain from sewage sludge to SNG was modeled.

6.1.1 Base case

The process chain is investigated as shown in Figure 6.1 and was modeled as detailed as necessary to achieve the aforementioned goals. To assess the process efficiency, special attention was drawn on the need of energy-intensive heating, cooling and compression of the process streams. All temperature and pressure changes are noted in Figure 6.1. Further energy requirements of individual process steps, such as electrical energy or auxiliary thermal energy (e.g. sorbent regeneration) were only considered for the most energy-demanding steps. Process steps with assumingly small influence on the overall efficiency (e.g. wet scrubbers) were simplified and the energy demand (e.g. pumps for washing liquid) neglected. Heat losses were also neglected. All considered process steps and the respective operation conditions and assumptions are summarized in Table 6.1.

Mechanically dewatered sewage sludge with a moisture content of 0.75 kg kg^{-1} is fed into the thin film dryer where the sludge is dried to a moisture content of 0.1 kg kg^{-1}. The dryer is partially supplied via heat integration but also needs additional drying heat, e.g. waste heat from a neighboring process. If no waste heat is on-site, it is also possible to use mixtures of sludges that are dried on-site and elsewhere. Another option would be solar drying to supply additional dry sludge.

Dried sewage sludge enters the gasifier with a moisture content of 0.1 kg kg^{-1}. The gasification agents oxygen and steam are pre-heated by heat integration and fed into the gasifier. Limestone is used as bed additive with n_{CaCO3} = 0.03 kg kg^{-1} according to the findings of the previous sections.

The raw syngas undergoes several conditioning steps, which were largely selected based on the state of the art from the GoBiGas demonstration plant [89] and commercial sewage sludge gasification plants by KOPF SynGas [9, 58]. After exiting the gasifier, the syngas is cooled to 200 °C, dedusted in a bag filter and then fed into a bio diesel (RME) scrubber at 50 °C for bulk removal of H_2O, tar, HCl, NH_3 and heavy metals. Especially due to the considerable amount of NH_3, H_2S and probably HCN, further scrubbing is needed. Several scrubbers may be applied in series using water, sour water and caustic water for sufficient impurity removal. Light tars, BTX but also ECN2 tar species that passed the scrubbers are removed in a steam-regenerated activated carbon fixed bed. The activated carbon bed will also absorb remaining mercury. The gas stream is then compressed to 12 bar absolute pressure, which is modeled by a 3-stage compressor using Aspen Plus® compressor blocks. The electrical energy for compression is calculated with the help of compressor efficiencies as given in Table 6.1.

After the compression, CO_2 is removed by pressure water scrubbing, which is a different technology choice than for the GoBiGas plant, with significant lower heat consumption. The next steps

are catalytic hydration of COS to H_2S and a ZnO fixed bed to remove residual H_2S, both at 300 °C, followed by catalytic hydration of olefins to saturated species. All gas-cleaning steps were modeled as simple separator blocks in Aspen Plus® assuming full separation of the respective impurities while omitting power consumption for liquid pumps.

The methanation section is based on the commercially available TREMP® process by Haldor Topsoe [135, 136], which is modeled by three "RGibbs" reactors assuming thermochemical equilibrium for each stage. The first methanation stage uses a recycle to control its temperature. The electrical energy consumption of the recycle fan is calculated with the same efficiencies as the syngas compressor (see Table 6.1 line 11). Water is condensed before methanation step 3 to shift the equilibrium towards high CH_4 concentrations. After the methanation, the SNG undergoes final conditioning by cooling and drying through a zeolite bed. The final SNG product has a residual absolute pressure of around 8 - 10 bar, which is sufficient for feeding into a local gas grid. For long distant transport or high-pressure gas storage, the SNG must be pressurized further, which is not considered in this work.

The heat integration follows the principle used in the dual fluidized bed gasifier CHP in Senden [131] using thermal oil circuits that are used to collect thermal energy from coolers and to supply it to heaters. This has the advantage that no gas-gas heat exchangers are needed, which reduces the required heat transfer surface and therefore the heat exchanger CAPEX. A terminal temperature difference of 15 K was assumed between gas and thermal oil. The thermal oil cold return flow comes from the sewage sludge thin-film dryer (stream A) with a temperature of 185 °C and is fed into all gas coolers, i.e. syngas cooler after gasifier and gas coolers after methanation steps where it is heated to 350 °C. All hot thermal oil steams are mixed to yield the hot supply flow (stream B). Slipstreams of stream B are used to supply the demand of heaters for oxygen pre-heating and part of the steam generation and pre-heating. The residual flow of stream B supplies heat to the dryer. The hot ash stream is used for steam generation and superheating. A fluidized bed heat exchanger is considered for this, alternatively a screw heat exchanger could be used.

Additional thermal oil circuits are used to cool and re-heat the syngas to obtain the desired temperature level for each process step. Circuit C-D re-heats the syngas to 300 °C before the COS hydration by using heat from SNG cooling after the third methanation reactor. Furthermore, circuit G-H is used for heat integration between cooling for H_2O removal after the second methanation and re-heating for the third methanation. Circuit E-F is used to transfer heat from compressor cooling to pre-heating of feed water for steam production. Cooling water was used whenever cooling to low temperatures of e.g. 50 °C was necessary (RME-scrubber, H_2O condensers).

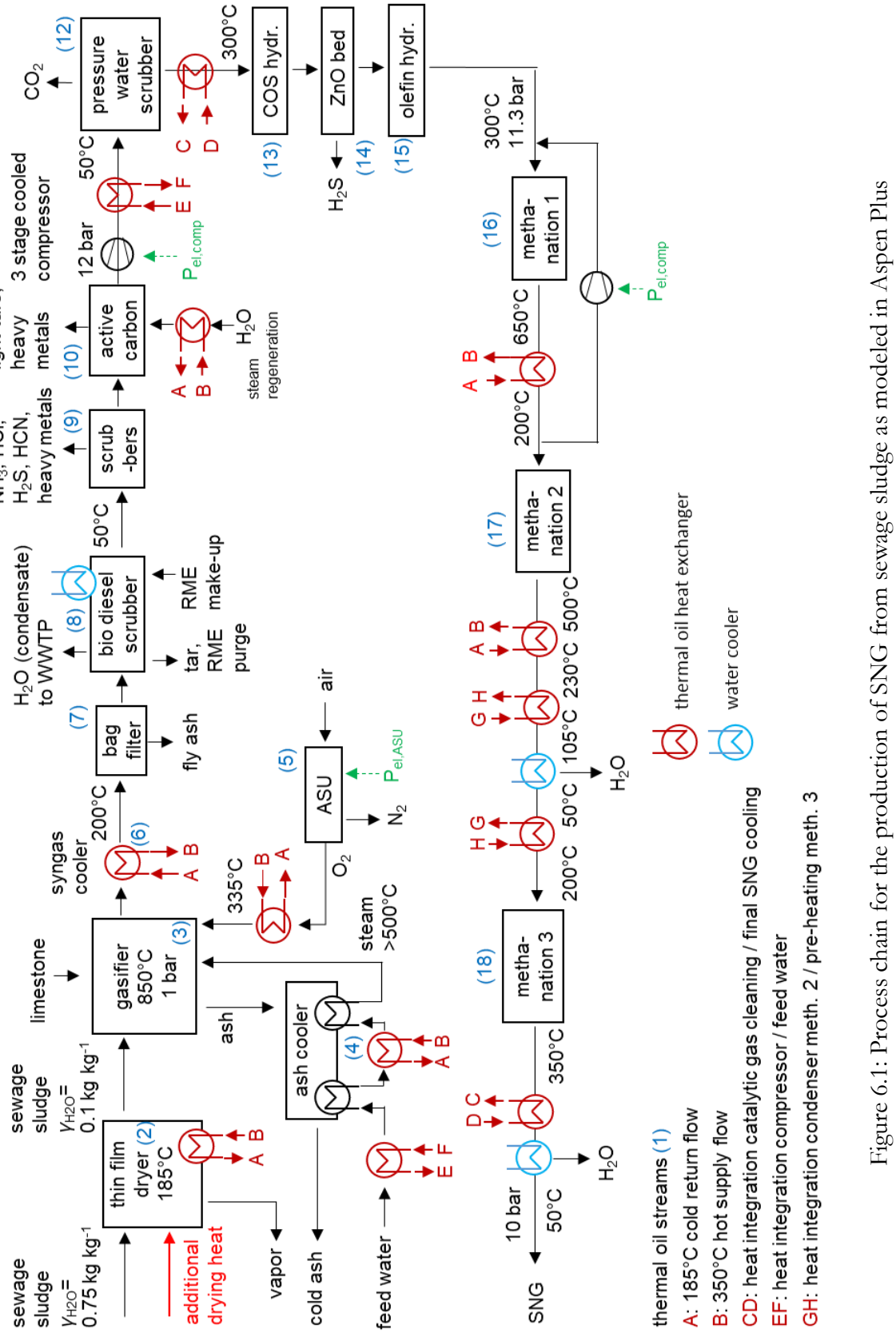

Figure 6.1: Process chain for the production of SNG from sewage sludge as modeled in Aspen Plus

Table 6.1: Description of process steps and values for modelling

no.	block/item	type	used values/assumptions	reference
1	heat integration media	thermal oil	• lowest temperatures in process: 185 °C • highest temperature in process: 350 °C • temperature difference for heat exchangers: 15 K	[137]
2	sewage sludge dryer	thin-film dryer	• drying efficiency η_{dryer} = 0.82 • thermal oil inlet: min. 200 °C, outlet 185 °C	[103]
4	steam production for gasifier fluidization	steam generator and superheater in ash cooler and by thermal oil	• 2 bar steam pressure • superheated to 480 - 750 °C, depending on heat availability	
5	O_2 production	cryogenic air separation unit (ASU)	• small scale cryogenic ASU • purity y_{O2} = 0.996 $m^3\ m^{-3}$ • power consumption 2.42 MJ per kg O_2 (considerably higher than large scale ASU)	[138]
6	syngas cooler	tube bundle heat exchanger	• gas outlet 200 °C • thermal oil inlet 185 °C, outlet 350 °C	
8	RME scrubber	bio diesel (RME) scrubber	• scrubber temperature 50 °C • 100% gravimetric tar removal • H_2O condensation up to equilibrium • thermal utilization of RME and tars is neglected • electric energy demand neglected	[139]
9	impurity scrubbers	atmospheric water scrubber, sour scrubber, caustic scrubber	• scrubbers for removal of NH_3, HCl, HCN, H_2S • scrubber temperature: 50 °C • energy demand neglected	[123]
10	light tar species removal	regenerated active carbon beds	• active carbon beds with cyclic regeneration with 250 °C-steam • complete removal of residual tar species • consumption of 9.2 kg steam per kg tar	[139]
11	compressor	3-stage centrifugal	• compression to 12 bar • three adiabatic stages, gas cooling to 50 °C after stage 1 and stage 2 • energy demand calculated by compressor block in Aspen Plus®: η_{isen} = 0.8, η_{mech} = 0.95, η_{el} = 0.85	[140–142]
12	CO_2 removal	pressure water washing	• complete CO_2-removal, ϑ = 50 °C • power consumption for liquid pumps and blower for stripping air was neglected, syngas compression included in (11)	[143]
13	COS hydration	catalytic fixed bed	• complete conversion of COS to H_2S, • ϑ = 300 °C	[139]
14	ZnO-bed	fixed bed sorbent	• complete H_2S removal • ϑ = 300 °C	
15	olefin hydration	catalytic fixed bed	• complete olefin conversion to alkanes • ϑ = 300 °C	[139]
16	methanation	TREMP® process	• 3 stage adiabatic fixed bed • first stage with pre-methanation and recycle (compressor efficiencies as in line 11 • modeled by thermodynamic equilibrium with Aspen Plus® RGibbs reactor	[136, 139]

6.1.2 Additional catalytic water-gas shift unit

The base case as described in section 6.1.1 does not include any water-gas shift unit. However, shifting of CO to H_2 according to R 11 may be necessary to provide a suitable stoichiometry for methanation. If required, a catalytic shift unit is considered downstream of the gasifier but before the RME scrubber since the syngas still contains steam that can be used as reactant for the shift reaction. Shift units operate at temperatures of around 400 °C, therefore the gas cooling was divided into two steps (Figure 6.2). The syngas is first cooled from gasification temperature to 400 °C, passes the ceramic candle filter, the catalytic shift unit and is finally cooled to 200 °C. This position requires catalysts that are resistant to the impurities in the raw gas such as sulfur and chlorine.

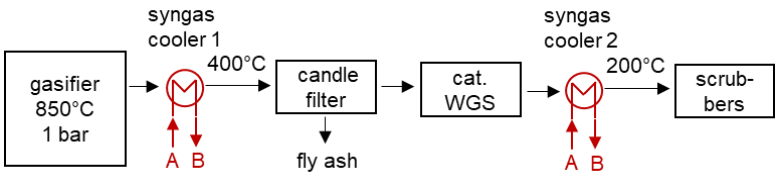

Figure 6.2: Process chain amendment for case with catalytic water-gas shift unit

6.1.3 Additional integration of SOEC water electrolysis

A further goal of this chapter is to assess the integration of a water electrolysis into the process chain. Water electrolysis provides oxygen that can be used as gasification agent and hydrogen that can be fed into the methanation for enhanced SNG yield. A solid oxide electrolyzer (SOEC) is suitable for this application due to its high efficiency. The SOEC is operated at 850 °C and uses steam as input. The anode produces pure oxygen that is directly fed into the gasifier at 850 °C. The cathode product stream is a mixture of H_2 and steam with an H_2 concentration of 0.7 $m^3\ m^{-3}$. The H_2/H_2O stream is cooled in a recuperator pre-heating the electrolysis steam input. The steam is afterwards condensed to obtain pure H_2. Steam generation is conducted by heat-integration with the process chain through thermal oil. The electrolysis is modeled with an "RStoic" reactor block in Aspen Plus®. An electrical efficiency of $\eta_{el,ELY} = 0.87$ was implemented as calculated from published data from the manufacturer Sunfire GmbH [90]. The integration of the SOEC into the process chain is depicted in Figure 6.3.

The minimum load of the electrolysis is defined by the O_2 demand of the gasifier. For higher electrolysis loads, only a part of the O_2 is used in the gasification. The CO_2-separation efficiency of the pressure water scrubber was adjusted to leave a suitable amount of CO_2 in the syngas for methanation with the additional H_2. A CO_2-removal unit is not required if the electrolysis is constantly operated at a load that allows full methanation of all CO and CO_2 in the syngas.

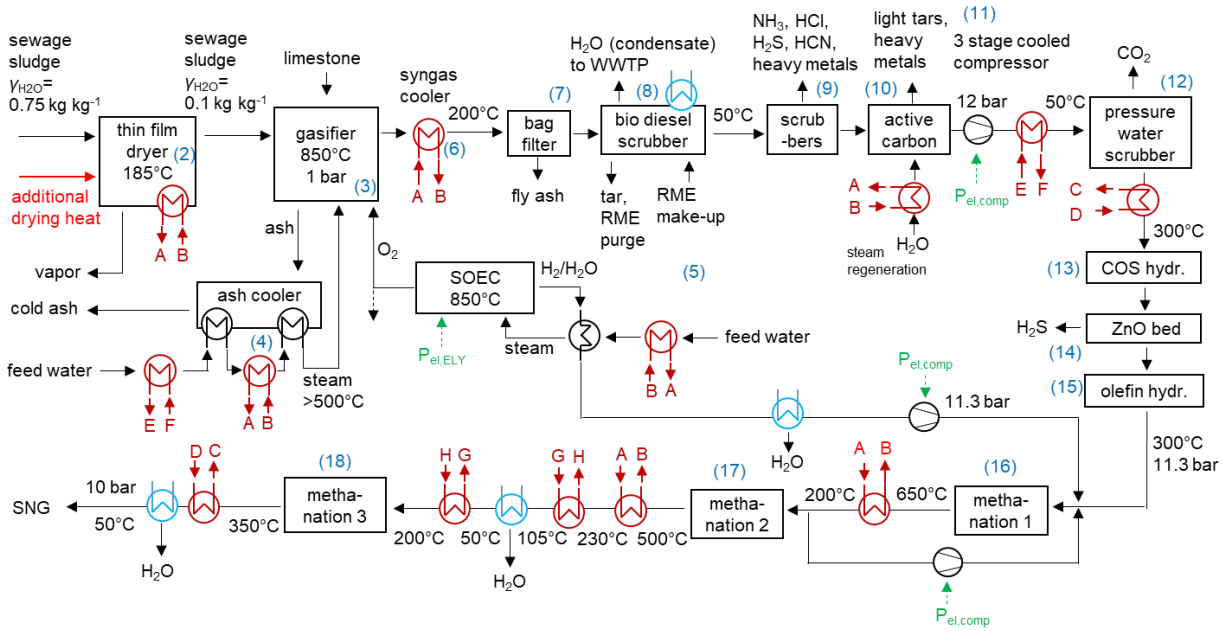

Figure 6.3: Process chain amendment for case integration of electrolysis

6.1.4 Additional integration of drying vapor

In the base case, the gasification agent steam is produced by evaporation of feed water with heat from heat integration. Especially for high n_{SC}, steam provision can consume a considerable fraction of the available heat. An innovative approach would be to use vapor from sewage sludge drying as gasification agent. According to the dryer manufacturer SMS-Buss-Cancler, it is possible to produce an air-free vapor with a thin-film dryer. Figure 6.4 shows how this option was implemented into the process chain. Part of the drying vapor is super-heated to above 500 °C in the ash cooler and then fed into the gasifier.

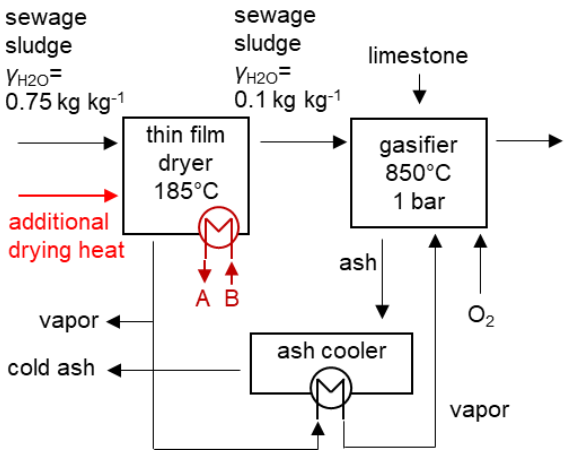

Figure 6.4: Process chain amendment for case drying vapor utilization as fluidization steam

6.1.5 Additional syngas quench

Heavy tar species can condense at temperatures below 400 °C. This can lead to clogging of pipes and heat exchangers requiring frequent maintenance. One measure to prevent this is to conduct syngas cooling only until 400 °C as shown in Figure 6.5. Fine particle removal must then be conducted by a ceramic candle filter at 400 °C since the temperature is too high for bag filters. The temperature needs to be further decreased by a quench unit before it is fed into the scrubber section. This arrangement has the downside of less heat recovery. The effect of syngas quenching on the energy balance of the integrated process chain is discussed in section 6.3.

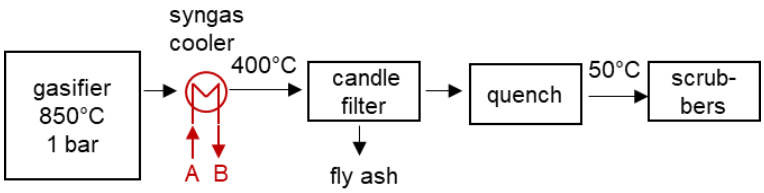

Figure 6.5: Process chain amendment for case syngas quenching to protect gas cooler from condensates

6.2 Selection of n_{SC} for integrated process chain

The steam to carbon ratio, n_{SC}, is an influential operation parameter. This subsection investigates its influence on the integrated process chain to determine the optimized design value for n_{SC}. Steam has the function to act as fluidization agent, but also as gasification agent for tar and char conversion and influences H_2S concentration. Steam is also consumed in the water-gas shift reaction to convert CO to CO_2, which can be used to adjust the H_2 to CO ratio, $\alpha_{H2,CO}$, for a downstream synthesis process. However, higher amounts of steam also increase the heat demand of the gasifier, as the steam needs to be heated to the gasification temperature. Since the integrated process chain model also considers steam-production and pre-heating through heat integration, the simulations are able to assess the trade-off between in-situ stoichiometry adjustment and energy consumption.

6.2.1 Steam amount and resulting pre-heating temperature

Figure 6.6 shows the specific mass of steam per water free sewage sludge, $m_{H2O,wf}$, over n_{SC}. The achievable steam pre-heating temperature by heat integration is dependent on the used steam amount, since the available high-temperature heat is limited (Figure 6.7). For n_{SC} = 2.3, a steam pre-heating temperature of 480 °C was achieved while significantly higher temperatures were possible for lower n_{SC}. The steam preheating temperature was limited to 750 °C since higher temperatures were not considered feasible due to limitation of heat exchanger materials.

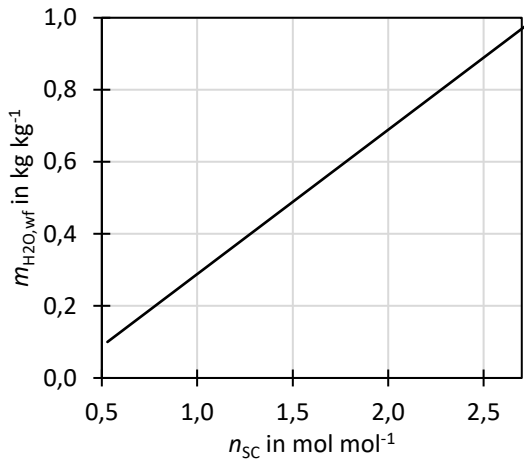

Figure 6.6: Specific steam to fuel mass ratio, $m_{H2O,wf}$, for different n_{SC} for the integrated process chain

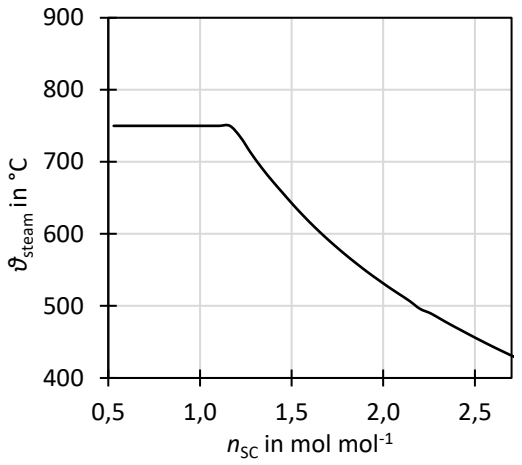

Figure 6.7: Steam pre-heating temperature for different n_{SC} for the integrated process chain

6.2.2 Oxygen ratio and cold gas efficiency

Figure 6.8 shows the oxygen ratio n_{O2} over n_{SC} which is constant at n_{O2} = 0.33 until n_{SC} = 1.1 and increases with further rising n_{SC}. The opposite trend is present for η_{CGE} as visible in Figure 6.9. The trend of increasing n_{O2} and decreasing η_{CGE} is due to the increased amount of steam that is fed into the gasifier that needs to be heated to gasification temperature and the decreasing steam-pre-heating temperature (see Figure 6.6 and Figure 6.7). This result is slightly different than in chapter 5, where the simulation was conducted without the integrated process chain.

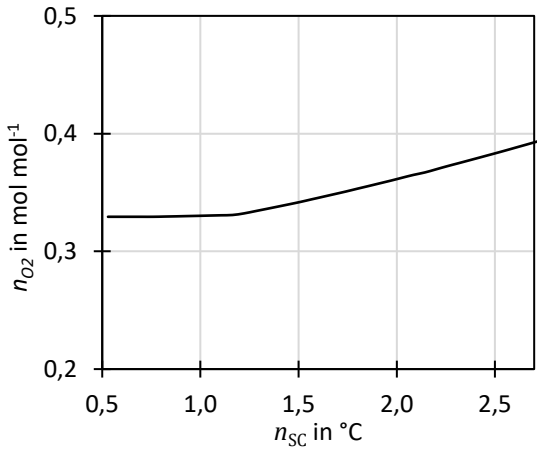

Figure 6.8: Oxygen ratio n_{O2} for different n_{SC} for the integrated process chain

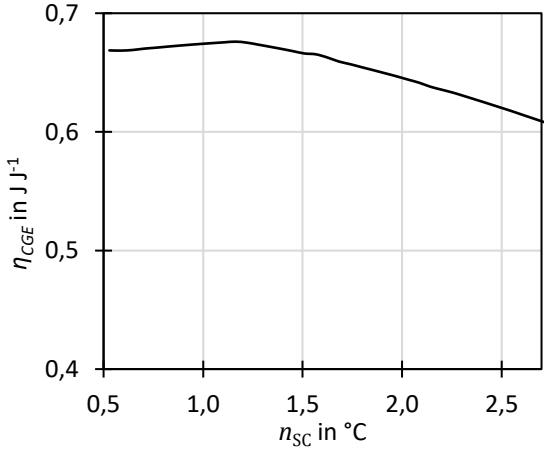

Figure 6.9: Cold gas efficiency η_{CGE} for different n_{SC} for the integrated process chain

6.2.3 Gas composition and H_2/CO-ratio $\alpha_{H2,CO}$

Figure 6.10 shows the gas composition after the gasifier. The permanent gases are shown on water free basis while the H_2O concentration is shown on wet basis. Naturally, the H_2O concentration is strongly increasing with rising n_{SC}. CO is decreasing and CO_2 increasing while H_2 is first increasing but strives to a constant value for higher n_{SC}. This behavior is due to the combination of increasing water-gas shift reaction but also increasing partial combustion (higher n_{O2}) with rising n_{SC}. Figure 6.11 shows the mole ratio of H_2 to CO, $\alpha_{H2,CO}$, which is increasing almost linearly with n_{SC}. This work's simulations have shown that $\alpha_{H2,CO} = 3.5$ is optimal for methanation of CO and C_2H_4 which according to Figure 6.11 corresponds to n_{SC}=2.3. This result is similar as in chapter 5. For lower n_{SC}, the stoichiometry of the syngas after the gasifier is not suitable for methanation and requires further shifting (e.g. a catalytic shift unit) before the CO_2 separation or addition of H_2.

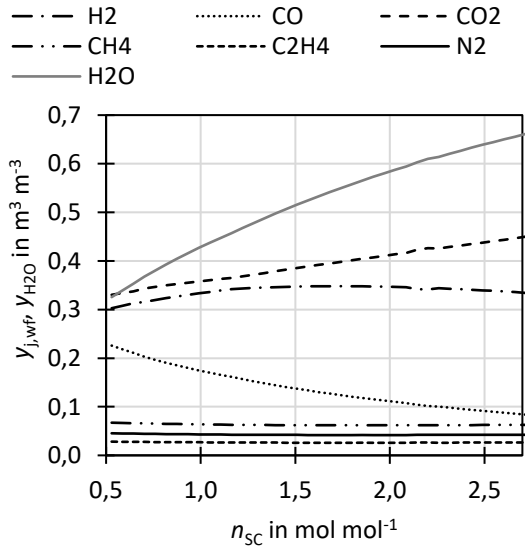

Figure 6.10: Gas concentrations for different n_{SC} for the integrated process chain

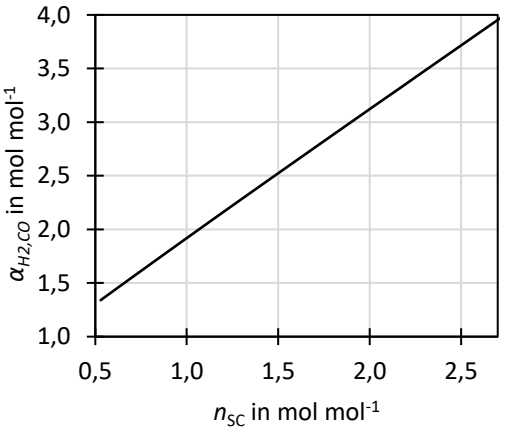

Figure 6.11: H_2 to CO ratio, $\alpha_{H2,CO}$, for different n_{SC} for the integrated process chain

6.2.4 Impurity concentrations

Figure 6.12 shows the impurity concentrations. It is visible that higher n_{SC} led to higher H_2S and COS concentrations since the steam decreases sulfur capture in CaS as described in section 4 and 5. The NH_3 concentration is approximately constant for different n_{SC}. Figure 6.13 shows the concentrations of GC tars (model component C_6H_6) and gravimetric tars (model component $C_{10}H_8$). Gravimetric tars are decreasing with rising n_{SC} since steam acts as oxidizer for tar reforming of heavy tars while the GC tar concentration stays almost constant, as described in chapter 4 and 5.

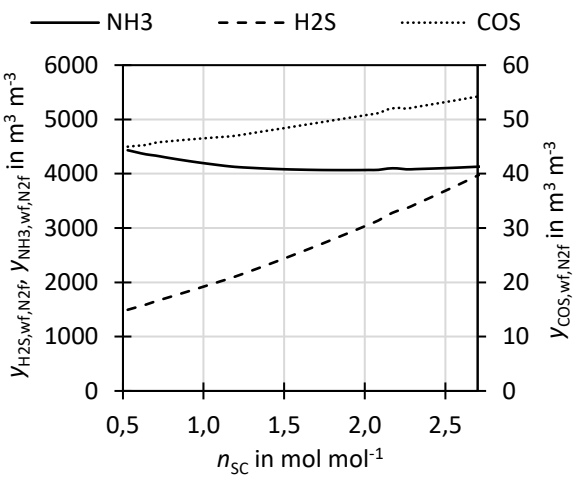

Figure 6.12: Impurity concentrations for different n_{SC} for the integrated process chain

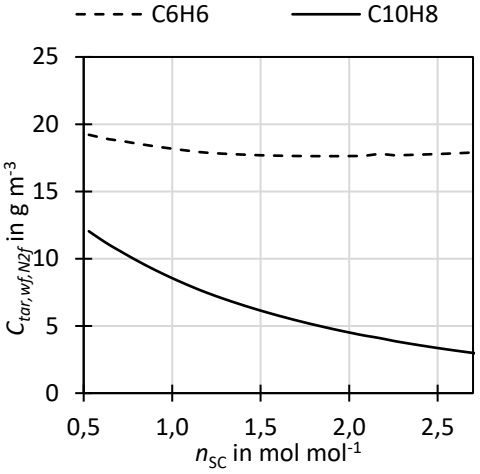

Figure 6.13: Tar concentrations for different n_{SC} for the integrated process chain

6.2.5 Drying ratio

Figure 6.14 shows the fraction of sewage sludge drying heat that can be supplied by heat integration, α_{drying} (see definition in 6.3.5). At n_{SC} = 0.7 mol mol^{-1}, around α_{drying} = 0.20 J J^{-1} of the drying heat can be supplied by heat integration while for n_{SC} = 2.3 mol mol^{-1} it drops to α_{drying} = 0.07 J J^{-1}. It can be concluded that a low n_{SC} should be chosen for enhanced heat provision for sewage sludge drying.

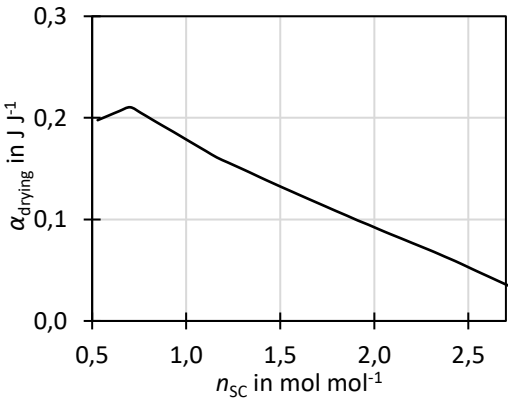

Figure 6.14: Fraction of sewage sludge drying heat that can be supplied by heat integration, α_{drying}, for different n_{SC} for the integrated process chain

6.2.6 Selection of n_{SC} design value

From this section's results it is concluded that n_{SC} has a considerable influence on the relevant performance values, $\alpha_{H2,CO}$ and α_{drying}. Other performance values are either not significantly dependent on n_{SC} or are not as relevant to the considered process chain. It is thus on the one hand possible to optimize the process chain for adjustment of $\alpha_{H2,CO}$ in the gasifier avoiding the CAPEX and OPEX of a catalytic water-gas shift unit. On the other hand, it is possible to operate the process with enhanced α_{drying} through availability of recovered heat for sewage sludge drying by reducing the required heat for steam generation by using a low n_{SC}. However, a minimum of steam is needed for sufficient fluidization and reduction of oxygen partial pressure at the gas distributors. Therefore, the following two cases are selected:

- n_{SC}=2.3 for in-situ WGS for achieving $\alpha_{H2,CO}$=3.5 after the gasifier
- n_{SC}=0.7 for enhanced heat availability for sludge drying, but need of catalytic WGS

6.3 Results of case simulations

This section uses four specific cases to analyze the performance of different operation modes of the integrated process chain.

6.3.1 Description of considered cases

Table 6.2 shows the operation parameters and configurations of the four selected cases. Case 1 uses the "base case" configuration as described in subsection 6.1.1. with n_{SC} = 2.3 for in-situ WGS. Case 2, 3 and 4 use a reduced n_{SC} for enhanced heat recovery for sewage sludge drying. As a result, case 2 requires a catalytic water-gas shift unit as described in 6.1.2.

Cases 3 and 4 use an electrolysis unit (ELY) as described in 6.3.1. Stoichiometry adjustments are not needed for case 3 and 4 since the additional H_2 is able to convert all CO to CH_4. While in case 3 the electrolysis is operated with a suitable load to provide the required oxygen for the gasification, the electrolysis provides in case 4 sufficient H_2 to convert all CO and CO_2 from the syngas into CH_4.

Table 6.2: Simulation cases for integrated process chain

	case 1	**case 2**	**case 3**	**case 4**
short name	**n_{SC}=2.3**	**n_{SC}=0.7**	**ELY O_2**	**ELY full C**
n_{SC}	2.3	0.7	0.7	0.7
catalytic WGS unit	no	yes	no	no
electrolysis	no	no	O_2-production with electrolysis	H_2-provision for complete methanation of CO and CO_2 from syngas
CO_2-removal	complete	complete	partial	no

6.3.2 Mass balance

This section shows the simplified mass balance of gasifier and methanation section.

Gasifier

Table 6.3 shows the mass balance of the gasifier based on the throughput of 1 kg water free sewage sludge. The input streams are sewage sludge with a moisture content of 0.1 kg kg^{-1}, oxygen, steam and limestone additive. The output streams are ash and syngas.

Case 1 uses n_{SC} = 2.3 resulting in a high steam input of 0.816 kg per kg dry sewage sludge. Case 2 to 4 use n_{SC} = 0.7 and are therefore quite similar among each other. The steam amount used is with 0.168 kg kg^{-1} significantly lower than for case 1. The syngas contains thus less steam for case 2, 3

and 4 compared to case 1, but also less H_2 and more CO. The lower steam input of case 2 to 4 also leads to a lower oxygen requirement compared to case 1. The oxygen for case 3 and 4 originates from the electrolysis and has thus a higher temperature than oxygen from ASU, which enables further reduction of the oxygen ratio. The additive and ash streams are identical for all cases.

Methanation

Table 6.4 shows the mass balance of the complete 3-stage TREMP® methanation section including gas cooling. The input stream is cleaned and compressed (12 bar) syngas. CO_2 was removed completely upstream of the methanation for case 1 and 2. Additionally, case 2 considers a catalytic water-gas shift step upstream of the gas cleaning. Partial CO_2-removal to ensure a suitable stoichiometry for methanation was used in case 3, while no CO_2 separation was considered in case 4. The hydrogen feed from electrolysis was 0.033 kg kg^{-1} in case 3 and 0.098 kg kg^{-1} in case 4.

For case 1 and 2 the methane yield in SNG based on water free sewage sludge was 0.11 kg kg^{-1}, while for case 3 and case 4, the methane yield could be enhanced to 0.18 kg kg^{-1} and 0.30 kg kg^{-1}, respectively.

Figure 6.15 shows the respective carbon utilization $S_{CH4,C}$ which resembles the fraction of sewage sludge carbon that was converted to CH_4 in the SNG. The carbon utilization of cases 1 and 2 are $S_{CH4,C}$ = 0.33, meaning that one third of the sewage sludge's carbon is converted to CH_4, the residual carbon is emitted mainly as CO_2 and to a lower extent as tar and char. Case 3 has a carbon yield of $S_{CH4,C}$ = 0.55, showing that more than half of the carbon can be utilized if the electrolysis load matches the O_2-requirement. Case 4 displays with $S_{CH4,C}$ = 0.92 an almost complete carbon methanation. The residual carbon is lost through tar and char formation in the gasifier and through residual CO_2 in the SNG.

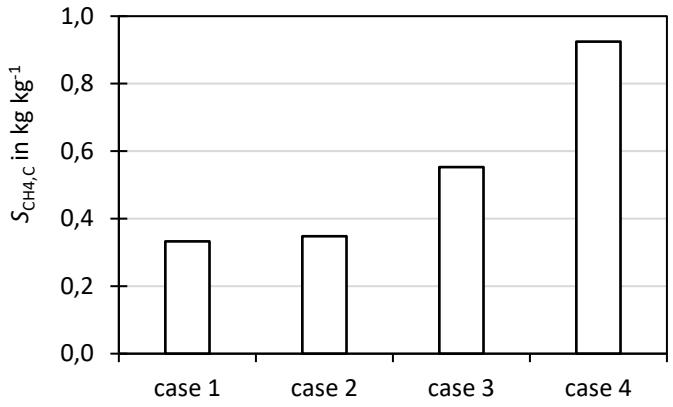

Figure 6.15: Carbon utilization based on water ash free sewage sludge

Table 6.3: Specific gasifier mass balance for integrated process chain

			unit	case 1	case 2	case 3	case 4
				n_{SC}=2.3	n_{SC}=0.7	ELY O_2 n_{SC}=0.7	ELY full C n_{SC}=0.7
input	sewage sludge	m_{SSwf}	kg kg^{-1}	1.000	1.000	1.000	
		$m_{H2O(l)}$		0.112	0.112	0.112	
	oxygen	m_{O2}		0.311	0.273	0.264	
	steam	$m_{H2O(g)}$		0.816	0.168	0.168	
	additive	m_{CaCO3}		0.030	0.030	0.030	
output	ash	m_{ash}		0.508	0.508	0.508	
	syngas	m_{H2}		0.022	0.019	0.020	
		m_{CO}		0.087	0.171	0.178	
		m_{CO2}		0.601	0.454	0.444	
		m_{CH4}		0.032	0.032	0.032	
		m_{C2H4}		0.023	0.023	0.023	
		m_{N2}		0.038	0.038	0.038	
		$m_{H2O(g)}$		0.937	0.314	0.308	
		m_{NH3}		0.0021	0.0021	0.0021	
		m_{H2S}		0.0036	0.0016	0.0016	
		m_{COS}		0.0001	0.0001	0.0001	
		m_{HCl}		0.0005	0.0005	0.0005	
		m_{C6H6}		0.0121	0.0121	0.0121	
		m_{C10H8}		0.0026	0.0068	0.0068	

Table 6.4: Specific methanation mass balance for integrated process chain

			unit	case 1	case 2	case 3	case 4
input	syngas after gas cleaning	m_{H2}	kg kg^{-1}	0.022	0.024	0.020	0.020
		m_{CO}		0.087	0.097	0.178	0.177
		m_{CO2}		0.000	0.000	0.076	0.444
		m_{CH4}		0.032	0.032	0.032	0.032
		m_{C2H4}		0.023	0.023	0.023	0.023
		m_{N2}		0.037	0.037	0.037	0.037
		m_{H2O}		0.006	0.006	0.009	0.015
	additional H_2	m_{H2}		-	-	0.033	0.098
output	SNG	m_{CH4}		0.107	0.112	0.179	0.299
		m_{N2}		0.037	0.037	0.037	0.037
		m_{H2}		0.000	0.000	0.001	0.003
		m_{CO}		0.000	0.000	0.000	0.001
		m_{CO2}		0.002	0.001	0.015	0.032
	condensate	m_{H2O}		0.061	0.069	0.176	0.474

6.3.3 SNG composition and heating value

The composition of SNG based on volumetric concentrations is shown in Figure 6.16. Case 1 and 2 exhibit similar SNG compositions. The major component is CH_4 with a concentration of 0.81 $m^3 m^{-3}$. N_2 has with 0.16 $m^3 m^{-3}$ the second-highest concentration. This N_2 comes from fuel-bound nitrogen that is converted to N_2 during gasification. The rather high N_2 concentration is due to the volume reduction of the total gas stream during CO_2-removal and methanation. The H_2 concentration is around 0.03 $m^3 m^{-3}$, while the CO and CO_2 concentrations are below 0.01 $m^3 m^{-3}$.

Case 3 and case 4 show slightly higher CH_4 concentrations of 0.84 $m^3 m^{-3}$. Since the N_2 mass flow is similar for all cases but the CH_4 mass flow is higher in case 3 and 4, the N_2 concentration is reduced to 0.10 $m^3 m^{-3}$ in case 3 and 0.05 $m^3 m^{-3}$ in case 4. For case 3 and 4, there are slightly higher residual CO_2 and/or H_2 concentrations, showing that the methanation was less complete than for case 1 and 2 with the considered methanation process. A possibility to enhance the conversion of CO_2 and H_2 to CH_4 would be to shift the equilibrium by adding a condensation step after methanation stage one or to add a fourth methanation stage.

The DVGW standard G260 [144] sets the requirement of $y_{CH4} > 0.9$ $m^3 m^{-3}$ for feeding SNG into the natural gas grid. It can thus be concluded that SNG produced by all cases does not meet this requirement since the N_2 concentration is too high. In case 4, the nitrogen concentration is reduced sufficiently and it would be possible to achieve the requirement $y_{CH4} > 0.9$ $m^3 m^{-3}$ by optimizing the methanation process to reduce CO and H_2 concentrations.

In terms of heating value, as shown in Figure 6.17, the SNG heating value is between 32.5 MJ m^{-3} and 34.2 MJ m^{-3} and can therefore be compared to natural gas of the L-gas group [145].

Even if the produced SNG does not comply with current DVGW regulations, it is still a high quality fuel. The SNG could be mixed with upgraded biogas from sewage sludge or biomass fermentation or even LPG to achieve the DVGW requirements. A further possibility would be the liquefaction to renewable LNG, which enables a partial removal of N_2 as flash gas. It may also be possible to apply less strict regulations for feeding into local distribution grids.

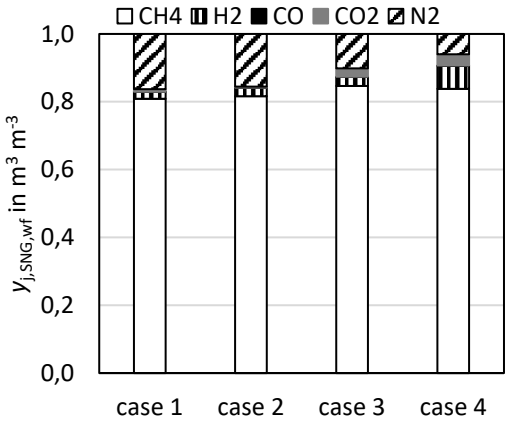

Figure 6.16: SNG composition

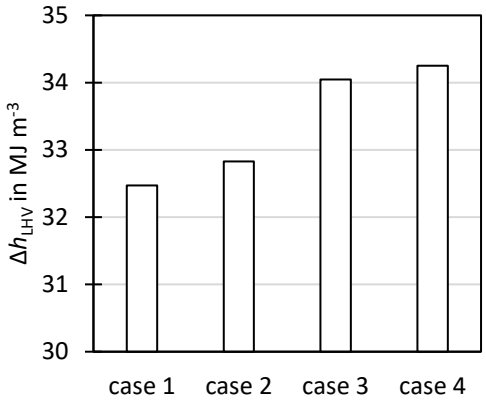

Figure 6.17: SNG lower heating value

6.3.4 Energy balance

This section discusses simplified specific energy balances for the process steps gasification, methanation, and the heat integration. The specific sensible and latent heat $q^{25°C}$ of each material stream was calculated by enthalpy difference from stream temperature ϑ to 25 °C and normalized to the higher heating value of sewage sludge:

$$q^{25°C} = \frac{H(\vartheta) - H(25°C)}{\Delta h_{\mathrm{HHV,SS,wf}}}. \tag{6-1}$$

Furthermore, chemical energy is considered by higher heating value Δh_{HHV} or reaction enthalpy Δh_{R}. The enthalpy of evaporation of sewage sludge moisture $\Delta h_{\mathrm{v,H2O}}$ is considered separately. Energy streams with value zero are omitted in the following tables, e.g. $q^{25°C}$=0 for streams with temperature 25 °C, Δh_{HHV} = 0 for streams without combustible species.

Gasification

Table 6.5 shows the gasification energy balance. The highest energy input stream is allocated to the sewage sludge feed in form of chemical energy (heating value). Followed by the sensible and latent heat of the gasification steam which is $q^{25°C}$ = 0.253 J J^{-1} for case 1, meaning that a quarter of the sewage sludge's higher heating value is needed to produce and pre-heat the gasification stream. The energy content in steam is significantly lower for case 2-4 due to the reduced steam amount. The energy needed for fuel moisture evaporation and additive calcination plays a minor role due to the low moisture content and low additive ratio.

The normalized syngas' chemical energy is equal to the cold gas efficiency and takes the value $\Delta h_{\mathrm{HHV,syn}} = \eta_{\mathrm{CGE}}$ = 0.63 for case 1 and could be enhanced to 0.67 for case 2 and 0.69 for case 3 and 4 due to lower n_{O2}. The chemical energy of tar is 0.055 J J^{-1} for case 1 and with 0.071 J J^{-1} slightly

higher for case 2, 3 and 4 as a result of increased tar yield at lower n_{SC}. The specific sensible and latent heat of the syngas is significantly higher for case 1 due to the high steam content than for case 2,3 and 4. The ash contains a specific sensible heat of around 0.043 J J^{-1} for all cases.

It can be concluded that cases 2, 3 and 4 are more energy efficient since less energy is required for steam generation and pre-heating and higher cold gas efficiencies could be achieved.

Methanation

Table 6.6 shows the energy balance of the methanation. The syngas is already compressed to 12 bar and heated to 300 °C. Since only impurities, CO_2 and steam have been removed from the syngas during gas cleaning; the chemical energy corresponds to the gasifier output. While case 1 and 2 do not use hydrogen addition, case 3 and 4 use hydrogen inputs with chemical energies of 0.43 J J^{-1} and 1.26 J J^{-1}, respectively. The chemical energy of hydrogen of case 4 thus exceeds the one from sewage sludge.

The SNG output has a temperature of 50 °C and has therefore a negligible heat content. The SNG's chemical energy equals the SNG cold gas efficiency with the values $\Delta h_{HHV,SNG} = \eta_{CGE,SNG} = 0.54$ and 0.57 for case 1 and 2, respectively. With the hydrogen addition, the cold gas efficiency could be significantly enhanced to 0.899 and 1.504 for case 3 and 4, respectively.

Heat integration

This section simplifies the analysis of the heat integration to one system with energy inputs and outputs as shown in Table 6.7. The actual simulated heat integration involves several heat exchangers as shown in section 6.1.

The hot syngas has a significant potential for heat recovery. The gas cooler brings the syngas from gasification temperature 850 °C to the filter temperature 200 °C while the heat is transferred to thermal oil, which is heated, from 185 °C to 350 °C. The thereby recovered heat stream for case 1 is 0.20 J J^{-1} while it is only 0.12 J J^{-1} for cases 2-4, due to the higher steam content in the syngas of case 1. If syngas quenching is applied as described in 6.1.4 and cooling is conducted only to 400 °C, the recovered heat is significantly reduced to 0.14 J J^{-1} for case 1 and 0.08 J J^{-1} for case 2 to 4.

Heat recovery is conducted accordingly after methanation step 1 and 2 where around 0.08 J J^{-1} could be transferred to the thermal oil circuit for case 1 and 2. Due to the enhanced yield of the exothermic methanation, more heat could be recovered for case 3 and 4 with 0.16 J J^{-1} and 0.28 J J^{-1}, respectively. Smaller heat flows are recovered from ash cooling and gas cooling after syngas compression.

Table 6.5: Gasification energy balance for integrated process chain

			unit	case 1 n_{SC}=2.3	case 2 n_{SC}=0.7	case 3 ELY O_2 n_{SC}=0.7	case 4 ELY full C n_{SC}=0.7
input	sewage sludge	ϑ	°C	25	25	25	
		Δh_{HHV}	J J^{-1}	1.000	1.000	1.000	
		$\Delta h_{V.H2O}$	J J^{-1}	-0.023	-0.023	-0.023	
	additive	ϑ	°C	25	25	25	
		$\Delta h_{R.calc}$	J J^{-1}	-0.005	-0.005	-0.005	
	oxygen	ϑ	°C	335	335	850	
		$q^{25°C}$	J J^{-1}	0.008	0.007	0.019	
	steam	ϑ	°C	484	750	750	
		$q^{25°C}$	J J^{-1}	0.253	0.060	0.060	
output	ash	ϑ	°C	850	850	850	
		$\Delta h_{HHV.char}$	J J^{-1}	0.035	0.035	0.035	
		$q^{25°C}$	J J^{-1}	0.043	0.043	0.043	
	syngas	ϑ	°C	850	850	850	
		$\Delta h_{HHV.syn}$	J J^{-1}	0.633	0.673	0.688	
		$\Delta h_{HHV.tar}$	J J^{-1}	0.055	0.071	0.071	
		$q^{25°C}$	J J^{-1}	0.450	0.210	0.208	

Table 6.6: Methanation energy balance for integrated process chain, all streams at 12 bar pressure, heat output through thermal oil, q_{meth}, is shown in Table 6.7, further heat is removed by cooling water

				case 1	case 2	case 3	case 4
input	syngas after gas cleaning	ϑ	°C	300	300	300	300
		Δh_{HHV}	J J^{-1}	0.633	0.673	0.687	0.687
		$q^{25°C}$	J J^{-1}	0.015	0.017	0.017	0.017
	H_2	ϑ	°C	-	-	120	120
		Δh_{HHV}	J J^{-1}	-	-	0.428	1.260
		$q^{25°C}$	J J^{-1}	-	-	0.003	0.006
output	SNG	ϑ	°C	50	50	50	50
		Δh_{HHV}	J J^{-1}	0.536	0.566	0.899	1.504
		$q^{25°C}$	J J^{-1}	0.007	0.007	0.011	0.017

Table 6.7: Heat integration of the integrated process chain mostly via thermal oil circuit

			unit	case 1	case 2	case 3	case 4
input	heat from coolers	q_{syn}		0.202	0.117	0.116	0.116
		q_{meth}		0.075	0.082	0.157	0.275
		q_{ash}		0.036	0.039	0.039	0.039
		q_{comp}		0.025	0.006	0.006	0.006
output	steam generation and heating	$q_{st,gasi}$	J J^{-1}	0.253	0.060	0.060	0.060
		$q_{st,ELY}$		0.000	0.000	0.103	0.271
		$q_{st,tar}$		0.028	0.028	0.028	0.028
	oxygen pre-heating	q_{O2}		0.008	0.007	0	0
	sewage sludge drying	q_{drying}		0.045	0.140	0.111	0.047

A significant part of the recovered heat is used for production and preheating of steam. For provision of gasification steam, case 1 requires 0.25 J J^{-1} whereas the lower n_{SC} reduced the energy demand of case 2 to 4 to 0.06 J J^{-1}. If pre-heated vapor from sewage sludge drying is used instead of steam, the heat demand can be lowered significantly to 0.05 J J^{-1} for case 1 and 0.02 J J^{-1} for case 2 to 4 for vapor pre-heating. Further recovered heat is used for steam provision for regeneration of the active char beds (light tar removal) and for oxygen pre-heating. In case 3 and 4, also significant heat of 0.10 J $J^{-1}$and 0.27 J J^{-1}, respectively, is required to produce steam for electrolysis. The residual recovered heat can be used for sewage sludge drying as discussed in 6.3.5.

6.3.5 Sewage sludge drying by heat integration

To better assess the available excess heat that can be used for sewage sludge drying; the ratio of drying heat supplied by the process chain's excess heat to total required drying heat is introduced:

$$\alpha_{\text{drying}} = \frac{Q_{\text{drying}}}{\Delta m_{\text{H2O,drying}}\, \Delta h_{v,H2O}\, \eta_{dryer}} = \frac{q_{\text{drying}}\, \Delta h_{HHV,SS,wf}}{\Delta m_{\text{H2O,drying}}\, \Delta h_{v,H2O}\, \eta_{dryer}} \text{ in J J}^{-1}. \quad (6\text{-}2)$$

Wherein q_{drying} is the available excess heat for drying as given in Table 6.7, $\Delta m_{\text{H2O,drying}}$ is the specific mass of water to be evaporated during drying and η_{dryer} is the efficiency of the used dryer (see Table 6.1). If dewatered sewage sludge with water content of $\gamma_{SS,ar}$ = 0.75 kg kg^{-1} is dried to a water content of $\gamma_{SS,au}$ = 0.1 kg kg^{-1}, the evaporated water amount is expressed by

$$\Delta m_{\text{H2O,drying}} = \frac{\gamma_{H2O,ar}}{1-\gamma_{H2O,ar}} - \frac{\gamma_{H2O,au}}{1-\gamma_{H2O,au}} = 2.889 \text{ kg kg}^{-1}. \quad (6\text{-}3)$$

Figure 6.18 shows α_{drying} for all four cases also considering the influence of quenching at 400 °C, using drying vapor as gasification steam and the combination thereof. For case 1 in base configuration, α_{drying} is 0.06 J J^{-1}, meaning that only a small fraction of the needed drying heat can be supplied by heat integration. Syngas quenching at 400 °C reduces available heat for drying to almost zero. By using drying vapor as gasification agent, α_{drying} could be slightly enhanced to around 0.10 J J^{-1}. The reduced n_{SC} of case 2 allows achieving α_{drying} = 0.19 J J^{-1} with the basic configuration. Syngas quenching decreases α_{drying} while vapor utilization only slightly enhances α_{drying}. For cases 3 and 4, α_{drying} is lower than for case 2 since the production of steam for electrolysis consumes additional energy.

Case 1 has the benefit of not needing a catalytic WGS unit and of lower tar concentrations; however, it can supply little to no heat for sludge drying. The case 1 configuration should therefore be selected if no or only very little drying heat is required on the plant site. If technically feasible, it can be recommended to use drying vapor as gasification agent instead of steam to enhance the available heat for drying especially for the case 1 configuration. The case 2 configuration is recommended for maximized α_{drying}, but still only one fifth of the sludge feed can then be dried by heat integration.

It can be concluded that by far not enough heat can be provided by heat integration to dry the utilized sewage sludge. This implies that either another heat source has to be used to dry the remaining sewage sludge, or that the majority of sewage sludge needs to be imported as pre-dried sludge from another site.

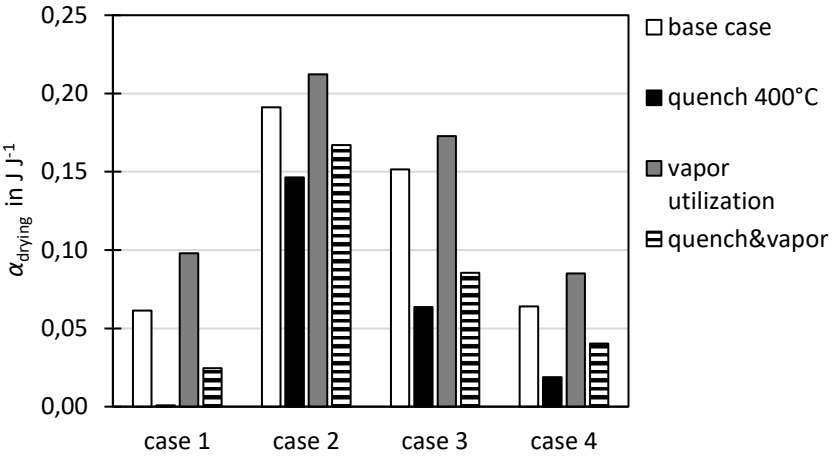

Figure 6.18: Fraction of sewage sludge drying heat that can be supplied by heat integration

6.3.6 Total efficiency of integrated process chain

The total efficiency also considers electrical power needed for process operation. This thesis focuses only on the three most significant power consumers, syngas compression, air separation and electrolysis. The electrical energy consumption based on the higher heating value of sewage sludge is given in Table 6.8. For case 1 and case 2, the electrical energy needed for syngas compression and air separation sums up to around 10 % of the sewage sludge's heating value. For comparison, the GoBiGas project reported electricity consumption of around 8 % based on the fuel's higher heating value [140].

No ASU is required for the cases 3 and 4; however, slightly more compression energy is required since also hydrogen compression is needed. The electrical energy consumption of the electrolysis is significant and corresponds for case 3 to around 44 % and for case 4 to around 130 % of the sludge's higher heating value.

Table 6.8: Electricity consumption for integrated process chain

		case 1	**case 2**	**case 3**	**case 4**
	unit	n_{SC}**=2.3**	n_{SC}**=0.7**	**ELY** O_2 n_{SC}**=0.7**	**ELY full C** n_{SC}**=0.7**
$P_{el,comp}$		0.035	0.035	0.051	0.086
$P_{el,ASU}$	J J^{-1}	0.067	0.060	-	-
$P_{el,ELY}$		-	-	0.442	1.302

Figure 6.19 shows the total efficiency of the process chain. It takes into account the higher heating values of the educt sewage sludge and the product SNG as well as the consumed electrical energy (see definition in section 2.2.6). External heat requirement for sludge drying is not considered. The total efficiency for case 1 and case 2 was calculated to $\eta_{tot,SNG}$ = 0.49 and 0.51, respectively. Since no suitable data on conversion of sewage sludge to SNG was found in literature, it was decided to compare with results from the GoBiGas project. From process data of the GoBiGas semi-commercial demo plant and process simulation, SNG "cold gas efficiency" of 0.62 and "plant efficiency" (comparable to $\eta_{tot,SNG}$) of 0.58 were reported [146]. The higher SNG efficiencies of GoBiGas are attributed to higher syngas cold gas efficiencies in the gasifier section since the GoBiGas process has lower losses through char and hot ash output than the process chain investigated in this work. In addition, the dual gasification system used in the GoBiGas plant did not need oxygen as gasification agent.

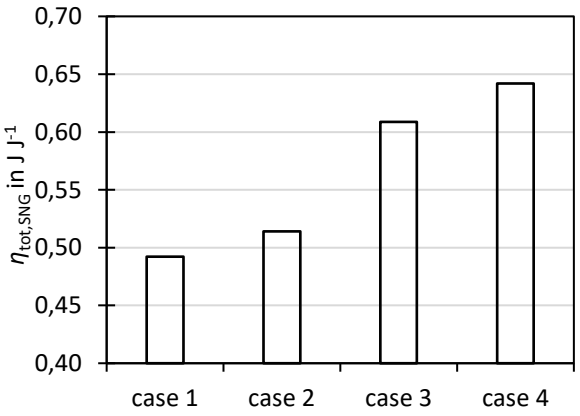

Figure 6.19: Total efficiency from sewage sludge to SNG of the integrated process chain including own consumption of electrical energy

The total efficiency for cases 3 and 4 are with $\eta_{tot,SNG}$ = 0.61 and 0.64, respectively, higher than for the cases without oxygen. The calculated efficiencies correspond well to literature data where a process chain from wood to SNG through steam-oxygen gasification with electrolysis integration was investigated [93].

6.4 Conclusions simulation of SNG production

In chapter 6, a process chain for SNG production from sewage sludge was modeled and simulations focusing on the performance of the process were conducted. Different cases were assessed including the integration of a water electrolysis. The main simulation results and conclusions are:

The predicted SNG composition for the case without electrolysis is rounded to $y_{CH4,SNG}$=0.81 m^3 m^{-3}, $y_{N2,SNG}$ = 0.16 m^3 m^{-3} and $y_{H2,SNG}$ = 0.03 m^3 m^{-3}. The high N_2 concentration is

due to the high nitrogen content in the sewage sludge. It needs to be noted that comprehensive experimental data on the fraction of fuel N that is converted to N_2 is not yet available to verify this prediction. The SNG does according to this prediction not meet current German regulations for feeding into the gas grid that require $y_{CH4,SNG} > 0.9$ m^3 m^{-3} [144]. However, less strict future regulations or blending with other gas qualities could still enable to feed sewage sludge-derived SNG into the existing grid.

The total efficiency of the conversion from sewage sludge to SNG without electrolysis is up to $\eta_{SNG,tot} = 0.51$, which is slightly lower than for other biomass to SNG processes (e.g. GoBiGas), but still is a promising result. The comparably lower efficiency is attributed to lower cold gas efficiency due to the heat off-stream from the gasifier through hot sewage sludge ash, comparably high yields of tar and char and the electrical energy demand of the O_2-provision.

The process chain has excess heat that can be used for sewage sludge drying. The amount thereof depends on the studied case, but is at maximum only sufficient to dry around 20 % of the sewage sludge feed. This implies that either another heat source has to be used to dry the remaining sewage sludge, or that the majority of the sewage sludge needs to be imported as dry sludge from other sites. A novel concept for utilization of vapor from sewage sludge drying as gasification agent instead of steam was studied in the simulations. It was found that the own consumption for steam generation can thereby be reduced enhancing the recovered excess heat for sewage sludge drying. The effect is more pronounced for higher n_{SC}.

Two possible cases were simulated regarding the choice of the steam to carbon ratio, n_{SC}, of the gasification step. On the one hand, $n_{SC} = 2.3$ mol mol^{-1} allows the in-situ adjustment of the H_2/CO-ratio to the desired value for methanation, saving the need of a catalytic water-gas shift unit thus enabling process intensification with potentially less CAPEX. However, the comparably high n_{SC} leads to a lower efficiency and lower excess heat for sewage sludge drying. On the other hand, a case with a low n_{SC} of 0.7 mol mol^{-1} was studied. The case was found to have a slightly higher cold gas efficiency and a higher recovery of excess heat.

Two cases for integration of an SOEC electrolysis into the process chain were studied. First, an operation with an electrolysis load that is sufficient to provide the required oxygen for the gasification process leads to an increase of over 60 % of the SNG yield and increased the total efficiency of the process chain. However, the electrical energy required for electrolysis is significantly higher than for O_2-production via air separation. Second, a case was studied that considers an even higher electrolysis load that provides sufficient H_2 to convert all CO and CO_2 in the syngas to CH_4. By this, an almost complete utilization of the sewage sludge's carbon could be achieved and the SNG yield could be enhanced by nearly 200 % compared to the case without electrolysis. The total efficiency of the process chain was enhanced as well.

Recommendations of the author for further investigations of this process chain are given in the following. A higher degree of detail could be used e.g. also covering thermal utilization of the tar from RME scrubbers and electrical consumption of more auxiliary units such as liquid pumps. Furthermore, a more detailed process simulation could be used to calculate CAPEX and OPEX and thus to study the economic assessment of the process. It could also be interesting to study alternative synthesis products such as methanol.

Finally, a simplified assessment of the potential of SNG production from sewage sludge in Germany is conducted. If all sewage sludge that is produced in Germany is used for SNG production without electrolysis, it would be possible to cover 0.3 % of the total German natural gas consumption (2021, [147]). This value seems low; however, it needs to be taken into account that natural gas is used mainly for domestic heating. A purpose that is assumed to decrease in the following years to be replaced by heat pumps or other technologies due to the energy transition. A more suitable comparison is that the SNG produced from sewage sludge could replace 8 % of the natural gas for material use in the German chemical industry [148]. If power to gas via electrolysis is added, the natural gas replacement could be up to 200 % higher (case 4).

7 Summary and conclusion

This thesis demonstrated and characterized steam-oxygen gasification of sewage sludge and assessed the conversion of sewage sludge to SNG as exemplary synthesis product. Since the used experimental gasifier was electrically heated and could thus not be operated under adiabatic conditions, it was necessary to complement the experiments with simulations. A gasifier model combining thermochemical equilibrium with empirical correlations deduced from the experiments was developed and used to obtain a complete mass and energy balance of the process.

The experimental work of this thesis demonstrated the feasibility of synthesis gas production from sewage sludge by steam-oxygen fluidized bed gasification. It was shown that the process works reliably in the investigated 20 kW scale and that the syngas contains high H_2 and CO concentrations and is thus suitable for synthesis of fuels and chemicals. The experimental results can be utilized for process design, since the yields of product gas, char, tar and impurities as well as their dependencies on the operation conditions were determined. The impurities NH_3, H_2S, COS and tar species were measured in considerable concentrations in the syngas. Hydrocarbons and tar species from sewage sludge consist of the known species from wood gasification such as benzene, toluene, naphthalene, but also of species with heteroatoms, such as pyridine and thiophene. Data from literature shows that also HCN may be present in the syngas in considerable amount. It is concluded that adequate gas cleaning steps (e.g. scrubbers, absorbers) are needed to remove the impurities in order to feed the syngas to synthesis processes. The impurity concentration measurements of this work provide a basis for designing the gas cleaning steps. The process is now ready to go into the next scale, which could be a TRL 7 demonstrator.

It was found by combination of simulation and experiments that the cold gas efficiency increases monotonously with rising gasification temperature, despite the increasing oxygen-requirement for autothermal operation, due to improved tar and char conversion at higher temperatures. It can therefore be concluded that the gasification temperature should be chosen as high as possible, but stay below the ash's shrinkage starting temperature under the reducing conditions of the gasifier. With this trade-off in mind, gasification temperatures should be set around 850 °C, requiring an oxygen ratio of n_{O2} = 0.33 and obtaining a cold gas efficiency of n_{CGE}=0.63.

Furthermore, the investigation of limestone as bed additive led to the conclusion that small amounts of limestone are sufficient to reduce the concentration of heavy tar species significantly, decreasing the potential risk of gas cooler clogging. Lighter hydrocarbons or tar species such as

benzene or naphthalene are only slightly reduced by the addition of limestone. Limestone addition also reduced the H_2S and COS concentrations. An additive ratio of 0.03 kg limestone per kg dry sewage sludge was found to be the optimum in respect of tar and sulfur reduction and cold gas efficiency.

It was further found that the H_2/CO-ratio could be controlled efficiently by altering the steam to carbon ratio, n_{SC}, as steam promotes the water gas shift reaction in the gasifier to achieve the desired stoichiometry for synthesis. It was concluded that there are two purposeful choices for n_{SC} in process design: The first option is a rather low n_{SC} of around 0.7 mol H_2O per mol fuel carbon, which requires less energy for steam generation making more excess heat available that can e.g. be used for sewage sludge drying. However, the low n_{SC} leads to a raw syngas with too low H_2/CO-ratio for SNG production. Thus, a downstream catalytic water-gas shift unit is needed to adjust the stoichiometry. The second option is an n_{SC} that leads to a suitable H_2/CO ratio in the raw gas without the need of a catalytic shift unit, which could be reached with n_{SC} = 2.3 mol mol^{-1}. Yet, significantly more heat is required for steam generation, reducing the available excess heat for sludge drying. In the best case, 20 % of the sewage sludge feed can be dried by excess heat. This implies that either another heat source has to be used to dry the remaining sewage sludge, or that the majority of the sewage sludge needs to be imported as dry sludge from another site.

Furthermore, an integrated process chain was simulated to assess the conversion of sewage sludge to synthetic natural gas (SNG) with and without inclusion of power-to-gas through electrolysis. The predicted SNG composition for the case without electrolysis is rounded to $y_{CH4,SNG}$ = 0.81 m^3 m^{-3}, $y_{N2,SNG}$ = 0.16 m^3 m^{-3} and $y_{H2,SNG}$ = 0.03 m^3 m^{-3}. The high N_2 concentration is due to the high nitrogen content in sewage sludge that is converted partially to N_2 during gasification. It is concluded that the sewage sludge-derived SNG does not meet current German regulations for feeding into the gas grid that require $y_{CH4,SNG}$ > 0.9 m^3 m^{-3} [144]. However, less strict future regulations or blending with other gas qualities could still enable feeding sewage sludge-derived SNG into the existing gas grid. In addition, comprehensive experimental data on the fraction of fuel N that is converted to N_2 is still needed to verify this prediction. The CH_4-yield of the whole process chain can be increased by adding hydrogen from electrolysis.

The total efficiency of the conversion from sewage sludge to SNG including own consumption of the plant for the case without electrolysis is up to 51 % with a carbon utilization of 33 %. The total efficiency, the SNG yield and the carbon utilization increased with increased hydrogen addition from electrolysis enabling almost full carbon utilization with a respective electrolysis load.

Overall, the steam-oxygen gasification proved to be an efficient and technically feasible process for sewage sludge treatment. The process can play a role in closing the loop for carbon by converting the organic fraction of sewage sludge to carbon-containing bio-fuels or chemicals as well as in

closing the loop for phosphorous that can be recovered from the heavy metal lean ash. This process can therefore be considered as alternative to fluidized bed incineration for future sewage sludge mono-treatment plants.

As an outlook, future experimental work should focus on determining practical data for gasifier design, such as the effect of solid and gas residence times on the product (gas and solid) qualities. Such data can be used to determine the dimensions of an industrial gasifier. Also, in the used electrically heated facility, n_{O2} was disconnected from the actual energy demand of the gasification. To study the process under more realistic conditions, it is recommended to conduct experiments in a refractory lined gasifier with a load of 200 kW or higher, allowing an autothermal operation under near-adiabatic conditions.

It is recommended to cast a deeper look onto the behavior of solids during gasification such as char conversion degree in dependency on operation conditions (ϑ, n_{SC}) and reactor design (n_{WHSV}, location of ash extraction). Also, different sewage sludges show a different behavior in respect to attrition, which could lead to a higher fly ash fraction. It would thus be interesting to correlate the waste water treatment process (e.g. utilized phosphorous precipitation additive), the drying process (dryer technology type) with the mechanic and thermochemical behavior of the sewage sludge in the gasifier. Also, analysis methods such as SEM microscopy and XRD mineral phase analysis could enhance the knowledge on the physical and chemical conversion of the solids during gasification. These insights are also important to optimize the ash for phosphorous extraction or direct fertilizer production from ash. More elaborate solid sample analysis may also help to optimize bed additives for sulfur capture and tar reduction.

The gasifier model and process simulation developed in this thesis are a great basis for in-depth techno-economic analysis of the application of steam-oxygen sewage sludge gasification. Such a study can be started by a more detailed calculation of OPEX such as consumption of electricity (also taking into account smaller auxiliaries such as washing water pumps, mechanical drives for solid transport), water and chemicals as well as the needed labor and spare part costs for operation and maintenance. Also, the energy demand of the CO_2-removal via pressure water scrubbing can be calculated more accurately. The second step would be an estimation of the plant's CAPEX. Such a techno-economic approach can be used to study different synthesis products (e.g. methanol, DME, Fischer-Tropsch alkanes) and different process integration scenarios (e.g. integration into a bio-refinery or chemical production site).

8 References

[1] Milieu Ltd, Environmental, economic and social impacts of the use of sewage sludge on land: Final Report Part I: Overview Report. https://www.svensktvatten.se/globalassets/avlopp-och-miljo/uppstromsarbete-och-kretslopp/revaq-certifiering/eu-sludge-summary-report-1.pdf (accessed 10 December 2023).

[2] T.E. Seiple, A.M. Coleman, R.L. Skaggs, Municipal wastewater sludge as a sustainable bioresource in the United States, Journal of Environmental Management 197 (2017) 673–680. https://doi.org/10.1016/j.jenvman.2017.04.032.

[3] G. Yang, G. Zhang, H. Wang, Current state of sludge production, management, treatment and disposal in China, Water Research 78 (2015) 60–73. https://doi.org/10.1016/j.watres.2015.04.002.

[4] K. Gorazda, B. Tarko, S. Werle, Z. Wzorek, Sewage sludge as a fuel and raw material for phosphorus recovery: Combined process of gasification and P extraction, Waste Management 73 (2018) 404–415. https://doi.org/10.1016/j.wasman.2017.10.032.

[5] AbfKlärV, Verordnung über die Verwertung von Klärschlamm, Klärschlammgemisch und Klärschlammkompost (Klärschlammverordnung - AbfKlärV), 2017. https://www.gesetze-im-internet.de/abfkl_rv_2017/AbfKl%C3%A4rV.pdf (accessed 5 January 2021).

[6] A. Zanelli, Producing Fertilizers with Recycled Phosphate, 2018. http://icl-group-sustainability.com/reports/producing-fertilizers-with-recycled-phosphate/.

[7] S. Arnout, E. Nagels, Modelling thermal phosphorus recovery from sewage sludge ash, Calphad 55 (2016) 26–31. https://doi.org/10.1016/j.calphad.2016.06.008.

[8] H. Herzel, O. Krüger, L. Hermann, C. Adam, Sewage sludge ash — A promising secondary phosphorus source for fertilizer production, Science of The Total Environment 542 (2016) 1136–1143. https://doi.org/10.1016/j.scitotenv.2015.08.059.

[9] J.W. Judex, M. Gaiffi, H.C. Burgbacher, Gasification of dried sewage sludge: Status of the demonstration and the pilot plant, Waste Management 32 (2012) 719–723. https://doi.org/10.1016/j.wasman.2011.12.023.

[10] M. Schmid, M. Beirow, D. Schweitzer, G. Waizmann, R. Spörl, G. Scheffknecht, Product gas composition for steam-oxygen fluidized bed gasification of dried sewage sludge, straw pellets and wood pellets and the influence of limestone as bed material, Biomass and Bioenergy 117 (2018) 71–77. https://doi.org/10.1016/j.biombioe.2018.07.011.

[11] E. Roche, J.M. de Andrés, A. Narros, M.E. Rodríguez, Air and air-steam gasification of sewage sludge. The influence of dolomite and throughput in tar production and composition, Fuel 115 (2014) 54–61. https://doi.org/10.1016/j.fuel.2013.07.003.

[12] P. Basu, Biomass Gasification and Pyrolysis, Academic Press, Boston, 2010.

[13] N. Abdoulmoumine, S. Adhikari, A. Kulkarni, S. Chattanathan, A review on biomass gasification syngas cleanup, Applied Energy 155 (2015) 294–307. https://doi.org/10.1016/j.apenergy.2015.05.095.

[14] K. Göransson, U. Söderlind, J. He, W. Zhang, Review of syngas production via biomass DFBGs, Renewable and Sustainable Energy Reviews 15 (2011) 482–492. https://doi.org/10.1016/j.rser.2010.09.032.

[15] J.M. de Andrés, E. Roche, A. Narros, M.E. Rodríguez, Characterisation of tar from sewage sludge gasification. Influence of gasifying conditions: Temperature, throughput, steam and use of primary catalysts, Fuel 180 (2016) 116–126. https://doi.org/10.1016/j.fuel.2016.04.012.

[16] D.J. Stevens, Hot Gas Conditioning: Recent Progress With Larger-Scale Biomass Gasification Systems :Update and Summary of Recent Progress, NREL report SR-510-29952 (2001) https://www.nrel.gov/docs/fy01osti/29952.pdf.

[17] B. Dou, C. Wang, H. Chen, Y. Song, B. Xie, Y. Xu, C. Tan, Research progress of hot gas filtration, desulphurization and HCl removal in coal-derived fuel gas: A review, Chemical Engineering Research and Design 90 (2012) 1901–1917. https://doi.org/10.1016/j.cherd.2012.04.009.

[18] M. Husmann, M. Müller, C. Zuber, T. Kienberger, V. Maitz, C. Hochenauer, Application of BaO-Based Sulfur Sorbent for in Situ Desulfurization of Biomass-Derived Syngas, Energy Fuels 30 (2016) 6458–6466. https://doi.org/10.1021/acs.energyfuels.6b00957.

[19] M. Schmid, S. Hafner, G. Scheffknecht, Experimental Parameter Study on Synthesis Gas Production by Steam-Oxygen Fluidized Bed Gasification of Sewage Sludge, Applied Sciences 11 (2021) 579. https://doi.org/10.3390/app11020579.

[20] M. Schmid, S. Hafner, S. Biollaz, J. Schneebeli, G. Waizmann, G. Scheffknecht, Steam-oxygen gasification of sewage sludge: Reduction of tar, H2S and COS with limestone as bed additive, Biomass and Bioenergy 150 (2021) 106100.

[21] M. Schmid, C. Schmidberger, G. Scheffknecht, Modelling and simulation of fluidized bed steam-oxygen gasification of sewage sludge using thermochemical equilibrium and experimental data, 10th Japan/China Symposium on Coal and C1 Chemistry 341 (2023) 127595. https://doi.org/10.1016/j.fuel.2023.127595.

[22] M. Schmid, C. Schmidberger, S. Hafner, G. Scheffknecht, Process simulation of SNG production from sewage sludge via steam-oxygen gasification, 10th Japan/China Symposium on Coal and C1 Chemistry 360 (2024) 130491. https://doi.org/10.1016/j.fuel.2023.130491.

[23] T.A. Milne, R.J. Evans, N. Abatzaglou, Biomass Gasifier "Tars": Their Nature, Formation, and Conversion, NREL/TP-570-25357 (1998).

[24] C. Di Blasi, Combustion and gasification rates of lignocellulosic chars, Progress in Energy and Combustion Science 35 (2009) 121–140. https://doi.org/10.1016/j.pecs.2008.08.001.

[25] CEN/TS 15439:2006, Biomass gasification - Tar and particles in product gases - Sampling and analysis, 2006.

[26] J. Kiel, S. Paasen, J. Neeft, L. Devi, K. Ptasinski, F. Janssen, R. Meijer, R. Berends, H. Temmink, G. Brem, E. Bramer, N. Padban, Primary measures to reduce tar formation in fluidised-bed biomass gasifiers, ECN publication(Energy research Centre of the Netherlands) 1 (2004) 1–108.

[27] J.M. de Andrés, A. Narros, M.E. Rodríguez, Behaviour of dolomite, olivine and alumina as primary catalysts in air–steam gasification of sewage sludge, Fuel 90 (2011) 521–527. https://doi.org/10.1016/j.fuel.2010.09.043.

[28] Z. Abu El-Rub, E.A. Bramer, G. Brem, Review of Catalysts for Tar Elimination in Biomass Gasification Processes, Ind. Eng. Chem. Res. 43 (2004) 6911–6919. https://doi.org/10.1021/ie0498403.

[29] B. Li, C.F. Magoua Mbeugang, Y. Huang, D. Liu, Q. Wang, S. Zhang, A review of CaO based catalysts for tar removal during biomass gasification, Energy 244 (2022) 123172. https://doi.org/10.1016/j.energy.2022.123172.

[30] L. Devi, K.J. Ptasinski, F.J. Janssen, A review of the primary measures for tar elimination in biomass gasification processes, Biomass and Bioenergy 24 (2003) 125–140. https://doi.org/10.1016/S0961-9534(02)00102-2.

[31] P. Yrjas, K. Iisa, M. Hupa, Limestone and dolomite as sulfur absorbents under pressurized gasification conditions, Fuel 37 (1996) 126. https://doi.org/10.1016/0140-6701(96)87879-9.

[32] Y.-H. Chen, M. Schmid, T. Kertthong, G. Scheffknecht, Reforming of toluene as a tar model compound over straw char containing fly ash, Biomass and Bioenergy 141 (2020) 105657. https://doi.org/10.1016/j.biombioe.2020.105657.

[33] Y.-H. Chen, M. Schmid, C.-C. Chang, C.-Y. Chang, G. Scheffknecht, Lab-Scale Investigation of Palm Shell Char as Tar Reforming Catalyst, Catalysts 10 (2020) 476. https://doi.org/10.3390/catal10050476.

[34] K.J. Andersson, M. Skov-Skjøth Rasmussen, P.E. Højlund Nielsen, Industrial-scale gas conditioning including Topsoe tar reforming and purification downstream biomass gasifiers: An

overview and recent examples, 10th Japan/China Symposium on Coal and C1 Chemistry 203 (2017) 1026–1030. https://doi.org/10.1016/j.fuel.2017.02.085.

[35] M. Husmann, C. Zuber, V. Maitz, T. Kienberger, C. Hochenauer, Comparison of dolomite and lime as sorbents for in-situ H2S removal with respect to gasification parameters in biomass gasification, Fuel 181 (2016) 131–138. https://doi.org/10.1016/j.fuel.2016.04.124.

[36] J. Delgado, M.P. Aznar, J. Corella, Calcined Dolomite, Magnesite, and Calcite for Cleaning Hot Gas from a Fluidized Bed Biomass Gasifier with Steam: Life and Usefulness, Industrial & Engineering Chemistry Research 35 (1996) 3637–3643. https://doi.org/10.1021/ie950714w.

[37] A.Y. Al-Otoom, Y. Ninomiya, B. Moghtaderi, T.F. Wall, Coal Ash Buildup on Ceramic Filters in a Hot Gas Filtration System, Energy & Fuels 17 (2003) 316–320. https://doi.org/10.1021/ef010275f.

[38] S. Hafner, M. Schmid, R. Spörl, G. Scheffknecht, Experimental Investigation of the Sorption Enhanced Gasification of Biomass in a Dual Fluidized Bed Pilot Plant, 27th European Biomass Conference (EUBCE), Lisbon (2019).

[39] D. Kunii, O. Levenspiel, Fluidization Engineering second edition, Butterworth-Heinemann, 1991.

[40] C.Y. Wen, Y.H. Yu, A generalized method for predicting the minimum fluidization velocity, AIChE J. 12 (1966) 610–612. https://doi.org/10.1002/aic.690120343.

[41] S.S.A. Syed-Hassan, Y. Wang, S. Hu, S. Su, J. Xiang, Thermochemical processing of sewage sludge to energy and fuel: Fundamentals, challenges and considerations, Renewable and Sustainable Energy Reviews 80 (2017) 888–913. https://doi.org/10.1016/j.rser.2017.05.262.

[42] P.H. Andrea Roskosch, Klärschlamm Entsorgung in der Bundesrepublik Deutschland, 2018.

[43] J. Oliva, A. Bernhardt, H. Reisinger, Domenig, M. & Krammer, H.-J, Klärschlamm – Materialien zur Abfallwirtschaft: REP-0221, Umweltbundesamt (2009).

[44] Y.-K. Choi, M.-H. Cho, J.-S. Kim, Steam/oxygen gasification of dried sewage sludge in a two-stage gasifier: Effects of the steam to fuel ratio and ash of the activated carbon on the production of hydrogen and tar removal, Energy 91 (2015) 160–167. https://doi.org/10.1016/j.energy.2015.08.027.

[45] F. Pinto, H. Lopes, André,, Rui Neto, M. Dias, I. Gulyurtlu, I. Cabrita, Effect of Experimental Conditions on Gas Quality and Solids Produced by Sewage Sludge Cogasification. 1. Sewage Sludge Mixed with Coal, Energy & Fuels 21 (2007) 2737–2745. https://doi.org/10.1021/ef0700836.

[46] L. Calvo, A. García, M. Otero, An Experimental Investigation of Sewage Sludge Gasification in a Fluidized Bed Reactor, TheScientificWorldJournal 2013 (2013) 479403. https://doi.org/10.1155/2013/479403.

[47] R. Migliaccio, P. Brachi, F. Montagnaro, S. Papa, A. Tavano, P. Montesarchio, G. Ruoppolo, M. Urciuolo, Sewage Sludge Gasification in a Fluidized Bed: Experimental Investigation and Modeling, Ind. Eng. Chem. Res. 60 (2021) 5034–5047. https://doi.org/10.1021/acs.iecr.1c00084.

[48] M. Niu, B. Jin, Y. Huang, H. Wang, Q. Dong, H. Gu, J. Yang, Co-gasification of High-ash Sewage Sludge and Straw in a Bubbling Fluidized Bed with Oxygen-enriched Air, International Journal of Chemical Reactor Engineering 16 (2018). https://doi.org/10.1515/ijcre-2017-0044.

[49] DüMV, Verordnung über das Inverkehrbringen von Düngemitteln, Bodenhilfsstoffen, Kultursubstraten und Pflanzenhilfsmitteln (Düngemittelverordnung - DüMV), 2012. https://www.gesetze-im-internet.de/d_mv_2012/D%C3%BCMV.pdf (accessed 5 January 2021).

[50] DIN EN ISO 21404:2020-06, Biogene Festbrennstoffe - Bestimmung des Asche-Schmelzverhaltens (ISO 21404:2020); Deutsche Fassung EN ISO 21404:2020, Beuth Verlag GmbH, Berlin.

[51] Y. Huang, K. Li, Effect of reducing conditions on sludge melting process, Chemosphere 50 (2003) 1063–1068. https://doi.org/10.1016/s0045-6535(02)00622-7.

[52] L. Wang, G. Skjevrak, J.E. Hustad, M.G. Grønli, Sintering characteristics of sewage sludge ashes at elevated temperatures, Fuel Processing Technology 96 (2012) 88–97. https://doi.org/10.1016/j.fuproc.2011.12.022.

[53] M. Beckmann, A. Hurtado (Eds.), Kraftwerkstechnik, Band 4: Sichere und nachhaltige Energieversorgung, TK-Verlag, 2012.

[54] Statistisches Bundesamt, Wasserwirtschaft: Klärschlammentsorgung aus der öffentlichen Abwasserbehandlung 2021, 2021. https://www.destatis.de/DE/Themen/Gesellschaft-Umwelt/Umwelt/Wasserwirtschaft/Tabellen/liste-klaerschlammverwertungsart.html#fussnote-1-633398 (accessed 16 February 2023).

[55] M. Rapf, Phosphorrückgewinnung aus Klärschlammasche vor dem Hintergrund der neuen deutschen Klärschlammverordnung, 14. Recy & DepoTech Konferenz, Leoben, Austria (2018).

[56] Kopf SynGas GmbH & Co. KG, SynGas Klärschlammverwertungsanlage Balingen, 2022. https://kopf-syngas.de/syngas-klaerschlammvergasungsanlage-in-balingen/ (accessed 2 April 2022).

[57] Kopf SynGas GmbH & Co. KG, SynGas Klärschlammverwertungsanlage Mannheim, 2022. https://kopf-syngas.de/syngas-klaerschlammvergasungsanlage-in-mannheim/ (accessed 2 April 2022).

[58] Kopf SynGas GmbH & Co. KG, SynGas Klärschlammverwertungsanlage Koblenz, 2022. https://kopf-syngas.de/syngas-klaerschlammvergasungsanlage-in-koblenz/ (accessed 2 April 2022).

[59] Y.-S. Jeong, T.-Y. Mun, J.-S. Kim, Two-stage gasification of dried sewage sludge: Effects of gasifying agent, bed material, gas cleaning system, and Ni-coated distributor on product gas quality, Renewable Energy 185 (2022) 208–216. https://doi.org/10.1016/j.renene.2021.12.069.

[60] T.-Y. Mun, J.-W. Kim, J.-S. Kim, Air gasification of dried sewage sludge in a two-stage gasifier: Part 1. The effects and reusability of additives on the removal of tar and hydrogen production, International Journal of Hydrogen Energy 38 (2013) 5226–5234. https://doi.org/10.1016/j.ijhydene.2012.10.120.

[61] N. Gao, K. Kamran, C. Quan, P.T. Williams, Thermochemical conversion of sewage sludge: A critical review, Progress in Energy and Combustion Science 79 (2020) 100843. https://doi.org/10.1016/j.pecs.2020.100843.

[62] F. Pinto, R.N. André, H. Lopes, M. Dias, I. Gulyurtlu, I. Cabrita, Effect of Experimental Conditions on Gas Quality and Solids Produced by Sewage Sludge Cogasification. 2. Sewage Sludge Mixed with Biomass, Energy & Fuels 22 (2008) 2314–2325. https://doi.org/10.1021/ef700767q.

[63] R.N. André, F. Pinto, H. Lopes, Study of Co-Gasification of Mixtrues with three Different Typers of Wastes. Control of H2S Release into Syngas, 21st International Conference on Fluidized Bed Combustion (2012) 813–820.

[64] J.J. Manyà, J.L. Sánchez, A. Gonzalo, J. Arauzo, Air Gasification of Dried Sewage Sludge in a Fluidized Bed: Effect of the Operating Conditions and In-Bed Use of Alumina, Energy & Fuels 19 (2005) 629–636. https://doi.org/10.1021/ef0497614.

[65] U. Lee, J. Dong, J.N. Chung, Experimental investigation of sewage sludge solid waste conversion to syngas using high temperature steam gasification, Energy Conversion and Management 158 (2018) 430–436. https://doi.org/10.1016/j.enconman.2017.12.081.

[66] S. Chen, Z. Sun, Q. Zhang, J. Hu, W. Xiang, Steam gasification of sewage sludge with CaO as CO2 sorbent for hydrogen-rich syngas production, Biomass and Bioenergy 107 (2017) 52–62. https://doi.org/10.1016/j.biombioe.2017.09.009.

[67] J. Schmid, A. Bartik, F. Benedikt, A.M. Mauerhofer, J. Fuchs, E. Schanz, S. Reisinger, B. Nowak, F. Bühler, M. Österreicher, A. Lunzer, C. Walcher, S. Müller, M. Fuchs, H. Hofbauer, Steam gasification of sewage sludge for synthesis processes, Proceedings of the ICPS 19 (2019). https://doi.org/10.34726/45.

[68] D. Schweitzer, A. Gredinger, M. Schmid, G. Waizmann, M. Beirow, R. Spörl, G. Scheffknecht, Steam gasification of wood pellets, sewage sludge and manure: Gasification performance and

concentration of impurities, Biomass and Bioenergy 111 (2018) 308–319. https://doi.org/10.1016/j.biombioe.2017.02.002.

[69] C. Freda, G. Cornacchia, A. Romanelli, V. Valerio, M. Grieco, Sewage sludge gasification in a bench scale rotary kiln, Fuel 212 (2018) 88–94. https://doi.org/10.1016/j.fuel.2017.10.013.

[70] M. Tomasi Morgano, H. Leibold, F. Richter, D. Stapf, H. Seifert, Screw pyrolysis technology for sewage sludge treatment, Waste Management 73 (2018) 487–495. https://doi.org/10.1016/j.wasman.2017.05.049.

[71] J. Neumann, J. Meyer, M. Ouadi, A. Apfelbacher, S. Binder, A. Hornung, The conversion of anaerobic digestion waste into biofuels via a novel Thermo-Catalytic Reforming process, Waste Management 47 (2016) 141–148. https://doi.org/10.1016/j.wasman.2015.07.001.

[72] Y. Chen, L. Yi, J. Yin, H. Jin, L. Guo, Sewage sludge gasification in supercritical water with fluidized bed reactor: Reaction and product characteristics, Energy 239 (2022) 122115. https://doi.org/10.1016/j.energy.2021.122115.

[73] Logan City Council, Logan City Biosolids Gasification Project, 2019. https://arena.gov.au/projects/logan-city-biosolids-gasification-project/ (accessed 21 November 2023).

[74] M. Schurz, A. Laugwitz, S. Krzack, B. Meyer, Comparison of Two Coal-Gasifier-Designs with Moving-Bed and Internal-Circulating-Fluidized-Bed Configuration in One Reactor, The Open Fuels & Energy Science Journal 10 (2017) 48–67. https://doi.org/10.2174/1876973X01710010048.

[75] M. Rapf, FlashPhos - The Complete Thermochemical Recycling of Sewage Sludge. https://flashphos-project.eu/ (accessed 21 November 2023).

[76] Bernd Buttker, Thomas Obermeier, Methanol aus Klärschlamm in der SVZ Schwarze Pumpe GmbH, 1997. https://www.tomm-c.de/fileadmin/pdf/2002/Methanol_aus_Klaerschlamm_in_der_SVZ_Schwarze_Pumpe_GmbH_2002.pdf (accessed 21 November 2023).

[77] Fritz Winkler: Verfahren zum Herstellen von Wassergas DE437970C. 1922. IG FARBENINDUSTRIE AG (ed.).

[78] D. Barisano, G. Canneto, F. Nanna, E. Alvino, G. Pinto, A. Villone, M. Carnevale, V. Valerio, A. Battafarano, G. Braccio, Steam/oxygen biomass gasification at pilot scale in an internally circulating bubbling fluidized bed reactor, Gasification and its Applications 141 (2016) 74–81. https://doi.org/10.1016/j.fuproc.2015.06.008.

[79] J. Gil, M.P. Aznar, M.A. Caballero, E. Francés, J. Corella, Biomass Gasification in Fluidized Bed at Pilot Scale with Steam−Oxygen Mixtures. Product Distribution for Very Different Operating Conditions, Energy Fuels 11 (1997) 1109–1118. https://doi.org/10.1021/ef9602335.

[80] A. Sebastiani, D. Macrì, K. Gallucci, M. Materazzi, Steam - oxygen gasification of refuse derived fuel in fluidized beds: Modelling and pilot plant testing, Fuel Processing Technology 216 (2021) 106783. https://doi.org/10.1016/j.fuproc.2021.106783.

[81] Y.-H. Chen, A.M. Parvez, M. Schmid, G. Scheffknecht, T.-L. Chen, 20 kW Pilot scale steam-oxygen gasification of solid recovered fuel with a focus on newly developed off-line and on-line tar measurement methods, Fuel Processing Technology 227 (2022) 107096. https://doi.org/10.1016/j.fuproc.2021.107096.

[82] C. Berrueco, D. Montané, B. Matas Güell, G. del Alamo, Effect of temperature and dolomite on tar formation during gasification of torrefied biomass in a pressurized fluidized bed, Energy 66 (2014) 849–859. https://doi.org/10.1016/j.energy.2013.12.035.

[83] C. Berrueco, J. Recari, B.M. Güell, G.d. Alamo, Pressurized gasification of torrefied woody biomass in a lab scale fluidized bed, Energy 70 (2014) 68–78. https://doi.org/10.1016/j.energy.2014.03.087.

[84] J. Koljonen, E. Kurkela, C. Wilén, Peat-based HTW-plant at Oulu, Bioresource Technology 46 (1993) 95–101. https://doi.org/10.1016/0960-8524(93)90059-K.

[85] E. Kurkela, M. Kurkela, I. Hiltunen, Steam–oxygen gasification of forest residues and bark followed by hot gas filtration and catalytic reforming of tars: Results of an extended time test, Gasification and its Applications 141 (2016) 148–158. https://doi.org/10.1016/j.fuproc.2015.06.005.

[86] X. Meng, W. de Jong, N. Fu, A.H. Verkooijen, Biomass gasification in a 100 kWth steam-oxygen blown circulating fluidized bed gasifier: Effects of operational conditions on product gas distribution and tar formation, Biomass and Bioenergy 35 (2011) 2910–2924. https://doi.org/10.1016/j.biombioe.2011.03.028.

[87] G.W. Huber, S. Iborra, A. Corma, Synthesis of Transportation Fuels from Biomass: Chemistry, Catalysts, and Engineering, Chemical Reviews 106 (2006) 4044–4098. https://doi.org/10.1021/cr068360d.

[88] A. Bolt, I. Dincer, M. Agelin-Chaab, A critical review of synthetic natural gas production techniques and technologies, Journal of Natural Gas Science and Engineering 84 (2020) 103670. https://doi.org/10.1016/j.jngse.2020.103670.

[89] Wikipedia, The Free Encyclopedia, Wikimedia Foundation, Electrolysis of water. https://en.wikipedia.org/wiki/Electrolysis_of_water (accessed 20 November 2023).

[90] Sunfire, SUNFIRE-HYLINK SOEC – TECHNICAL DATA. https://www.sunfire.de/files/sunfire/images/content/Sunfire.de%20(neu)/Sunfire-Factsheet-HyLink-SOEC-20210303.pdf (accessed 23 September 2022).

[91] Sunfire, Erfolgreiche Inbetriebnahme des weltweit größten SOEC-Elektrolyse-Moduls, 2021. https://www.sunfire.de/de/news/detail/erfolgreiche-inbetriebnahme-des-weltweit-groesssten-soec-elektrolyse-moduls (accessed 23 September 2022).

[92] G. Song, L. Wang, A. Yao, X. Cui, J. Xiao, Technical and Economic Assessment of a High-Quality Syngas Production Process Integrating Oxygen Gasification and Water Electrolysis: The Chinese Case, ACS Omega 6 (2021) 27851–27864. https://doi.org/10.1021/acsomega.1c03489.

[93] R. Anghilante, C. Müller, M. Schmid, D. Colomar, F. Ortloff, R. Spörl, A. Brisse, F. Graf, Innovative power-to-gas plant concepts for upgrading of gasification bio-syngas through steam electrolysis and catalytic methanation, Energy Conversion and Management 183 (2019) 462–473. https://doi.org/10.1016/j.enconman.2018.12.101.

[94] M. Beirow, M. Schmid, R. Spörl, G. Scheffknecht, Fluidized Bed Modelling for SER Steam Gasification Considering Partial Load Operation Points, in: 12th International Conference on Fluidized Bed Technology, 2017.

[95] M. Beirow, A.M. Parvez, M. Schmid, G. Scheffknecht, A Detailed One-Dimensional Hydrodynamic and Kinetic Model for Sorption Enhanced Gasification, Applied Sciences 10 (2020) 6136. https://doi.org/10.3390/app10176136.

[96] M. Schmid, Prozessmodellierung der AER- und Wasserdampfvergasung unter Berücksichtigung von Teillastbetriebspunkten: Masterarbeit Universität Stuttgart (2015).

[97] T. Kertthong, Entwicklung eines eindimensionalen Modells zur Beschreibung der autothermen Wirbelschichtvergasung: Masterarbeit Universität Stuttgart (2017).

[98] Ö.Ç. Mutlu, T. Zeng, Challenges and Opportunities of Modeling Biomass Gasification in Aspen Plus: A Review, Chem. Eng. Technol. 43 (2020) 1674–1689. https://doi.org/10.1002/ceat.202000068.

[99] J.M. de Andrés, M. Vedrenne, M. Brambilla, E. Rodríguez, Modeling and model performance evaluation of sewage sludge gasification in fluidized-bed gasifiers using Aspen Plus, Journal of the Air & Waste Management Association 69 (2019) 23–33. https://doi.org/10.1080/10962247.2018.1500404.

[100] P. Brachi, S. Di Fraia, N. Massarotti, L. Vanoli, Combined heat and power production based on sewage sludge gasification: An energy-efficient solution for wastewater treatment plants, Energy Conversion and Management: X 13 (2022) 100171. https://doi.org/10.1016/j.ecmx.2021.100171.

[101] S. Di Fraia, N. Massarotti, M.R. Uddin, L. Vanoli, Conversion of Sewage Sludge to combined heat and power: Modeling and optimization, Smart Energy 5 (2022) 100061. https://doi.org/10.1016/j.segy.2021.100061.

[102] N.P. Lumley, D.F. Ramey, A.L. Prieto, R.J. Braun, T.Y. Cath, J.M. Porter, Techno-economic analysis of wastewater sludge gasification: A decentralized urban perspective, Bioresource Technology 161 (2014) 385–394. https://doi.org/10.1016/j.biortech.2014.03.040.

[103] F. Drunsel, Buss-SMS-Cancler GmbH, Efficiency and heating medium temperatures of thin-film sewage sludge dryers. Email, 2021.

[104] P. Haro, F. Johnsson, H. Thunman, Improved syngas processing for enhanced Bio-SNG production: A techno-economic assessment, Energy 101 (2016) 380–389. https://doi.org/10.1016/j.energy.2016.02.037.

[105] A. Bartik, F. Benedikt, A. Lunzer, C. Walcher, S. Müller, H. Hofbauer, Thermodynamic investigation of SNG production based on dual fluidized bed gasification of biogenic residues, Biomass Conv. Bioref. 11 (2021) 95–110. https://doi.org/10.1007/s13399-020-00910-y.

[106] R. Gabbrielli, F. Barontini, S. Frigo, L. Bressan, Numerical analysis of bio-methane production from biomass-sewage sludge oxy-steam gasification and methanation process, Applied Energy 307 (2022) 118292. https://doi.org/10.1016/j.apenergy.2021.118292.

[107] VDI 3878, Measurement of ammonia (and gaseous ammonium compounds), manual method (2017).

[108] K. van Paasen, J. Kiel, Tar formation in a fluidised-bed gasifier, ECN publication (Energy research Centre of the Netherlands) 1 (2004) 1–58.

[109] M. Neubert, S. Reil, M. Wolff, D. Pöcher, H. Stork, C. Ultsch, M. Meiler, J. Messer, L. Kinzler, M. Dillig, S. Beer, J. Karl, Experimental comparison of solid phase adsorption (SPA), activated carbon test tubes and tar protocol (DIN CEN/TS 15439) for tar analysis of biomass derived syngas, Biomass and Bioenergy 105 (2017) 443–452. https://doi.org/10.1016/j.biombioe.2017.08.006.

[110] C.W. Bale, E. Bélisle, P. Chartrand, S.A. Decterov, G. Eriksson, K. Hack, I.-H. Jung, Y.-B. Kang, J. Melançon, A.D. Pelton, C. Robelin, S. Petersen, FactSage thermochemical software and databases — recent developments, Calphad 33 (2009) 295–311. https://doi.org/10.1016/j.calphad.2008.09.009.

[111] G. Ruoppolo, F. Miccio, P. Brachi, A. Picarelli, R. Chirone, Fluidized Bed Gasification of Biomass and Biomass/Coal Pellets in Oxygen and Steam Atmosphere, Chemical Engineering Transactions 32 (2013) 595–600. https://doi.org/10.3303/CET1332100.

[112] K. Sandeep, S. Dasappa, Oxy–steam gasification of biomass for hydrogen rich syngas production using downdraft reactor configuration, Int. J. Energy Res. 38 (2014) 174–188. https://doi.org/10.1002/er.3019.

[113] R. Xiao, M. Zhang, B. Jin, Y. Huang, H. Zhou, High-Temperature Air/Steam-Blown Gasification of Coal in a Pressurized Spout-Fluid Bed, Energy & Fuels 20 (2006) 715–720. https://doi.org/10.1021/ef050233h.

[114] S. Guo, X. Wei, J. Li, D. Che, H. Liu, B. Sun, Q. Wang, Experimental Study on Product Gas and Tar Removal in Air–Steam Gasification of Corn Straw in a Bench-Scale Internally Circulating Fluidized Bed, Energy & Fuels 34 (2020) 1908–1917. https://doi.org/10.1021/acs.energyfuels.9b04008.

[115] S. Chianese, S. Fail, M. Binder, R. Rauch, H. Hofbauer, A. Molino, A. Blasi, D. Musmarra, Experimental investigations of hydrogen production from CO catalytic conversion of tar rich syngas by biomass gasification, Catalysis Today 277 (2016) 182–191. https://doi.org/10.1016/j.cattod.2016.04.005.

[116] A. Molino, P. Iovane, A. Donatelli, G. Braccio, S. Chianese, D. Musmarra, Steam Gasification of Refuse-Derived Fuel in a Rotary Kiln Pilot Plant: Experimental Tests, Chemical Engineering Transactions 32 (2013) 337–342. https://doi.org/10.3303/CET1332057.

[117] N. Poboss, Experimental investigation of the absorption enhanced reforming of biomass in a 20 kWth dual fluidized bed system, Int. J. Thermo 15 (2012). https://doi.org/10.5541/ijot.321.

[118] U. Wolfesberger, I. Aigner, H. Hofbauer, Tar content and composition in producer gas of fluidized bed gasification of wood-Influence of temperature and pressure, Environ. Prog. Sustainable Energy 28 (2009) 372–379. https://doi.org/10.1002/ep.10387.

[119] C. Pfeifer, S. Koppatz, H. Hofbauer, Steam gasification of various feedstocks at a dual fluidised bed gasifier: Impacts of operation conditions and bed materials, Biomass Conversion and Biorefinery 1 (2011) 39–53. https://doi.org/10.1007/s13399-011-0007-1.

[120] J. Fuchs, J.C. Schmid, S. Müller, A.M. Mauerhofer, F. Benedikt, H. Hofbauer, The impact of gasification temperature on the process characteristics of sorption enhanced reforming of biomass, Biomass Conv. Bioref. (2019). https://doi.org/10.1007/s13399-019-00439-9.

[121] N. Poboss, Experimentelle Untersuchung der sorptionsunterstützten Reformierung. Dissertation, Universität Stuttgart, 2016. http://elib.uni-stuttgart.de/bitstream/11682/8873/1/Dissertation_Norman_Poboss.pdf (accessed 5 January 2021).

[122] S. Chen, Z. Sun, Q. Zhang, J. Hu, W. Xiang, Steam gasification of sewage sludge with CaO as CO2 sorbent for hydrogen-rich syngas production, Biomass and Bioenergy 107 (2017) 52–62. https://doi.org/10.1016/j.biombioe.2017.09.009.

[123] Kopf SynGas GmbH & Co. KG, Klärschlammverwertung: Nachhaltige Phosphornutzung aus Vergasungsaschen. https://suelzle-kopf.de/wp-content/uploads/sites/3/2018/07/aschenutzung-phosphor-suelzle-kopf-syngas.pdf (accessed 2 April 2020).

[124] W. de Jong, J. Andries, K.R. Hein, Coal/biomass co-gasification in a pressurised fluidised bed reactor, Renewable Energy 16 (1999) 1110–1113. https://doi.org/10.1016/S0960-1481(98)00432-7.

[125] J. Hongrapipat, W.-L. Saw, S. Pang, Removal of ammonia from producer gas in biomass gasification: integration of gasification optimisation and hot catalytic gas cleaning, Biomass Conv. Bioref. 2 (2012) 327–348. https://doi.org/10.1007/s13399-012-0047-1.

[126] N. Paterson, Y. Zhuo, D. Dugwell, R. Kandiyoti, Formation of Hydrogen Cyanide and Ammonia during the Gasification of Sewage Sludge and Bituminous Coal, Energy & Fuels 19 (2005) 1016–1022. https://doi.org/10.1021/ef049688h.

[127] C. Di Blasi, Modeling chemical and physical processes of wood and biomass pyrolysis, Progress in Energy and Combustion Science 34 (2008) 47–90. https://doi.org/10.1016/j.pecs.2006.12.001.

[128] I. Fonts, G. Gea, M. Azuara, J. Ábrego, J. Arauzo, Sewage sludge pyrolysis for liquid production: A review, Renewable and Sustainable Energy Reviews 16 (2012) 2781–2805. https://doi.org/10.1016/j.rser.2012.02.070.

[129] J.C. Schmid, F. Benedikt, J. Fuchs, A.M. Mauerhofer, S. Müller, H. Hofbauer, Syngas for biorefineries from thermochemical gasification of lignocellulosic fuels and residues—5 years' experience with an advanced dual fluidized bed gasifier design, Biomass Conv. Bioref. (2019). https://doi.org/10.1007/s13399-019-00486-2.

[130] D. Schweitzer, F.G. Albrecht, M. Schmid, M. Beirow, R. Spörl, R.-U. Dietrich, A. Seitz, Process simulation and techno-economic assessment of SER steam gasification for hydrogen production, International Journal of Hydrogen Energy 43 (2018) 569–579. https://doi.org/10.1016/j.ijhydene.2017.11.001.

[131] A. Larsson, M. Kuba, T. Berdugo Vilches, M. Seemann, H. Hofbauer, H. Thunman, Steam gasification of biomass – Typical gas quality and operational strategies derived from industrial-scale plants, Fuel Processing Technology 212 (2021) 106609. https://doi.org/10.1016/j.fuproc.2020.106609.

[132] F. Tang, Y. Jin, Y. Chi, Z. Zhu, J. Cai, Z. Li, M. Li, Effect of steam on the homogeneous conversion of tar contained from the co-pyrolysis of biomass and plastics, Environmental Science and Pollution Research 28 (2021) 68909–68919. https://doi.org/10.1007/s11356-021-15313-3.

[133] W. Song, C. Deng, S. Guo, Effect of Steam on the Tar Reforming during Circulating Fluidized Bed Char Gasification, ACS Omega 6 (2021) 11192–11198. https://doi.org/10.1021/acsomega.0c05861.

[134] Eurostat, Energy statistics - an overview, 2020. https://ec.europa.eu/eurostat/statistics-explained/index.php?title=Energy_statistics_-_an_overview (accessed 19 September 2022).

[135] J. H. Jensen, J. M. Poulsen and N. U. Andersen, From coal to clean energy, Nitrogen+Syngas (2011).

[136] Haldor Topsoe, Biogas-SOEC Electrochemical upgrading of biogas to pipeline quality by means of SOEC electrolysis, 2011. https://www.ea-energianalyse.dk/wp-content/uploads/2020/02/1110_biogas_soec_mail_final_report.pdf (accessed 8 February 2021).

[137] Fragol AG, Fragoltherm (R) heating liquid, 2021. https://www.fragol.de/de/waermetraeger/waermetraeger/produkte/fragolthermr-dpo.html.

[138] Cosmodyne, Poplar Series: Oxygen, Nitrogen, Argon generating systems. https://www.cosmodyne.com/wp-content/uploads/2015/10/Poplar_Series_Brochure1.pdf (accessed 17 February 2021).

[139] A. Alamia, S. Òsk Gardarsdòttir, A. Larsson, F. Normann, H. Thunman, Efficiency Comparison of Large-Scale Standalone, Centralized, and Distributed Thermochemical Biorefineries, Energy Technol. 5 (2017) 1435–1448. https://doi.org/10.1002/ente.201600719.

[140] H. Thunman, M. Seemann, T.V. Berdugo, J. Maric, D. Pallares, H. Ström, G. Berndes, P. Knutsson, A. Larsson, C. Breitholtz, O. Santos, Advanced biofuel production via gasification – lessons learned from 200 man-years of research activity with Chalmers' research gasifier and the GoBiGas demonstration plant, Energy Sci Eng 6 (2018) 6–34. https://doi.org/10.1002/ese3.188.

[141] John M. Campbell, How to Estimate Compressor Efficiency. http://www.jmcampbell.com/tip-of-the-month/2015/07/how-to-estimate-compressor-efficiency/ (accessed 16 February 2021).

[142] Y. Demirel, 5.2 Energy Conservation, in: I. Dincer (Ed.), Comprehensive Energy Systems, ELSEVIER, Oxford, 2018, pp. 45–90.

[143] P. Adler, E. Billig, A. Brosowski, W. Urban, J. Daniel-Gromke, I. Falke, E. Fischer, J. Grope, U. Holzhammer, J. Postel, J. Schnutenhaus, K. Stecher, M. Trommler, G. Szomszed, Leitfaden Biogasaufbereitung und -einspeisung, 2014. https://mediathek.fnr.de/media/downloadable/files/samples/l/e/leitfaden_biogaseinspeisung-druck-web.pdf.

[144] DVGW, G262 (A) Nutzung von Gasen aus regenerativen Quellen in der öffentlichen Gasversorgung: Technische Regel - Arbeitsblatt.

[145] E.ON Energie Deutschland GmbH, Was bedeutet L-Gas und H-Gas?, 2022. https://www.eon.de/de/pk/erdgas/l-gas-h-gas.html (accessed 25 December 2022).

[146] A. Alamia, A. Larsson, C. Breitholtz, H. Thunman, Performance of large-scale biomass gasifiers in a biorefinery, a state-of-the-art reference, Int. J. Energy Res. 41 (2017) 2001–2019. https://doi.org/10.1002/er.3758.

[147] BDEW Bundesverband der Energie- und Wasserwirtschaft e.V., Die Energieversorgung 2021 Jahresbericht (2022).

[148] bayernets GmbH et. al., Klimaschutz und Wettbewerbsfähigkeit gemeinsam sichern: der Beitrag der Gaswirtschaft und Industrie: Positionspapier, 2020. https://wintershalldea.com/sites/default/files/media/files/Positionspapier_Gaskoalition_Erdgas%20in%20der%20Industrie_de_0.PDF (accessed 29 March 2022).